AD-A120 286 NAVAL POSTGRADUATE SCHOOL MONTEREY CA F/G 8/3
OCEANIC MIXED LAYER RESPONSE TO TIDAL PERIOD INTERNAL WAVE MOTI--ETC(U)
JUN 82 R J BURGER

UNCLASSIFIED NL

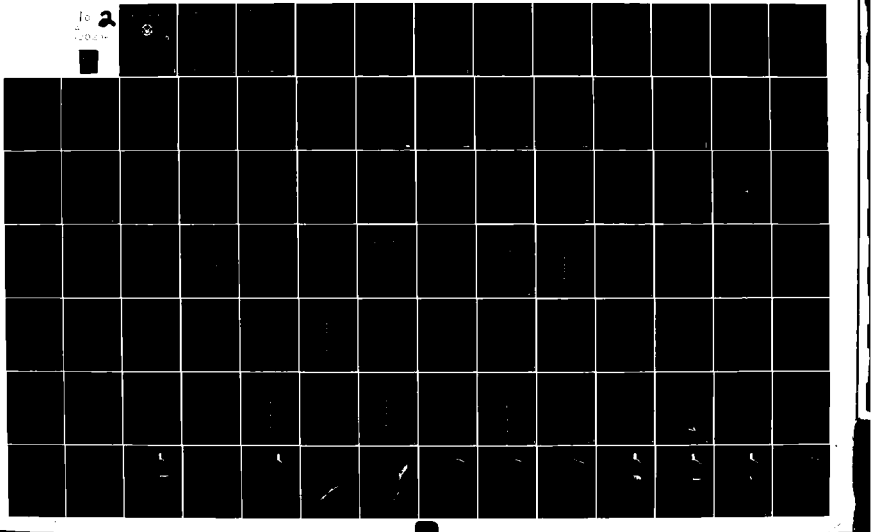

NAVAL POSTGRADUATE SCHOOL
Monterey, California

THESIS

OCEANIC MIXED LAYER RESPONSE TO TIDAL PERIOD INTERNAL WAVE MOTION

by

Rolf John Burger

June 1982

Thesis Advisor: R. W. Garwood, Jr.

Approved for public release, distribution unlimited

Unclassified
SECURITY CLASSIFICATION OF THIS PAGE (When Data Entered)

REPORT DOCUMENTATION PAGE	READ INSTRUCTIONS BEFORE COMPLETING FORM
1. REPORT NUMBER	2. GOVT ACCESSION NO. AD-A120396	3. RECIPIENT'S CATALOG NUMBER
4. TITLE (and Subtitle) Oceanic Mixed Layer Response to Tidal Period Internal Wave Motion	5. TYPE OF REPORT & PERIOD COVERED Master's Thesis June 1982
	6. PERFORMING ORG. REPORT NUMBER
7. AUTHOR(s) Rolf John Burger	8. CONTRACT OR GRANT NUMBER(s)
9. PERFORMING ORGANIZATION NAME AND ADDRESS Naval Postgraduate School Monterey, California 93940	10. PROGRAM ELEMENT, PROJECT, TASK AREA & WORK UNIT NUMBERS
11. CONTROLLING OFFICE NAME AND ADDRESS Naval Postgraduate School Monterey, California 93940	12. REPORT DATE June 1982
	13. NUMBER OF PAGES 131
14. MONITORING AGENCY NAME & ADDRESS(if different from Controlling Office)	15. SECURITY CLASS. (of this report) Unclassified
	15a. DECLASSIFICATION/DOWNGRADING SCHEDULE

16. DISTRIBUTION STATEMENT (of this Report)

Approved for public release, distribution unlimited.

17. DISTRIBUTION STATEMENT (of the abstract entered in Block 20, if different from Report)

18. SUPPLEMENTARY NOTES

19. KEY WORDS (Continue on reverse side if necessary and identify by block number)

Mixed layer modelling, vertical advection and mixed layer modelling, Tidal period internal waves and mixed layer modelling.

20. ABSTRACT (Continue on reverse side if necessary and identify by block number)

The purpose of this research was to investigate the effect of tidal-period internal wave vertical motion on oceanic mixed layer dynamics, and to discern the effect upon the diurnal evolution of thermoclines, as observed during MILE (mixed layer experiment). Vertical advection was added to a one-dimensional bulk model of the mixed layer with an assumed linear in z and sinusoidal in time dependence. The rate of mixed layer deepening was therefore due to the combination of vertical motion and entrainment. The first significant result was the finding that the

DD FORM 1 JAN 73 1473 EDITION OF 1 NOV 65 IS OBSOLETE S/N 0102-014-6601 | Unclassified
SECURITY CLASSIFICATION OF THIS PAGE (When Data Entered)

interaction between vertical mixing and vertical motion depended upon the wave frequency and its phase relation to the diurnal heating cycle. Second, linear and non-linear interactions of the wave induced vertical motion with the cyclical boundary conditions can generate two-dimensional (x-z) structure in the near-surface temperature field of an initially horizontally homogeneous ocean under the influence of horizontally homogeneous surface boundary conditions. Finally, this advective interaction increases the utility of the mixed layer model in single station forecasting.

Approved for public release; distribution unlimited.

Oceanic Mixed Layer Response to Tidal Period Internal Wave Motion

by

Rolf John Burger
Lieutenant, United States Navy
B.S., University of North Carolina, 1974

Submitted in partial fulfillment of the
requirements for the degree of

MASTER OF SCIENCE IN METEOROLOGY AND OCEANOGRAPHY

from the

NAVAL POSTGRADUATE SCHOOL
June 1982

Author: Rolf J. Burger

Approved by: Roland W. Garwood Jr
Thesis Advisor

Christopher N. K. Mooers for R. T. Williams
Second Reader

Christopher N. K. Mooers
Chairman, Department of Oceanography

William M. Tolles
Dean of Science and Engineering

ABSTRACT

The purpose of this research was to investigate the effect of tidal-period internal wave vertical motion on oceanic mixed layer dynamics, and to discern the effect upon the diurnal evolution of thermoclines, as observed during MILE (mixed layer experiment). Vertical advection was added to a one-dimensional bulk model of the mixed layer with an assumed linear in z and sinusoidal in time dependence. The rate of mixed layer deepening was therefore due to the combination of vertical motion and entrainment. The first significant result was the finding that the interaction between vertical mixing and vertical motion depended upon the wave frequency and its phase relation to the diurnal heating cycle. Second, linear and non-linear interactions of the wave induced vertical motion with the cyclical boundary conditions can generate two-dimensional (x-z) structure in the near-surface temperature field of an initially horizontally homogeneous ocean under the influence of horizontally homogeneous surface boundary conditions. Finally, this advective interaction increases the utility of the mixed layer model in single station forecasting.

TABLE OF CONTENTS

LIST OF FIGURES

I. INTRODUCTION

In recent years much study of internal waves has focused on the linear and non-linear wave interactions. Models for wave prediction have been developed and tested to match the theory. There have been attempts to measure the internal wave fields in situ. Some of the most useful of these have been the observations of temperature and pressure field variations with depth, providing a basis for computations of the vertical motions and interactions involved. These studies and analyses of data demonstrate the importance of the internal wave field in upper ocean and near surface dynamics.

Roth et al. (1981) presented clear evidence that internal waves are not as critical in an analysis of the dynamics of mixing at depth because they have little variability. However, near the surface, where they interact with other phenomena such as cyclical heat flux, wind stress, and other boundary conditions, their effect can be considerable when dealing with the budgets of heat and momentum. Holloway (1980) pointed out that internal waves are not weak waves (in the sense of weak resonant interaction theory) and have a high impact on mixed layer dynamics down to and including turbulent scales of motion. Pinkel (1981) showed that the near-surface wave field has a profound effect on the vertical velocity field in the upper ocean.

Some mixed layer experiments such as those by Linden (1975) and Kantha et al. (1977) have shown that internal wave radiation may play an important role in controlling the rate of deepening of a turbulent

mixed layer in a stratified fluid. Displacements induced by the turbulence in the base of the mixed layer served to form internal waves which removed kinetic energy of motion from the mixed layer. Since this energy is also important in the entrainment process, these induced internal waves, of relatively high frequency, serve to retard deepening of a mixed layer. Townsend (1968) has derived an expression for the rate of generation of the internal waves and their energy by a steady disturbance field which is advected relative to a stratified layer at a constant speed. The theory was extended by Bell (1978) to cover general space-time dependence of the disturbance field. These works indicate that internal waves could be a means of retarding the growth of mixed layers, through the removal of the kinetic energy in the layers.

Such studies all indicate that the presence of internal waves should be taken into account as a possibly important factor in the mechanical energy budget which controls mixing. It is hypothesized that internal waves which have periods comparable to the dominant time scales of the atmospheric forcing (surface heat flux and wind stress) will be the most likely to result in an interaction with the entrainment mixing process in terms of a positive feedback (increased mixing) effect.

A. BACKGROUND DATA ANALYSIS

During the period August-September 1977, a mixed layer experiment (MILE) was conducted at Ocean Station P (55° N, 145° W) in the North Pacific. The depth of the mixed layer varied between about five and thirty meters during the period of the experiment. Temperature was continuously observed at fixed depths for a period of three weeks. A spectrum analysis of this data (See Figure 10 in later section) shows some important features.

First, a major spectral peak was at about 12.79 $\pm$ .02 hours, with secondary peaks at 6.62 $\pm$ .13 and 3.94 $\pm$ .06 hours. Lower order spectral peaks are at 4.9 hours, and at several frequencies having periods under 3.5 hours. The peak at 12.79 hours is clearly associated with the semi-diurnal tide (12.45 hrs.), with the other two peaks at 6.62 and 3.94 hours probably being higher harmonics. At all three depths of the analysis it is clear that the semi-diurnal internal tidal wave, with its harmonics, is the dominant cause of vertical motion at the base of the mixed layer.

Second, the tidal peaks, including the harmonics, are very coherent vertically throughout the depths analyzed. They are present in all three depths analyzed, below the layer, and in the mixed layer, with very little frequency or phase shift.

Finally, the spectral peaks at other than tidal frequencies are not vertically coherent. Also, there is a large variation in non-tidal spectral densities for observations above and below the thirty meter depth--the top of the seasonal thermocline at this time of year. This suggests that something has happened to the higher frequency waves near the surface making the interpretation of their effect on mixed layer dynamics hard to judge from simple theories. However, at the same time it suggests that the effect of tidal internal waves may be quite easily discerned.

These results confirm the work of Pinkel (1981) whose studies showed that of the wave fields in the upper ocean, the tide and its harmonics have the greatest vertical coherence.

Studies by Simpson and Paulson (1979) demonstrated the variability of the temperature structure in the upper ocean during the POLE experiment.

Shook (1980) showed that these variations were a response to vertical and horizontal advective processes. In a study of Pacific Ocean ship track temperature data, Butler (1981) found definite cyclical variations in the sea surface temperature structure.

From these studies of actual data, it is obvious that (1) the tidal period internal waves and their harmonics are an important source of energy in the upper ocean, and (2) surface layer temperature patchiness exists in the ocean, and may in part be generated by interaction of mixing and internal wave motion.

B. ADVECTION IN MODELLING

To date little has been published concerning the interaction of tidal-period internal waves and entrainment by the mixed layer. De Szoeke (1980) has discussed advection in the mixed layer as a result of horizontal variability of the surface wind stress. He showed that advection, upwelling and downwelling, was an important parameter in mixed layer dynamics, resulting from the boundary forcing of the wind stress. Cushman-Roisin (1981), Garwood et al. (1981), and Price (1981) also demonstrated that advection can play an important role in the dynamics of the mixed layer, but the interaction with internal gravity waves is not treated. De Szoeke and Rhines (1981) discussed coastal upwelling at length, but the advective motion was conceived as a necessary factor to achieve a realistic balance for surface heating, transport, and mixing, in order to produce observed coastal temperature fields. Price et al. (1978) included vertical advection in the test of a mixed layer formulation during storm conditions. They found that the phase dependence between wind stress and mixed layer deepening, and the mixed layer deepening itself were reasonably simulated.

Within this discussion of a limited amount of relevant literature on the advective process it has been shown that vertical advection must play an important role in storm response, coastal circulation, and fronts. No one has examined the role of internal wave motion, on the tidal scale, in the open ocean where the geometry and boundary conditions are rather one-dimensional.

In possibly the most relevant previous effort, Spigel (1980) looked at the coupling of internal wave motion and entrainment in a two-layer lake model, having a mixed layer which is based upon the one-dimensional turbulent kinetic energy budget. Time scales of internal wave motion, wave decay, and entrainment were widely separated. Using a seiche effect in a basin, he demonstrated that internal waves did in fact play an important role in the entrainment zone.

With this background it was believed that the time has come for an investigation of the effects of internal vertical motion in the oceanic mixed layer. The motion is there. Observations show that it dominates Eulerian measurements in the upper thermocline. The importance of this motion to mixed layer evolution needs to be established.

C. SCOPE OF THIS STUDY

The scope of this initial study shall be confined to a limited number of wave frequencies. There is insufficient time to concentrate on all the types of internal vertical motion, and all of the possible couplings and interactions in this thesis. The purpose of this initial research was to investigate the effect of dominant tidal-period internal

wave vertical motion on oceanic mixed layer dynamics, and to discern the effect upon the transient thermocline as observed during the mixed layer experiment. The effects of the vertical motion are explored using a one-dimensional bulk model of the mixed layer originally proposed by Garwood (1976,1977) and expanded here to include a prescribed vertical velocity.

The first hypothesis to be examined is can alteration of the existing mixed layer model be reasonably done? Can a relatively simple mathematical transformation be applied to include a prescribed vertical motion without altering the basic physics of the entrainment process? The study will show that this in fact can be done, as revealed by a careful examination of the interactions at each step of the alteration of the original model.

A second hypothesis to be examined is that vertical motion produced by long period internal gravity waves for which the Rossby number is small, through interaction with cyclical boundary conditions (wind stress and heat flux) can produce two-dimensional (x-z) structures in the temperature field of a simple infinite ocean having horizontally homogeneous surface boundary conditions. An objective will be to demonstrate the frequency dependence of the internal vertical motion upon the phases of the cyclical heat fields, and the wind stress. It will be shown that there is a non-linear interaction between superimposed diurnal and semi-diurnal internal tidal waves. Finally, this study will show the relative strengths of the resultant two-dimensional structures, and relate these to their importance in forming an improved thermodynamic ocean model.

II. MIXED LAYER MODEL AND VERTICAL MOTION THEORY

A. MIXED LAYER MODEL

To study the effects of internal vertical motion on mixed layer evolution, the Garwood (1976, 1977) mixed layer model was used in a one-dimensional form. Garwood developed an ocean mixed layer model using the Navier-Stokes equation of motion with the geostrophic component eliminated, the continuity equation for incompressible water, the heat equation from the first law of thermodynamics, the conservation of salt equation, and a linearized equation of state. The entrainment hypothesis depends upon the relative distribution of turbulent energy between horizontal and vertical components and is offered as a plausible mechanism for governing both entrainment and layer retreat.

Garwood suggested that planetary rotation influences the dissipation of turbulence for deeper mixed layers and enables a cyclical steady state to exist on an annual basis. Furthermore, the rate of entrainment for the stable regime cannot be a simple linear extrapolation of the unstable situations. Unlike the atmospheric boundary case, most of the solar radiation does not penetrate the layer. Therefore, downward turbulent heat flux in the oceanic boundary layer is as important as the upward flux during the course of both diurnal and annual cycles. The non-linearity of the interface entrainment tendency parameter, which is greatest for stable surface boundary conditions, results in a modulation of the long term trend of the mixed layer depth by the diurnal component of surface heat flux. In this model, buoyant production is somewhat more efficient than shear production as a source

of energy for vertical mixing because of its unique effect on the vertical component of the turbulent velocity.

The governing heat equation for this model assumes two forms: one for the mixed layer, the other for below the mixed layer. For the mixed layer, the equation has the form

$$\frac{\partial \langle T \rangle}{\partial t} = \frac{(\overline{w'T'})_{-h} - (\overline{w'T'})_0}{h} + \frac{\alpha g}{\rho C_p h}\int_{-h}^{0} Q\, dz \qquad (1)$$

where $\langle\ \rangle$ denotes the mixed layer average and Q is the net heat flux, a product of downward solar radiation, upward turbulent heat flux to the surface, and surface back radiation. Below the mixed layer the heat equation becomes

$$\frac{\partial T}{\partial t} = -\frac{\partial (wT)}{\partial z} + \frac{\alpha g Q}{\rho C_p} + \frac{K \partial^2 T}{\partial z^2} \qquad (2)$$

where K is the eddy viscosity, and $-\partial(wT)/\partial z$ is the term added for the vertical motion.

The buoyancy flux at the entrainment zone is modelled according to

$$\alpha g(\overline{w'T'})_{-h} = -\frac{\langle \overline{w'w'} \rangle^{1/2} \langle \bar{E} \rangle}{h} \qquad (3)$$

which is derived from the local turbulent kinetic energy (TKE) budget where

$$z = -h \qquad (3a)$$

In the entrainment zone, the buoyant damping attributed to $(\overline{w'T'})_{-h}$ is assumed to be balanced by the convergence of TKE flux. This convergence is modeled as a function of the TKE kinetic energy components and the vertical distance over which this energy must be transported. $\langle \overline{w'w'} \rangle$ and $\langle \bar{E} \rangle$ are the bulk values of the vertical component and the total TKE,

respectively. The prognostic equations for these mixed-layer turbulence variables are derived using the bulk second-order closure methods of Garwood (1977), and are

$$\frac{\partial}{\partial t}\left(\frac{h\langle\bar{E}\rangle}{2}\right) = mu_*^3 - \frac{\alpha g h(\overline{w'T'})_{-h}}{2R_i^*} + \alpha g h\left[\frac{(\overline{w'T'})_{-h} + (\overline{w'T'})_0}{2}\right] - (\langle\bar{E}\rangle^{1/2} + fh)\langle\bar{E}\rangle \quad (4)$$

$$\frac{\partial}{\partial t}\left(\frac{h\langle\overline{w'w'}\rangle}{2}\right) = \alpha g h\left[\frac{(\overline{w'T'})_{-h} + (\overline{w'T'})_0}{2}\right] + (\langle\bar{E}\rangle - 3\langle\overline{w'w'}\rangle)\langle\bar{E}\rangle^{1/2} - \frac{(\langle\bar{E}\rangle^{1/2} + fh)\langle\bar{E}\rangle}{3} \quad (5)$$

where

$$u_* = (\tau/\rho_a)^{1/2}$$

with τ being the magnitude of the surface wind stress and ρ_a is the air density, assumed to be a constant, and

$$R_i^* = \frac{\alpha g h \Delta T}{(\Delta u^2 + \Delta v^2)}$$

is the bulk Richerdson number. The change in the total TKE, $\langle\bar{E}\rangle$, is a function of wind stress shear production, entrainment shear production, bouyant production/damping, and dissipation. The change in the vertical component, $\langle\overline{w'w'}\rangle$, is a function of bouyant production/damping, pressure redistribution, and dissipation. The quantities ΔT, Δu, and Δv are the jump values between the mixed layer (assumed to be vertically uniform), and the underlying stable waters. These bulk TKE equations are solved algebraically assuming quasi-steady state for the TKE budgets

$$\frac{\partial}{\partial t}(h\langle\overline{E}\rangle) = 0$$

and

$$\frac{\partial}{\partial t}(h\langle w'w'\rangle) = 0$$

With this assumption the computed values of $\langle\overline{w'w'}\rangle$ and $\langle\overline{E}\rangle$ are in phase with the surface boundary conditions--the wind stress, ρu_*^2, and the buoyancy flux, $\alpha g(\overline{w'T'})_0$.

Once the entrainment bouyancy flux is known from (3), the downward fluxes of momentum associated with entrainment at the base of the mixed layer, $(\overline{w'u'})_{-h}$ and $(\overline{w'v'})_{-h}$ are given by

$$-(\overline{w'u'})_{-h} = w_e \Delta u = -(\overline{w'T'})_{-h} \frac{\Delta u}{\Delta T} \qquad (6)$$

$$-(\overline{w'v'})_{-h} = w_e \Delta v = -(\overline{w'T'})_{-h} \frac{\Delta v}{\Delta T} \qquad (7)$$

Here the entrainment velocity is

$$w_e = \frac{-(\overline{w'T'})_{-h}}{\Delta T} \qquad (8)$$

and the entrainment velocity is also defined as

$$w_e = \frac{dh}{dt} + w_{-h} \qquad (9)$$

if w_e is greater than zero. If w_e is not greater than zero, equations (10) and (11) are applied.

1. Boundary Layer Deepening by Entrainment

The entrainment heat flux $(\overline{w'T'})_{-h}$ is determined algebraically from (3), and the steady-state forms of (4) and (5) in terms of given values of u_*, $(\overline{w'T'})_0$, h and R_i^*. This heat flux is then applied to the given temperature profile. The new h and new momentum and temperature

profiles are unique solutions provided that (i) the mixed layer is homogeneous, (ii) the value of h is just large enough to prevent unstable density profiles ($\partial T/\partial z$ greater than zero), and (iii) heat is conserved.

2. Boundary Layer Shallowing

Shallowing occurs when there is adequate vertical turbulent energy to transport heat down to the base of the existing mixed layer. The depth at which the vertical heat flux ($\overline{w'T'}$) vanishes establishes the new layer boundary, and will be the base of the new mixed layer. In this model, this occurs when ($\overline{w'w'}$) approaches zero. Then (3) is no longer applicable, and the steady state forms of (4) and (5) reduce to

$$0 = mu_*^3 - (\langle\bar{E}\rangle^{1/2} + fh)\langle\bar{E}\rangle + \frac{\alpha g h(\overline{w'T'})_0}{2} \qquad (10)$$

$$0 = \langle\bar{E}\rangle^{3/2} - \frac{(\langle\bar{E}\rangle^{1/2} + fh)\langle\bar{E}\rangle}{3} + \frac{\alpha g h(\overline{w'T'})_0}{2} \qquad (11)$$

Without the planetary rotation term, or if the downward surface buoyancy flux is dominant, h is proportional to the Obukhov length scale

$$L = u_*^3/\alpha g(w'T')_0$$

If, on the other hand, $(\overline{w'T'})_0 = 0$, h is proportional to u_*/f. In general, however, the depth of the shallowing mixed layer is a function of the two non-dimensional parameters, h/L and hf/u_*.

Heat and momentum are conserved in the profile specifications and, because the mechanical energy budget requires conservation of potential energy on the time scale of the turbulence, a numerical procedure is used that also preserves potential energy. This is

intended to ensure that the deepening rate is as correct as possible when the mixed layer deepens to its former position.

B. VERTICAL MOTION THEORY

By following a water particle as it is vertically advected by a prescribed velocity field, $w(x,z,t)$, the distortion of any temperature profile, $T(z)$, after a small, but finite length of time, (Δt), may be computed by non-linear theory.

If we assume

$$w = -\frac{Az}{D}\cos(\omega t + kx) \tag{12}$$

is prescribed, then

$$\frac{dz}{dt} = -\frac{Az}{D}\cos(\omega t + kx) \tag{13}$$

This may be reformed and integrated

$$\int_{z_1}^{z_2}\frac{dz}{z} = \int_{t_1}^{t_2}-\frac{A}{D}\cos(\omega t + kx)\,dt$$

where a water particle starting at time t_1 at position z_1 is advected to position z_2 at time t_2. Or following any constant isotherm initially at position z_1, to z_2 at t_2 gives

$$z_2 = z_1 \exp\left\{\frac{A}{\omega D}\left[\sin(\omega t_2 + kx) - \sin(\omega t_1 + kx)\right]\right\} \tag{14}$$

If $t = t_2 - t_1 << \omega^{-1}$, then

$$z_2 \cong z_1 \exp\left\{\frac{A\Delta t}{D}\left[\cos(\omega(t_1 + \tfrac{1}{2}) + kx)\right]\right\} \tag{15}$$

or

$$z_2 \cong z_1 e^{R} \tag{16}$$

which is the general form approximated by the progression of equations in this study of internal vertical motion. Internal vertical motion is applied to the mixed layer model through equation (10). dh/dt, due to the internal vertical advection, w_{-h}, is derived from equation (16).

For future study, the salinity budget can be handled in a like manner.

III. EXPERIMENTS

A. PRODUCTS

The products used to identify features in the model runs and used for comparison are:

1. Table (Sample Figure 1a) showing the hourly change in the mixed layer primary variables:

   H is the mixed layer depth in meters.

   T is the mixed layer temperature in degrees centigrade.

   S is the mixed layer salinity in parts per thousand.

   TAU is the surface wind stress in dynes per square centimeter.

   QNET is the net heat flux out of the mixed layer in watts per square meter.

   WDD is the value of the vertical motion parameter affecting the model in centimeters per second.

   DH is the change in mixed layer depth due to the vertical motion for that time period.

2. Contours of the temperature variation, T(z,t), (Sample Figure 1) between z = 0 and z = -60 meters over the initial 24 hours of the model run. Varying resolution is used to better resolve the evaluation of T(z,t). Temperature contours are in degrees centigrade.

3. Contours of temperature variation similar to 2, in a quasi two-dimensional mode. This is accomplished by running the model 24 times, each time passing the prescribed vertical motion through the 24 hour cycle of the model at a different, progressive phase. The 24 runs are then sorted by hour giving 24 data sets of 24 independent points with a spatial separation of kx from hour one through hour twenty-four.

DAY	HR	H	T	S	TAU	QNET	WDD	DH
1	1	6.3	14.956	34.000	0.50	- 3.5	0.0	0.0
1	2	7.3	14.939	34.000	0.50	-100.8	0.0	0.0
1	3	8.0	14.935	34.000	0.50	-184.3	0.0	0.0
1	4	8.5	14.939	34.000	0.50	-248.4	0.0	0.0
1	5	8.9	14.949	34.000	0.50	-288.7	0.0	0.0
1	6	9.2	14.958	34.000	0.50	-302.5	0.0	0.0
1	7	9.5	14.968	34.000	0.50	-288.9	0.0	0.0
1	8	9.8	14.976	34.000	0.50	-248.7	0.0	0.0
1	9	10.1	14.978	34.000	0.50	-184.7	0.0	0.0
1	10	10.4	14.974	34.000	0.50	-101.3	0.0	0.0
1	11	10.7	14.963	34.000	0.50	- 4.1	0.0	0.0
1	12	11.1	14.963	34.000	0.50	100.2	0.0	0.0
1	13	11.4	14.926	34.000	0.50	100.8	0.0	0.0
1	14	11.8	14.909	34.000	0.50	100.8	0.0	0.0
1	15	12.1	14.883	34.000	0.50	100.8	0.0	0.0
1	16	12.4	14.877	34.000	0.50	100.8	0.0	0.0
1	17	12.7	14.862	34.000	0.50	100.8	0.0	0.0
1	18	13.0	14.847	34.000	0.50	100.8	0.0	0.0
1	19	13.3	14.833	34.000	0.50	100.8	0.0	0.0
1	20	13.6	14.819	34.000	0.50	100.8	0.0	0.0
1	21	13.9	14.806	34.000	0.50	100.8	0.0	0.0
1	22	14.1	14.793	34.000	0.50	100.8	0.0	0.0
1	23	14.4	14.781	34.000	0.50	100.8	0.0	0.0
1	24	14.7	14.767	34.000	0.50	100.8	0.0	0.0
2	1	14.9	14.762	34.000	0.50	- 3.5	0.0	0.0
2	2	15.1	14.762	34.000	0.50	-100.8	0.0	0.0
2	3	15.2	14.768	34.000	0.50	-184.1	0.0	0.0
2	4	15.3	14.777	34.000	0.50	-248.4	0.0	0.0
2	5	15.3	14.789	34.000	0.50	-288.7	0.0	0.0
2	6	15.4	14.801	34.000	0.50	-302.5	0.0	0.0
2	7	15.4	14.814	34.000	0.50	-288.9	0.0	0.0
2	8	15.5	14.823	34.000	0.50	-248.7	0.0	0.0
2	9	15.6	14.829	34.000	0.50	-184.7	0.0	0.0
2	10	15.7	14.830	34.000	0.50	-101.3	0.0	0.0
2	11	15.9	14.825	34.000	0.50	- 4.1	0.0	0.0
2	12	16.1	14.814	34.000	0.50	100.2	0.0	0.0
2	13	16.3	14.803	34.000	0.50	100.8	0.0	0.0
2	14	16.5	14.793	34.000	0.50	100.8	0.0	0.0
2	15	16.6	14.783	34.000	0.50	100.8	0.0	0.0
2	16	16.8	14.773	34.000	0.50	100.8	0.0	0.0
2	17	17.0	14.763	34.000	0.50	100.8	0.0	0.0
2	18	17.2	14.753	34.000	0.50	100.8	0.0	0.0
2	19	17.4	14.743	34.000	0.50	100.8	0.0	0.0
2	20	17.5	14.734	34.000	0.50	100.8	0.0	0.0
2	21	17.7	14.725	34.000	0.50	100.8	0.0	0.0
2	22	17.9	14.716	34.000	0.50	100.8	0.0	0.0
2	23	18.1	14.707	34.000	0.50	100.8	0.0	0.0
2	24	18.2	14.697	34.000	0.50	100.8	0.0	0.0

(a)

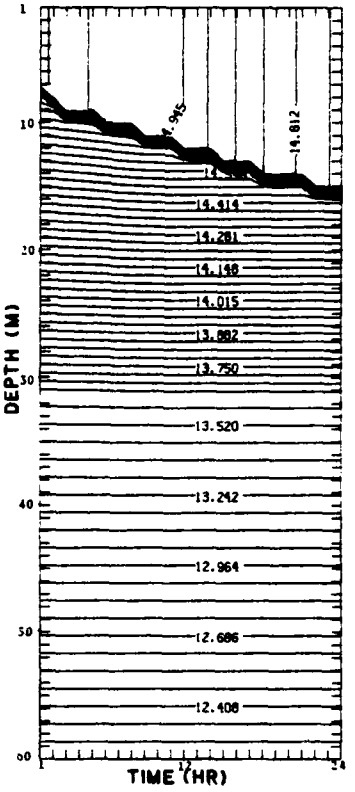

(b)

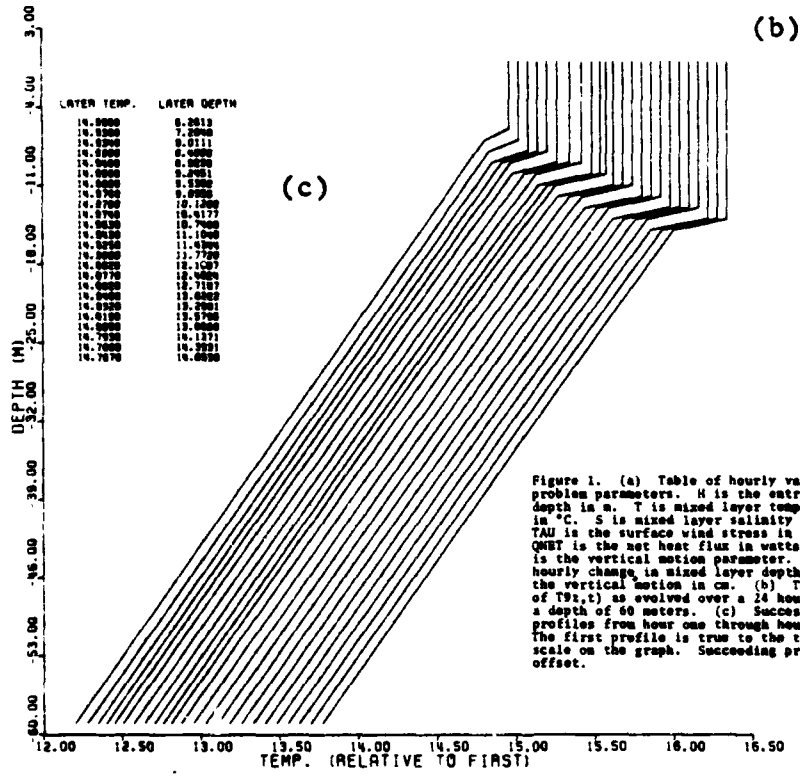

(c)

Figure 1. (a) Table of hourly values of problem parameters. H is the entrainment depth in m. T is mixed layer temperature in °C. S is mixed layer salinity in o/oo. TAU is the surface wind stress in dynes/cm^2. QNET is the net heat flux in watts/m^2. WDD is the vertical motion parameter. DH is the hourly change in mixed layer depth due to the vertical motion in cm. (b) The contours of T(z,t) as evolved over a 24 hour period to a depth of 60 meters. (c) Successive temperature profiles from hour one through hour twenty four. The first profile is true to the temperature scale on the graph. Succeeding profiles are offset.

It is assumed that there is a two-dimensional internal wave in x and z passing through this ocean system. Heat flux and wind stress are taken to be the same at all points, with no interaction between any of the points (advection is limited to the vertical).

4. Progressive temperature profiles, T(z), to a depth of 60 meters (Sample Figure 1c). Only the first profile matches the horizontal temperature scale which is degrees centigrade. The remaining profiles have been consecutively offset. The accompanying table has the mixed layer temperatures in degrees centigrade, and the mixed layer depth in meters.

5. Progressive temperature profiles as in 4, but in the two-dimensional mode of 3. Profiles are offset from the first, again, to provide an insight to the two-dimensional nature to the data.

B. STANDARDS

Prior to the examination of the addition of vertical motion to the mixed layer model (MLM), it is beneficial, here, to examine the results of running the mixed layer model in the two modes which will be used as the standards for comparison with the vertical motion modelling experiments. Both standard cases are runs of the mixed layer model from which the effects of evaporation and precipitation have been removed. This has been done to aid in the interpretation of later results by limiting the number of interaction variables to a manageable quantity. The first standard is a run of the MLM in the primarily wind-driven deepening mode. The second standard is for the MLM in a cyclical shallowing/deepening response to a strong downward heat flux.

1. Standard 1 (S1)

This run was initialized with a temperature profile having a surface and mixed layer temperature of 15.0°C. At 5.0 m the initial temperature decreases linearly with the form

$$T(z) = T_1 - 5.0 \times 10^{-4}(Z - H) \qquad (17)$$

Where Z is the absolute value of z in centimeters, and H is the mixed layer depth in centimeters. This profile extends to 200m. The resulting profile is shown in Figure 2.

The surface wind stress (TAU) is a constant 0.50 dynes per square centimeter for the entire run. Net heating reaches a maximum of 302.5 watts per square meter at hour six (local noon). Net heat loss after sunset is a constant 100.8 watts per square meter.

With no vertical motion the layer deepens continuously over the two-day period of the model run (Figure 1), as expected for primarily wind-driven mixing. In examining the first twenty-four hour period it is seen that the mixed layer deepens from an initial depth of 4.5 m to a depth of 14.7 m. The layer cools from 15°C to 14.767°C over the period, with a short period of mixed layer temperature increase of six hours related to that time when the net heat flux is sufficient to overcome the cooling attributed to the entrainment of cooler water into the layer.

The salinity in the layer remains constant because there is no precipitation or evaporation allowed which could change the surface salinity, and the below layer salinity is assumed to be a constant 34.00 part per thousand. Therefore, there are no sources of water with a salinity other than 34.00 parts per thousand.

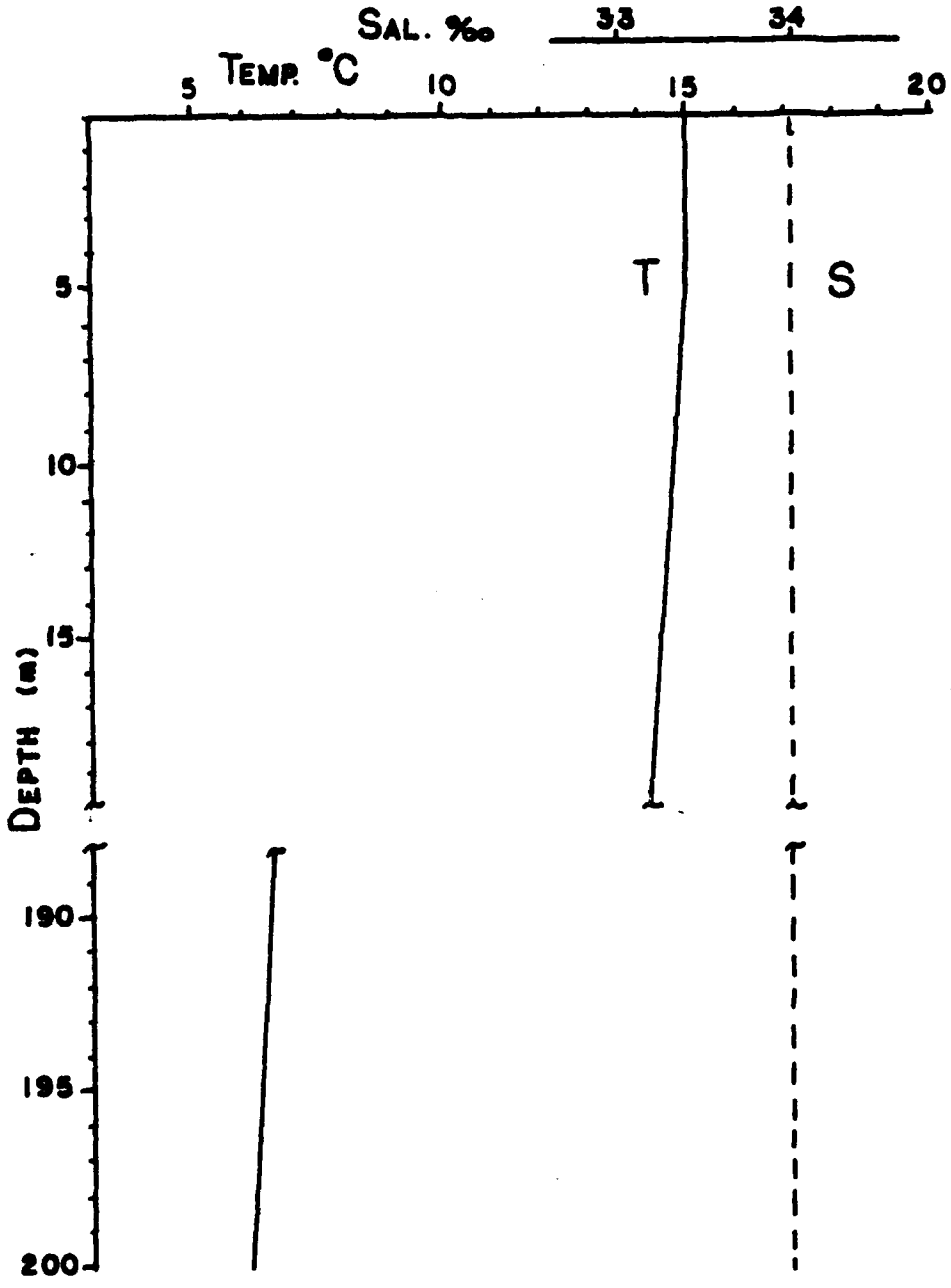

Figure 2. Initial temperature and salinity profiles for Case S1.

The downward solar radiation, Q_s, increases from sunrise (hour 1) to noon (hour 6), and then decreases to zero at sunset (hour 12.) A constant is assumed for the net upward turbulent heat flux to the atmosphere, plus back radiation of 100.8 watts per square meter for the entire day.

The one-day response to this cycle can be seen in the contours (Figure 1b). The mixed layer deepens continuously over the first 24 hours. Below the layer temperature, at any given depth not penetrated as the layer deepens, remains constant over time. In the layer the temperature is seen to cool slightly initially, then warm to a maximum value at about hour nine (1500 local time), and then cool again for the remainder of the period.

In the T(z) graph this sequence is seen again (Figure 1c). Here it is seen that all of the slopes of the profiles below the layer are the same from hour one to twenty-four, indicating that with no vertical motion, the characteristics below the layer will not change with time. The included table shows the relationship of the temperature, in degrees centigrade, and the layer depth, in meters, and indicates the rate and magnitude of the deepening.

The rate of deepening (Table 1) reflects the surface boundary conditions at any given time as well as layer depth and stratification below. As the run begins, the layer deepens quickly in response to the surface wind stress and the short distance over which it must act, as seen in equations (3) and (4). At hour one the layer deepens beginning at a shallow value where the wind flux has a high impact from equation (4), during a period where the heat flux into the layer

is a minimum. As the heat flux increases and the layer deepens the wind stress is relatively less effective in deepening, and the entrainment now effected by equation (5) slows until hour nine when the solar radiation goes to zero, and the deepening rate increases. This increase is relatively small because of the relatively large temperature jump (ΔT) in the entrainment zone by this time. After hour eleven (1800 local time) the minor heat loss, small wind stress and increased depth involved all act to slowly decrease the deepening rate.

Table 1. Deepening Rate in Meters Per Hour for Case S1

Hour	Deepening Rate	Hour	Deepening Rate
1	1.7613	13	0.3296
2	1.0227	14	0.3376
3	0.7271	15	0.3287
4	0.4877	16	0.3017
5	0.4242	17	0.3083
6	0.3221	18	0.3115
7	0.2941	19	0.2759
8	0.2964	20	0.2815
9	0.2904	21	0.2872
10	0.2917	22	0.2703
11	0.3291	23	0.2560
12	0.3580	24	0.2607

2. Standard 2 (S2)

This run is begun with the same initial layer temperature as for standard 1. Here, however, the initial mixed layer depth is taken to be 49.5 meters. At 50.0 meters, the profile again assumes the linear variability of equation (18), extending to 200.0 meters (Figure 3).

All other parameters are the same as those of S1 except for the prescribed surface heat flux. The net heat flux has increased to

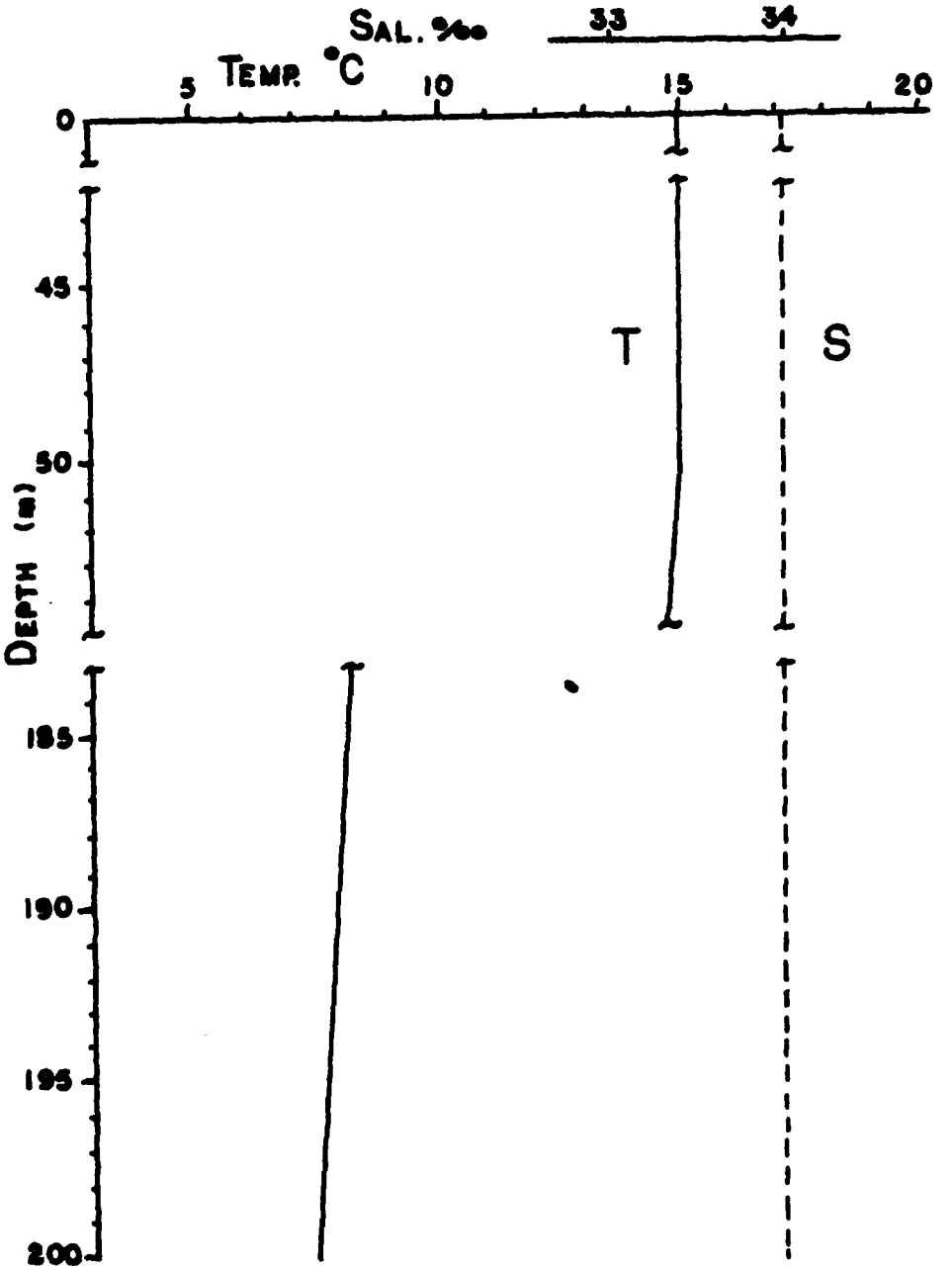

Figure 3. Initial temperature and salinity profiles for Case S2.

a maximum of 504.2 watts per square meter by assuming an extremely strong solar heating maximum (Q_s) of 600 watts per square meter at local noon.

In this case the layer depth remains at 49.5 meters for the first hour (Figure 21a) because the wind stress is not strong enough, coupled with the available heat energy, to cause further entrainment at this depth, and the solar heating is not yet strong enough to cause ($\overline{w'w'}$) to go to zero so that equations (10) and (11) are applied. By the second hour the net downward surface heat flux and the surface wind stress are sufficient to cause ($\overline{w'w'}$) to go to zero, and a new h is formulated through the solution of equations (10) and (11), forming a new surface mixed layer with a depth of about 18 m. The layer then continues to shallow until hour 6 (local noon) in response to the increased downward heat flux. Stirring by the wind stress is relatively small as its effect is overcome by the buoyancy flux associated with net surface heat flux. The layer temperature increases as long as there is heating sufficient to overcome the minor cooling due to the entrainment of cooler below layer water which resumes at local noon, but is not strong until hour 10 (1600 local time). At that time the layer cools due to the combined effects of the surface heat loss, and the entrainment of the cooler below layer waters.

The salinity, again, remains constant because there is no source of water of a salinity other than 34.00 parts per thousand. As shown by the contours (Figure 11b) the original layer of 50 meters shallows to hour 6, not forming a distinct layer, since equations (10) and (11) are applied at each hourly step, until hour 7. The transient thermocline prior to hour 7 is weak. This is seen more

clearly, perhaps, on the T(z) profiles (Figure 11c). The originally sharp interface at 50 meters becomes diffuse with time due to small (K_T = 0.2 cm^2/s) below-layer diffusion. This is clearly seen in the T(z) profiles, and it is the reason for the non-horizontal contours near the 50 m depth. The variability of the temperature structure below the newly formed surface mixed layer is a function of the shallowing adjustment by equations (10) and (11) as applied from hour two through six.

Again it is evident in the T(z) profiles that the profiles keep the same slope below the layer except for the originally sharp interface at 50 meters where diffusion of the layer occurs with time. This diffusion area is also seen to hold at a relatively constant depth with time.

The T(z,t) evolution reflects the turbulent kinetic energy budget for this problem (Table 2). The initial decrease in h from a deep layer to a shallow layer is clearly the result of the surface heating and the surface wind stress acting to form a new, warmer, shallower surface layer. Energy is increased in the surface mixed layer due to excessive solar insolation during the day. The Obukhov length is reduced from hour two through six, and the newly forming mixed layer adjusts accordingly. By hour seven the solar insolation begins to reduce. As this happens, the Obukhov length increases, allowing the newly formed layer to deepen. Deepening does not keep up with the Obukhov length because of the damping due to the energy transport which must take place during the mixing process. By hour 11 the net heat flux is negligible decreasing to a constant surface

loss after sunset. The relative magnitude of the depth increase ($\partial h/\partial t$) with time when compared with that of S1 is due to the strength of the temperature jump (ΔT) at the layer, and the available energy in the layer. In S1 a ΔT of the order of .4°C was encountered, while in S2, due to the slow formation of the new surface layer, a ΔT of the order .08°C is the maximum encountered. This allows for more rapid deepening. The rate of deepening increases after hour 16 (2200 local time) because, as seen in the T(z) profiles (Figure 11c) the ΔT at the entrainment zone is decreasing with time due to the net upward surface heat flux.

Table 2. Deepening Rate in Meters Per Hour for Case S2.

Hour	Deepening Rate	Hour	Deepening Rate
1	0.0152	13	0.8464
2	-31.4079	14	0.8317
3	-1.9247	15	0.8252
4	-3.1646	16	0.8235
5	-0.9575	17	0.8278
6	-0.2935	18	0.8404
7	0.3766	19	0.8596
8	0.3445	20	0.8879
9	0.4944	21	0.9186
10	0.5383	22	0.9516
11	0.6793	23	0.9870
12	0.8371	24	1.0256

C. EXPERIMENTS

The addition here to the existing theory of Garwood (1976-77) is approached in a step-by-step procedure, gradually increasing the complexity of the problem. A quick reference for this progression can be seen in Table 3. A basic assumption that was made in all of the

Table 3. Initial conditions, boundary conditions, and progression of vertical motion inputs for all experiments.

For all Cases:

1. Net surface heat loss is constant at 100.8 watts/m^2.
2. Surface wind stress is constant at 0.5 dynes/cm^2.
3. The initial layer temperature is 15.0°C.
4. The salinity is constant to 200 m at 34.00°/oo.
5. No precipitation or evaporation is allowed during the run.
6. The vertical motion is exponentially decreasing to the surface. Maximum motion is held at 36.0 cm/hr at 10 m, except for Case IVb, where it is 18.0 cm/hr at 10 m.

Case	B. C. Q_B max. (watts/m^2)	I. C. Temp. Profile	I. C. MLD (m)	Vertical Motion
S1	400.00	Fig. 2	4.5	None
S2	600.00	Fig. 3	49.5	None
Ia	S1	S1	S1	Constant downwelling during model run.
Ib	S2	S2	S2	
Ic	S1	S1	S1	Constant upwelling during model run.
Id	S2	S2	S2	
IIa	S1	S1	S1	Pulsed downwelling, 12 hour cycle. Phase shifted to peak at hours 5, 18, and 24.
IIb	S2	S2	S2	
IIc	S1	S1	S1	Pulsed upwelling, 12 hour cycle. Phase shifted to peak at hours 5, 18, and 24.
IId	S2	S2	S2	
IIIa	S1	S1	S1	Single diurnal wave passage. Phase shifted to give maximum downward motion at all hours. Hours 1, 7, 13, and 19 discussed.
IIIb	S2	S2	S2	
IVa	S2	S2	S2	Continuous diurnal wave system passage. Same phase shifts as Case III. Hours 6, 12, 18, and 24 discussed.
IVb	S2	S2	S2	Continuous semi-diurnal wave system passage. Phase shifted as in Case III. Runs with peak motions at hours 6 and 18, and 12 and 24 are discussed.
Va	S2	S2	S2	Superimposed diurnal and semi-diurnal continuous wave system passage. Both waves in phase. Input phase shifted as in Case III.
Vb	S2	S2	S2	As in Case Va, but phases of diurnal and semi-diurnal waves varied relative to one another.

work was that the vertical motion moved the water up and down, but did not directly induce turbulence (i.e., mixing). This is a valid assumption if no shear is associated with this motion.

The cases of progressively complicated vertical motion examined were:

1. Linearly (in z) varying vertical motion, constant over the entire period.
   a. Upwelling
   b. Downwelling
2. Linearly varying vertical motion pulsed in time.
   a. Short daily upwelling/downwelling events.
3. Linear internal wave motion.
   a. Passage of a single wave pulse through the experimental point over the 24 hour daily cycle.
4. Non-linear wave variations coupled with diurnal and semi-diurnal boundary conditions (heating, wind).
5. Non-linear response to superimposed waves of different periods. Diurnal and semi-diurnal tidal waves are combined and phase-shifted to determine non-linear interactions.

1. Case I

Both upwelling and downwelling are realistically induced with the realization that in a mixed homogeneous layer the vertical displacement due to a linear w(z) can be shown to be exponential, going to zero at the surface. Mathematically we know that

$$\frac{dz}{dt} = w(z) \tag{18}$$

if

$$w(z) = \frac{Az}{D}$$

where D is a scaling depth, it follows that

$$\frac{dz}{dt} = \frac{Az}{D}$$

or

$$\frac{dz}{z} = \frac{A\,dt}{D}$$

Integration from t_1 to t_2 yields

$$z_2 = z_1 e^{\frac{A\Delta t}{D}} \tag{19}$$

which is the equation upon which the following work is based, and which agrees with equation (16) derived earlier.

The temperature and salinity profiles must reflect "correct" variation if equations (16) and (19) are correct. Upwelling and/or downwelling will not cause isolines to break the surface or each other. Mixing must be done to induce this. Therefore, above the mixed layer depth T_{new} and S_{new} must equal T_{old} and S_{old} when there is vertical motion without mixing or surface exchange. Below the entrainment depth the profiles must be altered to reflect the type of vertical motion (upward or downward) in accordance with equation (16). Figure 4 shows the expected result from upwelling on a temperature profile. The mixed layer depth has decreased from time one to time two (after upwelling), and the slope of the profile below the mixed layer has been decreased. In all the cases the ΔT at the entrainment zone has been preserved.

a. Constant Downwelling (Case Ia) (Figure 12)

The initial conditions used are the same as those for S1 (See Table 3). A constant downward vertical motion is introduced giving the vertical motion parameter, WDD, (WDD = A t/D) a value of .03600, which equates to a value of vertical motion of .01 cm/s or 36 cm/hr at

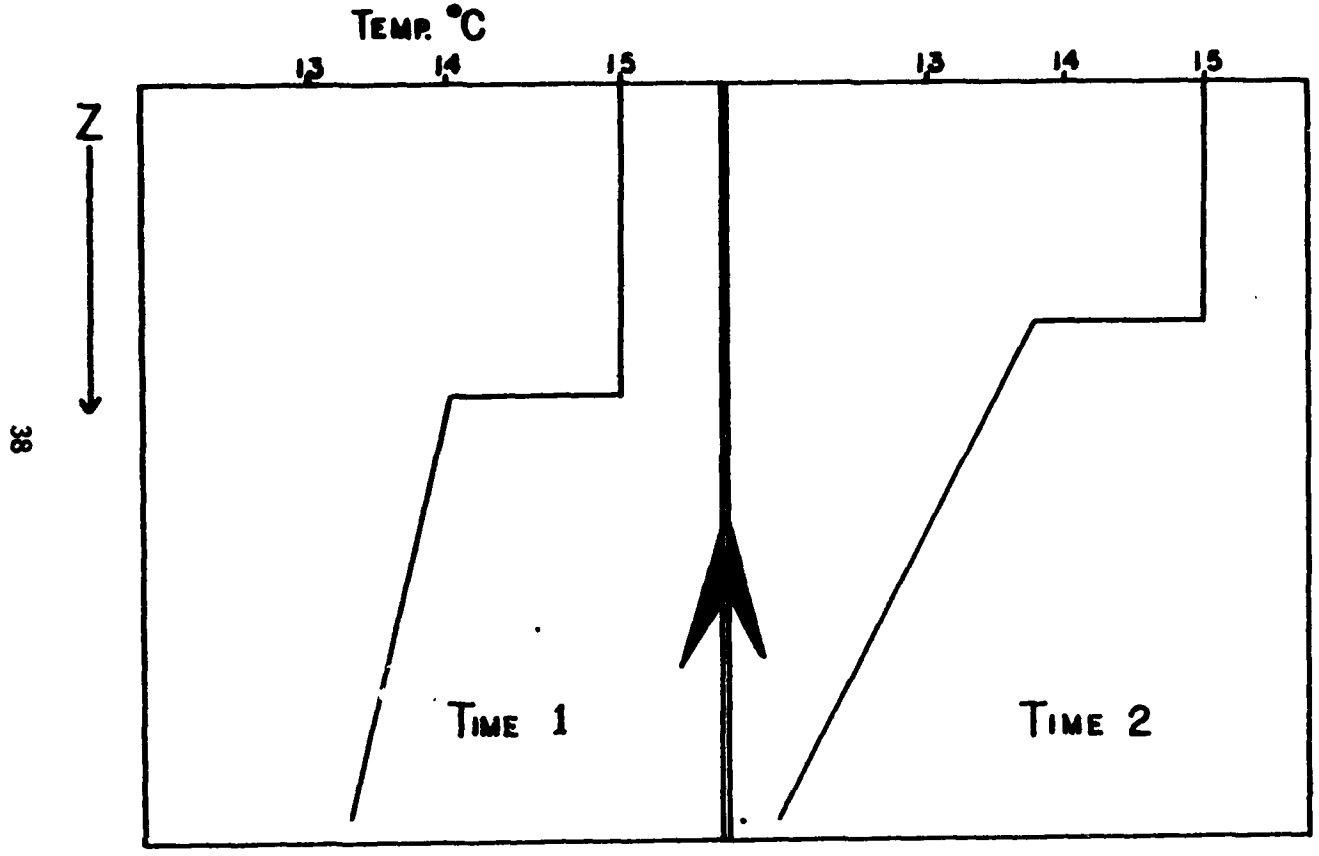

Figure 4. Temperature profile variation from t_1 to t_2 under upwelling conditions.

ten meters. This is a rather large value, but it demonstrates the interactions well. The vertical motion is applied beginning the first hour, and is not applied as the initial condition on the temperature and salinity profiles.

The result of this downward motion is, as expected, a more rapid deepening of the surface mixed layer (Figure 12a) when compared to S1. Comparing the depth change due to the mixing in this case (Table 4) to the S1 mixing, the same sequence of events as described for S1 is seen, and the values are comparable, indicating that the physics of the model has not been altered by the addition of the vertical motion parameter in the downwelling mode. It is noted that the effect of the vertical motion quickly becomes greater than the effect of mixing due to the large value of vertical mixing assigned in this run of the model.

Table 4. Deepening Rate in Meters Per Hour for the Mixing and Vertical Motion of Case Ia.

Hour	Mixing Deepening Rate	Vertical Motion Deepening Rate	Hour	Mixing Deepening Rate	Verticle Motion Deepening Rate
1	1.7613	0.2295	13	0.3201	0.5729
2	0.9705	0.2735	14	0.3169	0.6055
3	0.6606	0.3077	15	0.3134	0.6392
4	0.4759	0.3365	16	0.3102	0.6740
5	0.3535	0.3618	17	0.3068	0.7099
6	0.2945	0.3858	18	0.3034	0.7471
7	0.2444	0.4089	19	0.3017	0.7855
8	0.2282	0.4323	20	0.2983	0.8252
9	0.2394	0.4569	21	0.2949	0.8663
10	0.2513	0.4828	22	0.2914	0.9087
11	0.2793	0.5108	23	0.2881	0.9526
12	0.3219	0.5413	24	0.2094	0.9952

The sequence is vividly displayed in the contours (Figure 12b) where it is seen that the temperature contours deepen as time progresses

as one would expect in a downwelling case. The surface heating due to the incoming solar radiation is noted again, followed by cooling as the sun sets and heat is then lost at the surface and colder water is entrained at the bottom of the mixed layer. It is also noted that in only twenty-four hours, the vertical motion added here has deepened the layer to almost twice the value of S1.

The T(z) plot (Figure 12c) demonstrates the deepening involved and the effects on the temperature profile below the mixed layer. Note the increased slope (dT/dz) with time, as warmer near-surface temperatures (water) are carried downward by the downwelling. Also, one can see the effect of the preservation of the ΔT profile at the entrainment zone from the mixing step through the vertical motion progression in the model where at times there is an apparent discontinuity in the profile. This does not appear to cause a problem in the execution of the model, and will be seen in many of the following T(z) plots. One can further see that the vertical motion addition has caused a slight decrease in the jump strength of ΔT at the layer over that in S1. This can be attributed to the reduced mixing for the larger mixed layer depths. Where, with no downwelling a ΔT of 1.0°C may have occurred in 18 meters, it now occurs at a greater depth. This effect is transmitted into the entrainment zone as this below layer water is mixed in, causing the ΔT to be reduced.

b. Constant Downwelling (Case Ib) (Figure 13)

The initial conditions are those of S2 (See Table 3). A constant downward motion is introduced equal to that used in the previous case.

The result of the downward motion is again, as expected, a more rapid deepening of the layer after the new surface mixed layer is formed through the surface wind stress and heat flux as applied by equations (10) and (11) (Figure 13a). Comparing the depth change due to the mixing here (Table 5) to the S2 mixing shows that the values are of the same order, which shows that the energy relations of the original model are not impaired by the addition of vertical motion in this mode of the model either. Here it is noted that mixing drives the production of a new surface mixed layer beginning at hour 2 (0800 local) (Figure 13b). The shallowing due to the surface heating is dominant until hour seven (1300 local) when the downwelling becomes the dominant factor until hour nine. From hour nine to hour fifteen the effects of mixing and downwelling are of the same order. After hour fifteen the downwelling again, slowly, becomes the dominant factor for layer deepening.

Table 5. Deepening rate in meters per hour for the Mixing and Vertical Motion in Case Ib.

Hour	Mixing Deepening Rate	Vertical Motion Deepening Rate	Hour	Mixing Deepening Rate	Vertical Motion Deepening Rate
1	0.0152	1.8150	13	0.8093	0.6986
2	-33.4052	0.6571	14	0.7343	0.7511
3	-2.5282	0.5885	15	0.7445	0.8059
4	-3.7245	0.4735	16	0.7131	0.8616
5	-1.4432	0.4392	17	0.7029	0.9190
6	- .7286	0.4286	18	0.6768	0.9775
7	0.1233	0.4489	19	0.6716	1.0379
8	0.3275	0.4773	20	0.6628	1.1002
9	0.4266	0.5104	21	0.6420	1.1641
10	0.5787	0.5504	22	0.6316	1.2299
11	0.6446	0.5942	23	0.6224	1.2978
12	0.8003	0.6986	24	0.6120	1.3678

It is seen that the layer temperature, again, immediately begins to warm (Figure 13c), and in fact, while the dominant factor is the large amount of surface heating, the layer warms at exactly the same rate as in S2. After hour ten the layer again begins to cool, but because of the deepening of the mixed layer due to downwelling, the mixing of the surface wind stress is reduced. This, along with the fact that a deeper layer has available more mass of water to dilute the effect of the entrained water, results in less cooling over the remaining twelve hours.

Because of the downwelling effect on diffusing the temperature gradient it is also seen (Figure 13b) that the entrainment zone (layer boundary) remains rather diffuse until hour eight, while in S2 it was sharpened by hour six. This helps explain the magnitude of the deepening effect in the period from hour nine to fifteen, though the depth of the entrainment zone is increasing faster than that in S2 and reaches a difference of five meters from that in S2 by hour fifteen. The ΔT across the bottom of the layer for the downwelling case is slightly less than that in S2, allowing the mixing to be a more important factor for deepening in this case. The following decrease in the mixing is then due to the ever increasing depth through which the mixing must take place. The wind stress must act over distances that are twice as large as those in S2, and although the ΔT at the layer depth is not as great, the effect of the depth is quite noticeable.

The original deep layer is seen to begin to diffuse, but is quickly carried below the 60 meter level of the graphs. As stated above, the new surface mixed layer begins to show a significant ΔT

at hour eight. Extremely close examination of the T(z) profiles for S2 and the profiles for this run does show a smaller ΔT at the entrainment zone for this case during the period from hour seven to hour sixteen. After hour 16 there is no discernable difference in the ΔT in the profiles.

c. Constant Upwelling (Case Ic) (Figure 14)

The initial conditions are those of S1. A constant upward vertical motion is introduced beginning at hour one giving the vertical motion parameter, WDD, a value of .03600, or about 36 cm/hr at ten meters. Again, this is high, but it is done with the realization that later work will be with wave motion where this will not be an unrealistic value, and using it here provides a good benchmark for the effects produced by this motion.

Table 5. Deepening Rate in Meters Per Hour for the Mixing and Vertical motion of Case Ic.

Hour	Mixing Deepening Rate	Vertical Motion Deepening Rate	Hour	Mixing Deepening Rate	Vertical Motion Deepening Rate
1	1.7613	-.2214	13	0.4239	-.3026
2	1.1031	-.2526	14	0.4528	-.3079
3	0.6746	-.2675	15	0.4845	-.3142
4	0.6103	-.2796	16	0.4774	-.3199
5	0.4954	-.2873	17	0.2909	-.3189
6	0.3417	-.2892	18	0.2871	-.3178
7	0.3184	-.2902	19	0.3046	-.3173
8	0.3097	-.2909	20	0.3223	-.3175
9	0.3133	-.2917	21	0.3407	-.3183
10	0.3254	-.2929	22	0.2596	-.3163
11	0.3435	-.2947	23	0.2739	-.3148
12	0.3938	-.2982	24	0.2891	-.3138

The result of the addition of this upward motion is, as anticipated, a slowing of the deepening rate of the mixed layer (Figure 14a) when compared to S1. In fact, due to the size of the vertical

motion parameter, an effect is produced which almost holds the mixed layer at a constant depth. This is displayed more dramatically after two model days have been executed, and can be seen to reach a near equilibrium condition after four to five days. Comparing the deepening rates due to the effect of the mixing in the model and the vertical motion in this case (Table 5) to the S1 mixing it can be seen quite clearly that the effects described for the mixed layer model standard, S1, are still present. From equations (1) and (3) the slightly increased magnitude of the cooling of the mixed layer by entrainment and the subsequent heating are attributed to the reduced depth over which the wind stress and heat flux must be distributed. Again, it can be seen, that the model TKE balance, equations (3-5), is not violated by the addition of this upwelling motion.

The layer temperature initially falls (Figure 14a), then rises until 1400 local time. It then falls again in response to the mixing and the surface heating cycle, as in S1. The heating of the layer is not as great here as in the downwelling case (Figure 13), because the entrainment is sufficiently enlarged due to the smaller h, and because cooler water becomes available for entrainment more quickly due to the upwelling. This is more clearly seen in comparing the contoured fields, T(z,t), (Figure 14b) of this case with those of the downwelling case (Figure 13b). By the end of the twenty-four hour period this has resulted in a very strong temperature jump, ΔT, at the entrainment zone, as is seen best in the T(z) profiles (Figure 14c). It is seen that ΔT grows with time.

The strengthening of the jump, and the lifting of the cooler water is demonstrated clearly by the contours, and it is

clearly evident the contours not only lift, but also merge in time, indicating the ΔT grows with time. This effect is seen in the T(z) profiles by the increased gradient of the profiles with time.

Equilibrium is reached in this case as the jump gets too large for the mixing to have an effect greater than the effect of the vertical motion. Equation (8) shows that dh/dt vanishes as w_e approaches w_{-h}.

d. Constant Upwelling (Case Id) (Figure 15)

The initial conditions applied are identical to those of S2. A constant upward vertical motion is introduced at hour one of about 36 cm/hr at ten meters, as before.

The net result of the vertical motion after 24 hours is a reduced layer depth in comparison to the case having no vertical motion (S2). The total reduction in depth of six meters, however, is not as great as the previous case (Ic). After two days it is seen that the mixed layer is approaching an equilibrium depth of near eleven meters (Figure 15a).

The deepening rates (Table 6), when compared to those of S2, demonstrate that the basic model is still preserved in this run. From hours two through five the model is in the shallowing mode, and the new layer depth is established by equations (10) and (11), while there is a massive influx of solar radiation to the sea surface. The increased deepening rate due to the mixing seen from hour twelve through twenty-three is attributed to the effect of equations (1), (4) and (5). The mixed layer is maintained at a shallow level by the upward vertical motion, therefore, the mixing takes place over a much smaller distance than in S2.

Table 6. Deepening Rate in Meters Per Hour for the Mixing and Vertical Motion of Case Id.

Hour	Mixing Deepening Rate	Vertical Motion Deepening Rate	Hour	Mixing Deepening Rate	Vertical Motion Deepening Rate
1	0.0152	-1.7509	13	0.9465	-.4751
2	-29.4675	-0.6470	14	0.9470	-.4917
3	-1.3404	-0.5767	15	1.0159	-.5103
4	-2.6147	-0.4639	16	1.0611	-.5298
5	-0.5166	-0.4292	17	1.1449	-.5515
6	0.1312	-0.4186	18	1.2301	-.5755
7	0.3085	-0.4148	19	1.3043	-.6013
8	0.4578	-0.4163	20	1.4087	-.6298
9	0.5885	-0.4224	21	1.5577	-.6626
10	0.6775	-0.4314	22	1.6638	-.6980
11	0.7113	-0.4413	23	1.3743	-.7219
12	0.9078	-0.4578	24	0.6909	-.7208

Further, there is a concentration of energy in this shallower layer. The great variance in the last hour is a direct result of the magnitude of the upwelling, which, by hour four, has set up a large gradient in the temperature (Figure 15b). By hour twenty-four a gradient has been set up with such a large slope that mixing is becoming very difficult. Continued upward motion of this magnitude, without shallowing as is seen on the second day, would quickly make it extremely difficult to entrain much water into the mixed layer.

The progression in the change of the mixed layer temperature (Figure 15a) shows that as the model is shallowing, governed by equation (10) and (11), the same adjustment takes place as is seen in S2. The temperatures produced are exactly those seen in S2. This is another indication that the model is performing as before. Since w_e is zero, the upwelling has no effect on the setup of the new layer. If the H values had been listed immediately after the mixing phase of the computation, this could be seen more clearly. After the layer again begins

to mix downward, however, the upwelling begins to have some effect on T and h due to the upward transport of the entrainment zone. Though the layer is one to two meters shallower than in S2, the temperature of the layer is the same as that in the deeper standard to hour ten. At hour ten the heat flux of equation (1) has been reduced sufficiently so that wind mixing again becomes the dominant deepening force. At this point the upwelling has moved water cooler than that in S2 at the same time to the entrainment zone. The change in entrainment rate due to the upwelling, the entrainment of cooler waters, and the net surface heat loss after hour eleven combine to produce a cooling of .147°C from the maximum warm temperature, as compared to .109°C for S2. For the mass of water involved, and the relatively short time involved, this is a significant difference.

The effect of the upward vertical motion is perhaps best shown in the T(z) diagram (Figure 15c), where it is seen that the model initially adjusts, through equations (10) and (11), to a new surface layer which slowly strengthens, in terms of the jump, ΔT, as it entrains. As the process continues the profiles below the layer rise by upwelling and the initial deep interface is smoothed by diffusion until it disappears. By hour twenty-four a sufficiently stable profile has been set up to make deepening of the layer more difficult. This indeed is the case in the second day of the run (Figure 15a) as the layer reaches a temporary equilibrium. It is temporary, in that once the profile has been reached which makes deepening sufficiently difficult through equations (4) and (5), the dominant force becomes the upwelling, w_{-h} of equation (9).

The contours (Figure 15b) further demonstrate the effect of the upward lifting of the cooler water, as the contours tend to converge with time. The initial interface is quickly lost, as the model smooths this into its uplifted profile.

2. Case II

The next step of this progressive series of tests is to explore the effects of a simple pulsed motion varying in time. This is accomplished by varying the input motion in a sinusoidal pattern. By using the equation

$$w_o(t) = AA \sin\left(\frac{2\pi t}{24} + kx\right) \tag{20}$$

as the particular form of equation (12) applied for this case, where AA is the velocity scale factor such that AA = Az/D is scaled for an appropriate motion at 100 meters, and limiting the value of $w_o(t)$ to only values in one direction (+ or -), and zero, a pattern of motion can be produced such as that seen in Figure 5. A pulse of vertical motion of twelve hour duration is produced, followed by a twelve hour period of no motion. To determine the relationship of this motion with the cyclical boundary conditions one need only shift the phase of the pulse relation. This will cause the motion to peak at varying selected times during any twenty-four hour period run.

a. Pulsed Downwelling (Case IIa) (Figure 16, 17 and 18)

The initial conditions are the same as those of SI. Three different phase relationships of the downwelling to the cyclical boundary conditions are presented. In the first (Figure 16) the maximum of the downwelling occurs 180° out of phase with the heating

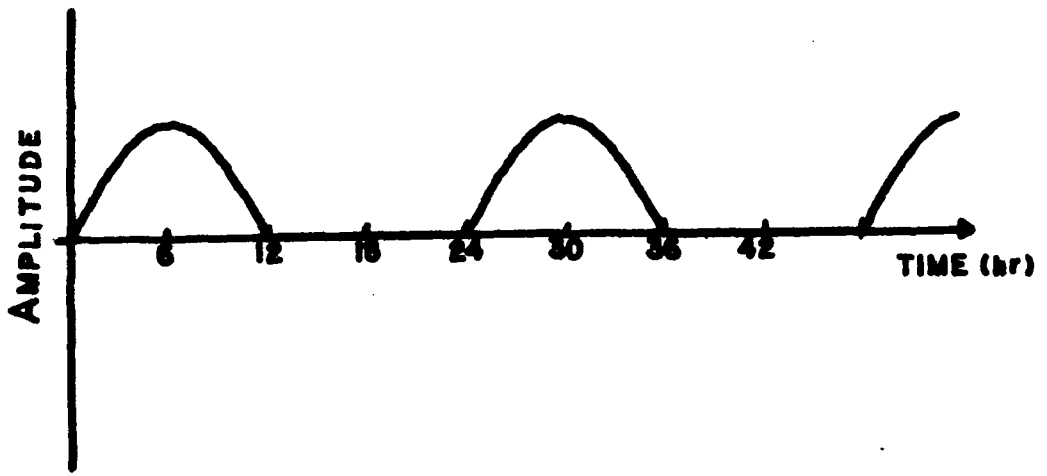

Figure 5. Pulsed upwelling form (in relation to model time/hrs at point x. Amplitude is variable).

cycle (that period of the model defined as night, or the cooling cycle). In the second (Figure 17), the downwelling occurs during the last seven hours of night, and during the first five hours of daylight. The maximum downwelling occurs six hours before the heating maximum. Finally, in the third case (Figure 18), the downwelling occurs in phase with the maximum heating cycle. In all three cases, the downwelling event is a twelve hour pulse with a maximum value of 36 cm/hr at ten meters.

(1) 180° Out of Phase (Figure 16). For this case it is seen that the model evolves exactly as does S1 until hour thirteen when downwelling begins (Figure 16a). All the fields produced are exactly the same as in S1 until hour thirteen for which the evolution has been discussed.

After hour thirteen the downwelling begins to transport the surface water downward, and causes a decrease in the jump, ΔT, strength of a few hundredths of a degree. This combined effect causes the deepening of the mixed layer to increase here over that of S1 by about four meters over the twenty-four hour period. Additionally, it decreases the change of temperature of the mixed layer because the layer is initially deeper, thereby, reducing mixing, and increasing the dilution of the entrained waters, and by causing entrainment of water which is not as cool as that of S1, over the same period. These effects are apparent in the contours (Figure 16b), and in the T(z) profile (Figure 16c). The downwelling effect is seen most dramatically in the contours, where the downward pulse is evident, along with the described temperature variations.

(2) Maximum Downwelling Before Heating (Figure 17). Here, the downwelling is applied during the last six hours of the mixing,

and during the first five hours of the heating cycle. The six hours of downwelling during the last six hours of night serve only to deepen the layer in the manner previously described. The first five hours of downwelling coupled with the heating and wind stress through equation (9), produces a noted change in the temperature fields (Figure 17c) from that of S1. This coupling leads to an increase of the layer temperature at the peak heating period of .008°C for this run over that of the previous (δT increase), and over that of the standard, S1. After twenty-four hours this difference has decreased to .005°C as compared to the previous run, and by two days the difference in temperatures is negligible, though the layer depth is slightly shallower after two days for this run. By only partially coupling the effects of downwelling and heating, a shallower mixed layer has been produced with somewhat warmer temperatures.

The surface temperature evolution and the below layer evolution are best revealed by the contoured fields (Figure 17b). It is apparent here that another phenomenon is present. As the downwelling commences the near layer contours do in fact diverge as expected. The deeper contours, however, initially narrow as the pulse forms, then widen to the below layer temperature spreading effect described previously. This convergence during the peak motion period is a direct result of the mathematical treatment of the below layer temperature profiles through equation (16).

(3) Coupled Heating and Downwelling (Figure 18). Here the downwelling peaks one hour before the maximum surface heat flux. The combination of downwelling and wind stress, equation (9) through equations (16) and (8), are sufficiently strong to cause the effect of

the heat flux, equation (1), to be negligible, and the layer deepens to almost three meters more than that of S1 by hour eleven. Also, the layer temperature has been increased significantly over S1 due to the downwelling effect on the layer which causes the entrainment of less water than previously during the period of maximum surface heating. By combining the downwelling with the heating, a maximum temperature change of .211°C for S1 has been reduced to .162°C for this run over the first twenty-four hours. This has also produced a mixed layer which is .06°C warmer and three meters deeper than S1 after only twenty-four hours. This reflects a substantial change in the energetics of the system, and may be a significant mechanism for the generation of horizontal temperature structure. After the pulse, the layer is mixed by the action of the wind stress in the presence of a smaller ΔT--reduced by the downwelling accompanied by a small downward surface heat flux. This explains why the deepening is not as great after the downwelling pulse as would be expected if one considered only the reduced jump strength.

In combination these three phased runs demonstrate the effect of the interaction of the downwelling and the diurnal heating cycle. In all cases a relative heating of the mixed layer is seen because of the depth increase. The deeper layer reduces the effect of the mixing, and reduces the entrainment. As the downwelling event couples with the heating, the final mixed layer depth is reduced, over that of the uncoupled cases, and greater surface temperatures (layer temperatures) are achieved. The rudiments of a pattern in surface features which could be induced over a large ocean by simply varying the coupling of these two basic effects is now seen.

b. Pulsed Downwelling (Case IIb) (Figures 19, 20 and 21)

The initial conditions are those of S2. The magnitudes of the downwelling, and the phase relations are the same as the previous case.

(1) 180° Out of Phase with Heating (Figure 19). Because the downwelling event occurs after the surface heating has stopped (at night), the model has gone through the shallowing mode, equations (10) and (11), and produced a new surface mixed layer exactly as in S2 during the daylight period. The effect of the downwelling is seen at hour fourteen when mixed layer deepening is first observed. The cumulative effect of the downwelling is to deepen the layer by about five meters more than in S2 in the twenty-four hour period (Figure 19a). The layer temperature, due to the downwelling effect, remains .011°C warmer after the period. Destruction of the original layer at 50 m is caused by diffusion, and the model's mathematical smoothing in the production of new temperature contours due to the downwelling in accordance with equation (16).

(2) Maximum Downwelling Before Heating (Figure 20). The shallowing of the model through equations (10) and (11) during the surface heating period overrides the downwelling, so that by hour five this run is essentially the same as S2, with only a slight temperature difference. Comparing the contours (Figure 11b and Figure 20b) shows that this run is the same as S2 until the downwelling pulse begins at hour nineteen, except the early downwelling has deepened the layer and moved the cooler water away from the entrainment zone, relative to the temperatures in S2. The layer then deepens due to wind stress mixing, and downwelling. The net result of this coupled action is a

layer about four meters deeper than S2 after twenty-four hours, but with a temperature essentially equal to that of S2.

(3) Coupled Heating and Downwelling (Figure 21). Here the shallowing mode is still the dominant factor, with the downwelling playing only a minor role in that it deepens the newly forming layer, and moves the relatively cooler water away from the entrainment zone. Because the model is in the shallowing mode, as w_e approaches zero, the new value of h is dependent on equations (10) and (11), as is the temperature of the new mixed layer through equation (1). Since the downwelling adjustment is done after the evaluation of the shallowing h, the downwelling does deepen the newly formed layer, but no temperature adjustment is made. This results in a layer that appears to be deeper than in S2, and yet maintains the same temperature. The net result of these interactions after twenty-four hours is a layer that is one meter deeper than in S2, and .012°C warmer. Here the coupling effect was negligible.

In combination these three runs of the model in the downwelling mode with S2 initial conditions showed the opposite progression of those runs using the S1 initial conditions. The maximum variations of temperature and mixed layer depth occurs in the case of 180° out of phase downwelling with the heating cycle, where a deeper, warmer mixed layer is formed during the twenty-four hour period. In the case of the S1 initial conditions the maximum deviations occurred during the coupled run.

C. Pulsed Upwelling (Case IIIc) (Figure 22, 23 and 24)

The initial conditions are those of S1. The phase

relationships used are the same as in the pulsed downwelling case, as are the magnitudes of the effects.

(1) 180° Out of Phase with Heating (Figure 22). The effect here is negligible until hour thirteen, and this run is exactly the same as S1 until then. At hour thirteen the upwelling begins to increase the magnitude of ΔT. Colder water is moved up toward the entrainment zone below the layer, and the layer itself is moved upward, as the wind stress acts to deepen the layer by mixing. At hour twenty-one it is seen that the combination of the upwelling and the magnitude of ΔT are great enough to actually shallow the layer for that hour.

The net effect of the upwelling in this case is to create a mixed layer that is about 2.6 meters shallower than in S1 over the twenty-four hour period, and .03°C cooler (Figure 22a). Also, there is a maximum δT in the mixed layer of .241°C, where mixing only produced a δT of .211°C in S1. This has the potential of producing an observable surface temperature effect.

The effect of contour convergence during the pulse mentioned in the downwelling case is seen here again (Figure 22b). The overall effect of the upwelling, to converge the contours from before to after upwelling, is seen as expected.

(2) Maximum Upwelling Before Heating (Figure 23). In this case the upwelling immediately begins to lift the entrainment zone against the effect of the wind stress, causing an increase in the effect of the mixing, and reducing the water available for dilution of the entrained, cold water. In equation (9), w_{-h} is of opposite sign to that of w_e, reducing, or changing the sign of dh/dt.

This results in cooler layer temperatures over the same period as described for S1, and shallower mixed layer depths. Numerically, the net result of this effect over the twenty-four hour period is to produce a layer that is 2.5 m shallower than that of S1, and .04°C cooler (Figure 23c). The maximum δT of the layer over the period is .240°C, or about the same as in the previous upwelling case.

(3) Coupled Heating and Upwelling (Figure 24). The coupling of the upwelling and the heating cycle produce a mixed layer that is only 1.9 meters shallower than that of S1 in the twenty-four hour period, but a layer that is much cooler. The reduction of the layer depth during the heating period causes the maximum temperature to be .013°C colder, and causes the layer temperature at the end of the twenty-four hour period to be .071°C colder than S1, a significant change. The maximum δT of the layer for this period is .269°C.

As in the downwelling case with the shallow initial layer conditions, the maximum surface variations in temperature is in the coupled upwelling case.

d. Pulsed Upwelling (Case IId) (Figure 25 and 26)

The initial conditions are those of S2. The phase relationships used are the same as those in the previous three model runs. Magnitudes of the upwelling are the same as in the previous run.

(1) 180° Out of Phase with Heating (Figure 25). The shallowing proceeds as in S2 for the first six hours, and a new layer is formed (Figure 25b). At hour thirteen the upwelling begins and several effects are noted. First, the deepening immediately slows, relative to that in S2, as the upwelling lifts the layer, and

increases the ΔT at the entrainment zone. Second, the layer temperature decreases faster relative to that in S2, due to the shallowing of the layer, and entrainment of relatively cooler water into the layer. Finally, there is an effect not previously observed. The initial layer, which is being diffused in the previous runs is now reinforced during the upwelling (Figure 25c), and a two-layer system is formed over the first twenty-four hours.

The net result of this case is a surface layer that is 2.4 meters shallower and .022°C cooler than S2 over the period. This leads to a slightly increased surface signature over the non-upwelling case. Because of the reinforcement of the initial layer there is also a potential for a substantially recognizable T(z) signature for this case.

(2) Maximum Upwelling Before Heating (Figure 26). The shallowing and upwelling combine to make this a relatively uninteresting case. Though the large upwelling has some initial effect, the fact that w_e goes to zero forcing the model to be driven by equations (10) and (11) soon overcomes the upwelling, and by hour four this case is identical to S2 and the previous run with the exception that the upwelling has advected cooler water closer to the entrainment zone. The difference in water temperature and mixed layer depth between this case and S2 are negligible by hour eighteen. At hour nineteen upwelling begins again, increasing the relative effect of the wind stress mixing, causing increased entrainment of cool water. The net effect of the upwelling and the wind stress mixing over the depth involved is to produce a layer that is 2.2 meters shallower than in S2, but at only .004°C cooler after twenty-four hours. This would

not produce a noticeable effect at the surface. The two-layer type system seen in the previous case could, again, provide a signature to this sort of upwelling event.

(3) Coupled Heating and Upwelling (Figure 26). The shallowing prescribed by equations (10) and (11) due to the excessive heating tends, initially, to override any effect of the upwelling. By hour six there is only a .4 meter depth difference over that of S2, and essentially no temperature difference in the mixed layer. After that point, the upwelling begins to combine with the mixing to augment the cooling of the layer, and slowing its deepening.

The net result after twenty-four hours is to produce a layer that is about as deep as that of S2, but that is as cool as the case of the evening upwelling. This represents a substantial energy difference in the runs. Again, a slight surface temperature signature could be seen with this run in comparison with the standard.

3. Case III

The next test is that of the interaction of mixing with a single cycle internal wave. By stepping the phase of an input sinusoid through the twenty-four hour progression of the model, a quasi two-dimensional motion can be prescribed.

For a wave of the form

$$\text{wave amplitude} \propto A \sin(\omega t + kx)$$

the vertical motion would be of the form

$$w(x,z,t) \propto A_w \cos(\omega t + kx) \qquad (21)$$

as seen in Figure 6. By increasing the value of kx, the wave is made to travel in the -x direction.

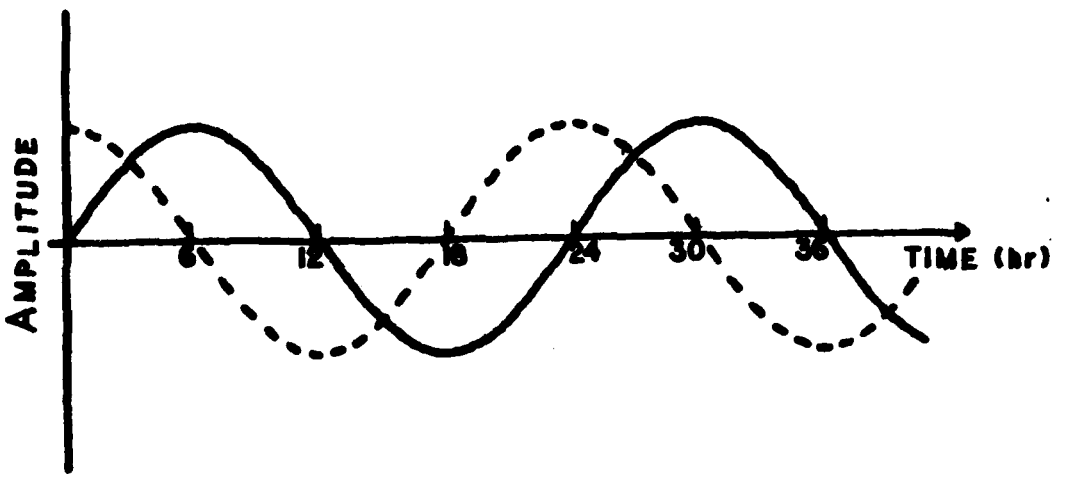

Figure 6. Vertical motion-wave form relationship: Vertical motion (dashed line) relative to wave (solid line) passing through a given point (x) at time t (hr). Amplitudes are not absolute (See equation 21).

The initial conditions used were those of cases S1 and S2. The vertical motion was introduced at hour one, and the amplitude was varied as t varied in equation (21), to give a wave induced vertical motion. This was then run twenty-four times, each time starting at a different phase of the wave, to test the interrelation of the wave input with the cyclical heat flux. For simplicity, only four major phase relationships are discussed here, as they will demonstrate the primary effects. Also, here, the two-dimensional field will be discussed for the first time.

The wave form of the desired vertical motion does appear in all four of the displayed runs. The difference in each run is the phase of the vertical motion in relation to the heat flux (daily solar heating cycle).

a. Shallow Initial Layer (Case IIIa) (Figures 27-33)

In all four phase relationships presented, maximum downward motion at hours 1, 7, 13, and 19, the initial conditions are those of S1. The magnitude of the peak upward and downward motions is 36 cm/hr at ten feet, as before. The wave is introduced at hour one, and progresses through the system through hour twenty-four.

(1) Peak Upward at Hour 7 (Figure 27). In this case the initial upward motion, hours one through twelve, the heating and the surface wind stress combine to give a slowly deepening layer, which, due to the upward advection of the layer and of cooler, below layer water, is almost .1°C cooler at its maximum temperature than S1. At the end of the upward cycle the layer has deepened about two meters less than S1 at the same time, and has set up a slightly larger ΔT at

the entrainment zone. As a result, the following downward cycle produces a smaller effect in combination with the wind stress in deepening than that seen previously. Because of the initial upward motion effects on the temperature profile, the combined effect of wind stress mixing, surface cooling, and the downward motion produce a layer that, after twenty-four hours, is only two meters deeper than S1. Additionally, the downward effect of the motion on the temperature gradient is sufficient only to make up about 60 percent of the deviation in temperatures caused by the upwelling motion, as to that of S1.

The maximum δT for this case is .245°C. It, also, produced the deepest layer of the four runs discussed here, over the twenty-four hour period.

(2) Peak Upward at Hour 1 (Figure 28). In this case the upward motion was present during the first six hours of the heating cycle only. The downward motion cycle then progressed for twelve hours, followed by six hours of upward motion to complete the twenty-four hour sequence.

During the first six hours the layer deepened to within less than one meter of the depth reached by hour six in S1, but the layer temperature is seen to be about .01°C cooler. The reversal of the motion was too late in the heating cycle to overcome that trend, and by hour nine, the time of the maximum surface temperature for S1, this experiment produced a surface temperature that is .013°C cooler. The layer depth reached here is within half a meter of the S1 depth for the same time. The difference is attributed to the initial lifting of the entrainment zone.

As the downward motion continues, along with the surface cooling, the layer deepens more quickly while the cooling of the layer slows as the effect of mixing is reduced. A maximum depth is reached two hours after the downward motion has stopped, when the upward motion is of sufficient magnitude to overcome the wind stress mixing. The layer becomes shallower from its extreme depth of 15.56 meters to 14.94 meters by hour twenty-four, with associated layer cooling due to surface heat loss, and increased entrainment due to the increased effect of the wind stress mixing.

The maximum δT for this run is .189°C. The final layer depth is within .3 meters of S1 for hour twenty-four. The variations of depth and temperature during the run are obviously much greater than for S1.

(3) Peak Upward Motion at Hour 19 (Figure 29). The fact that the downwelling and the heating cycle are in phase, as in Case IIa, produces, by hour nine, a layer that is two meters deeper and .006°C warmer than S1 for this same time. The following upward motion is sufficient to halt layer deepening at hour sixteen in opposition to the mixing, but is not sufficient to cool the layer as much as for S1. The final layer temperature is .035°C warmer than that in S1, while the final layer depth is about one meter less, though at hour sixteen a depth of 14.2 meters was reached. The maximum δT for the mixed layer in this case was .181°C.

(4) Peak Upward Motion at Hour 13 (Figure 30). This case produced the warmest layer temperature at hour nine, though the downward motion was only present during the first six hours of the

surface heating cycle. The initial downward motion deepened the layer, and thereby reduced mixing in this period, over the S1 case, allowing the surface layer to be heated to 14.988°C, an increase of .01°C over that in S1. The following upward motion was sufficient, hours eleven through fourteen, to hold the mixed layer at a relatively constant depth. This allowed a relatively constant, and strong wind stress entrainment to combine with surface cooling to rapidly cool the layer. The result after twenty-four hours is to produce a layer of about the same depth as that of S1, but one that is slightly cooler.

The ∂T here was .237°C, a very noticeable difference from S1, though the final product did not vary much in layer temperature or layer depth.

(5) Two Dimensional Data (Figure 31, 32 and 33). The two dimensional oceanic field was produced as previously discussed. The data covered here is that of the evolution of the ocean system at hours 6, 12, 18, and 24.

By hour six the wave has progressed into the oceanic field, and its effect below the layer is dramatic, (Figure 31a). It has produced a mixed layer that has a mean depth of about 9 meters (initial h was 4.5 meters) with a mean temperature of 14.957°C. A temperature structure, as could be measured at the surface in x, is being formed. The present maximum difference in surface temperatures (in x) is .016°C.

By hour twelve (Figure 31b) the effect of the wave is at its maximum, as seen in the amplitude of the contours below the layer. The layer is generally deeper than at hour six with a mean depth of about 11.5 meters. The deviation from the mean is much

greater for this time, however. The mean of the layer temperature has gone to 14.950°C, a slight decrease from hour six, but more significant is the deviation of the surface temperatures in the x direction. There is now a very definite variation in x of .051°C.

The layer has deepened to a mean depth of about 13 meters by hour eighteen (Figure 31c), with the effect of the wave beginning to be reduced in the system. The mean layer temperature has dropped to 14.846°C, a cooling of almost .05°C in the six hours between illustrations. The surface temperature deviation has reached .091°C. Warm and cold temperature bands are becoming defined in x.

The single wave has passed through the ocean by hour twenty-four, and only the remnant of its passage is seen (Figure 31a). In an ocean that is defined by S1 conditions everywhere, the twenty-four hour product would be an ocean with a mixed layer depth constant at 14.65 meters, and mixed layer temperature of 14.767°C. With the introduction of a single diurnal wave cycle, a variable condition ocean has been produced. The mean depth of this ocean is 15.012 meters, with local variations of up to +1.73 meters and -1.32 meters, with depths at small x being somewhat greater than depths at large x. The mean layer temperature is 14.764°C, but more importantly, the surface temperature variation is now .095°C, in a clearly defined pattern. The pattern that exists is that of a narrow zone of relatively cool water centered near kx = 5, with a wider zone of relatively warmer water centered near kx = 18. Below the layer the isotherms are found to be parallel after the passage of this single wave cycle.

b. Deep Initial Layer (Case IIIb) (Figures 34-40)

The initial conditions for these runs were the same as

for S2. The wave cycle passed through the system as in the previous runs (IIIa). The wave form is harder to discern in these runs, but looking at the contours below the original layer (Figures 34-37) the same forms as the previous run are apparent.

(1) Peak Upward Motion at Hour 7 (Figure 34). As in the previous deep initial layer cases, the shallowing due to the surface heating drives the model in the first six hours. The coincident upward motion during this time combines with the shallowing and mixing to produce a layer that is about 1.5 meters shallower, but at the same temperature as in S2, by hour ten. Two noticeable effects during this period of upward motion are (i) a slight shallowing of the newly formed surface layer, and (ii) the upward transport of cooler below layer water, setting up a larger ΔT at the entrainment zone for this case over that of the standard. The downward motion then contributes to the deepening of the layer as does the mixing which must initially act over a relatively shallow depth. This entrains cool water, forming a quickly deepening and cooling surface mixed layer. As the downward motion decreases the cooling slows, and the increase in the depth of the layer is seen to be caused mostly by the vertical motion. Of all the phases examined this produced the deepest layer (30.34m) and has the second coolest layer at the end of the period (15.059°C) in relation to the other three cases discussed.

The δT for this case is .115°C. This is about half that for the shallow layer case discussed previously. The original deep interface can be followed on the contours (Figure 34b) over the twenty-four hour period. During the downward motion it, again, is

diffusing, while during the upward case there is a slight reinforcement of the interface.

(2) Peak Upward Motion at Hour 1 (Figure 35). Again it is seen that the shallowing mode of the mixed layer model, equations (10) and (11), controls the layer development to hour ten. The layer depth reached through the shallowing, upward, and downward motion combination by hour ten has reached a depth that is about .5 meters deeper than that in S2 for the same time. The temperature is the same as S2. Also, the downward motion makes entrainment of water into the mixed layer due to mixing more difficult, such that cooling after hour ten progresses much more slowly than in that of the previous case, and that of S2. The net result in the layer depth of this run is a layer that is about as deep as that of S2 after the twenty-four hour period. The model did not deepen more than S2 due to the dominant upward motion during the last six hours. The mixed layer temperature was slightly warmer than that of S2 at the end of the run (.071°C). Also, it can been seen that the below layer water is somewhat warmer than in S2 for the end of the period, due to the combined effects of the heating and downward vertical motion timing.

The δT for this case is .092°C. This is less significant than in the previous run.

(3) Peak Upward Motion at Hour 19 (Figure 36). Again, the shallowing mode of the model controls the initial ten hour layer temperature adjustment. The downward vertical motion, however, drives the layer two meters deeper during this time causing reduced mixing due to the surface wind stress. The upward motion keeps the layer

from deepening as quickly as before after hour twelve. Because of the below layer temperature adjustment by the downward motion and the initial deepening of the layer, the layer, also, does not cool as quickly. This case produced the shallowest final layer depth, and the second warmest layer at the end of the period, relative to the other three runs.

The δT for this case is .103°C, which is about the same as the first case which was 180° out of phase with this run.

(4) Peak Upward Motion at Hour 13 (Figure 37). The coincident shallowing, wind stress mixing, heat flux, and cycled vertical motion over the first ten hours produce a surface mixed layer that has the same temperature as S2, and almost the same layer depth (to within less than .5 meters). Below the layer, however, the upward motion has made relatively cooler water available by hour ten (in comparison with S2), and the layer, though not rapidly deepening due to the continued upward motion, cools quickly as large quantities of water are entrained over a relatively shallow depth, a trend which continues to the end of the period. The net result is a mixed layer that is 1.5 meters deeper than that of S2, but is also the coolest layer of the four runs. Because of the below layer temperature profiles which are set up by the upward motion for the mid-twelve hours, the continued run of this model over a second day gives continued rapid cooling of the layer due to increased entrainment of cooler, upward advected water, and to increased effects of mixing. A noticeable deepening does take place at the end of the period due to the downward motion, which accounts for the fact that this run ended deeper than S2.

The δT for this run is .125°C. This is the largest of the four runs, but it is still only half of the maximum δT seen for the shallow initial layer case.

(5) Two-Dimensional Data (Figure 38, 39 and 40). The two-dimensional oceanic field is produced, here, as previously discussed, for the single wave cycle. The data covered is for hours 6, 12, 18, and 24. A common feature is the varying below layer temperature structure set up because of the introduction of the initial deep layer. Because of this, the changes in the thermocline below the initial deep interface best show the effect of the wave progression through the system.

As in the shallow case, by hour six, the wave has progressed into the oceanic system producing some horizontal sea surface temperature structure. However, the effect on the surface temperature is almost negligible, in that the variability of the surface temperature in x is only .001°C. This is due to the shallowing mode response of the model over the first six hours. Even with this, however, the depth structure has varied (Figure 38a) so that there has been a change from the constant structure that would be seen in S2 of 11.767 meters for the layer depth, to a layer of mean depth of 11.769 meters $\pm$ .35 meters, indicating that an adjustment due to the wave is taking place.

By hour twelve much more temperature and layer (h(x)) variation is beginning to take shape. At hour twelve the case without the vertical motion has a layer depth of 15.037 meters, and a layer temperature of 15.159°C everywhere. In this case, where the maximum effect of the wave has been reached, the layer depth has a mean of

15.231 meters with a deviation of ± 2.5 meters. The variability in the surface temperature in x has reached .01°C. Though the variability in the surface temperature is not very large, a pattern is again beginning to emerge in the x direction. At small x cooler water is forming, while at large x a band of warmer water is emerging.

The layer has continued to deepen to hour eighteen. The layer depth has increased to a mean of 19.46 m, ± 3.4 m, and the variation in the surface temperature structure in x has reached .03°C. The warm-cold pattern seen at hour six is repeated and strengthened. Though the temperature difference between warm and cool water is not as great as in the shallow case, the banding of the patches is much more distinct here (Figure 38, Figure 31).

At the end of the period the wave has, again, been removed from the system, and only the remnant of its passage is seen. The final layer depth is deeper than in the previous hours, and much deeper than in the shallow case. The variability of h in x is also much greater here than in the shallow case. The surface temperature patchiness is well-defined, but the variability of the temperature in x is only .035°C.

Comparing the two cases, shallow and deep initial layers, it is seen that for the same amplitude wave the model produces two distinct ocean types. For the shallow case an ocean is formed that has a relatively shallow layer with a large temperature variation in the x direction, but with that temperature variation primarily in wide bands. For the deep case a deep surface layer is formed with smaller variability in the surface temperature. However, the temperature structure in x is much better defined. Also in the deep case,

the patches of warm and cold water are much closer to each other (in x). This could suggest a mechanism for generating or sharpening SST fronts through surface heating, and internal solitary wave passage.

4. Case IV

It was noted in Case III that after twenty-four hours the wave form had passed through the ocean system, and had left behind only the residue of its effect on the system, over and above the standard effects. This can be compared to a solitary wave passing through an ocean system. While this has theoretical advantages, it is not a very realistic problem, in that wave forms seldom take on this sort of motion. One possible exception may be solitons generated at extreme tidal stages (Apel, 1982).

The next progression, therefore is to look at a continuous wave system that passes through the ocean with constant form, until the run is terminated. This is done by simply modifying the mathematics of the previous case to include initialization of the temperature and salinity profiles with the wave form according to the following.

We know that

$$w(x,z,t) = \frac{AAz}{D}\cos(\omega t + kx)$$

and

$$w = -\frac{\partial \delta h}{\partial t}$$

or

$$\delta h = -\int w \partial t$$

therefore

$$\delta h = -\frac{AAz}{\omega D}\sin(\omega t + kx)$$

For initial displacement

$$\delta h(x,z,0) = \delta h_0$$

therefore

$$\delta h_0 = -\frac{AAz}{\omega D}\sin(kx) \qquad (22)$$

Applying equation (22) to form the initialized layer depth, and combining this with equation (16) to initialize the temperature profile, a continuous wave field can now be passed through the model ocean (Figure 7).

From this point on the discussion will be confined to the deep initial layer case, S2 standard, and variations thereof. This is done because all the primary effects discussed to this point appear in both the shallow and deep cases, as do the effects to be discussed in varying degrees, and it is not necessary to continuously reiterate this discussion.

a. Diurnal Wave (Case IVa) (Figures 41, 42 and 43)

Because of the overriding effect of the shallowing mode of the model in the first six hours of the runs, the results produced here were exactly the same as those discussed in Case IIIb, for the phase relationships. This was of course expected from the theory.

(1) Two-Dimensional Data (Figure 44, 45 and 46). Again, because of the dominance of the shallowing mode, the hour 6, 12, 18, and 24 two-dimensional fields produced here are the same as those of Case IIIb for the area of the entrainment zone, and the mixed layer. Below the layer, however, the wave form is now seen to progress through the system in a continuous mode. This is best seen in the contours

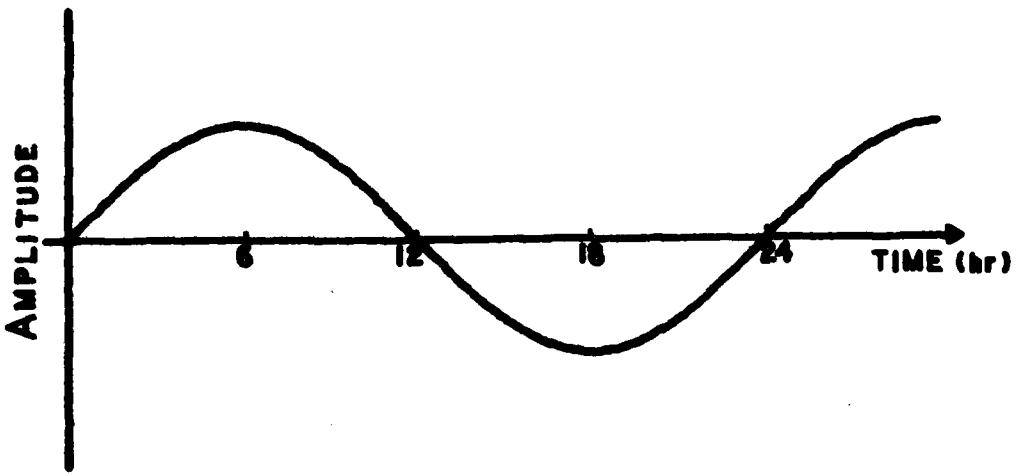

Figure 7. Diurnal wave relationship (of continuous diurnal waveform to model location (x). Amplitude variable.)

in which the amplitude of the system remains a constant, but the wave form is shifted with time.

It can be seen that the patch of warmer waters forms (Figure 44) and takes a phase that barely leads the peak of the wave system. The entrainment zone ($h(x)$) now takes the form of the passing wave system, as would be expected, and yet was not obvious in the previous case. The divergence and convergence of below layer fields is also obvious here, where previously it was not particularly obvious.

b. Semi-diurnal Wave (Case IVb) (Figures 47-50)

A dominant internal wave system of the temperate oceans is the semi-diurnal tidal cycle. South of 30° N there is also a strong diurnal tidal cycle. A semi-diurnal tidal field can be produced for testing in this model by simply adjusting the frequency of the prescribed w for equation (21), and setting the initial profiles with the appropriate frequency of equation (22) and (17).

The amplitude of the motion remains the same as the diurnal cycle case. Because the cycle of wave mixing interactions repeats itself after a 2π phase shift, which occurs after 12 hours in this case, only the cases of six and twelve hour phase shifts will be discussed. The 18 and 24 hour phase shifts are merely repeats.

(1) Six Hour Shift (Figure 47a and b). Figure 8 shows the relationship of the heating cycle to the wave motion in this case. The vertical motion is seen to immediately combine with the shallowing mode of the model through the initialization to give a somewhat shallower initial layer. The shallowing mode of the model holds the layer temperature the same as in S2 to hour six, while the vertical

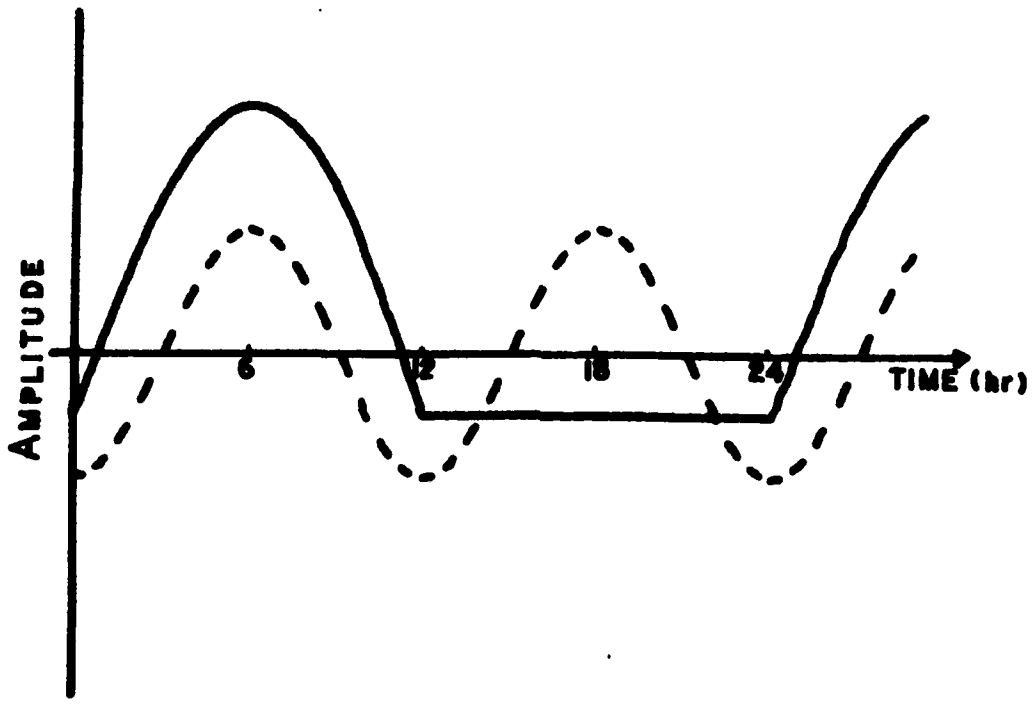

Figure 8. Phase relationship of Case IVb (six hour shift) of semi-diurnal waveform to diurnal surface heating cycle over time (hrs). Amplitudes are not proportional.

motion varies the layer depth, and alters the below layer temperature structure. By hour six a half-cycle of the wave has passed through the model point, and a layer has been produced that is almost one meter deeper than S2 at this time, but which has the same layer temperature. Continued but decreasing downward motion combines with the downward heat flux until hour nine to slowly deepen the layer, but the layer continues to warm. This process continues through hour ten, though upward motion has begun because the heating and entrainment of relatively warm water are greater than the effect of the resistance to deepening due to the surface heat flux, and the small upward motion. By hour eleven the upward motion dominates, and the layer shallows while it cools slightly due to the increased entrainment. At hour twelve the layer is as shallow as it will ever get, and the first wave has passed. Now decreased upward motion followed by downward motion, combined with surface cooling and mixing through a progressively cooler surface mixed layer quickly increases the layer depth to a maximum of 26.7 meters at hour twenty-one. This is deeper than S2 gets in the entire twenty-four hour period. Yet, the layer is not as cool as in the S2 case. By hour twenty-one the upward motion is again dominant and the layer shallows.

(2) Twelve Hour Shift (Figure 47c and d). Figure 9 shows the relationship of the heating cycle with the wave in this case. The initialization combines with the vertical motion and shallowing mode to produce an initial layer that is deeper than that in S2, but soon becomes shallower, as the new surface layer is established. By hour six a layer of the same temperature as S2, but .72 meters shallower

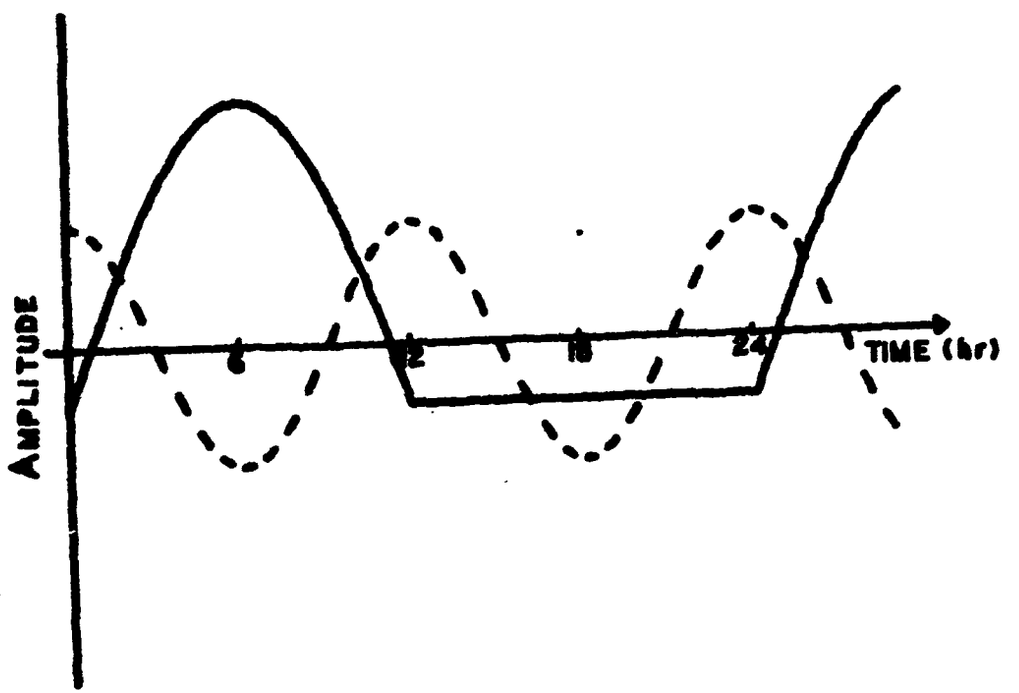

Figure 9. Phase relationship of Case IVb (twelve hour shift).

has been formed. The net result of the cyclical interactions in this case is a layer that is 1.5 meters deeper than in S2, but which is at about the same temperature. The difference in the layer temperature between this run, and the previous is .004°C. However, the layer depth is 2.2 m different.

(3) Two-Dimensional Data (Figure 48, 49 and 50). At hour six a very discernable depth structure has been set up at the bottom of the mixed layer which reflects the structure of the passing wave. Above the entrainment zone the temperature structure, as produced by the shallowing mode, is homogeneous. Below the layer the structure is highly varied in x reflecting the combined effects of the vertical motion to this time. The mean layer depth is 11.75 meters, while that of S2 is 11.77 m, showing the domination of the shallowing to this point. A variation of h in x of $\pm$ .75 meters is already exhibited.

By hour twelve the mixed layer depth structure in x, and the layer temperature variability in x have evolved considerably over that of hour six. At the entrainment zone the structure is approximately sinusoidal, as expected. Over the last six hours a large amount of water from below the layer has been entrained while surface heating has occurred, and the mixed layer has heated and cooled accordingly to begin to set up the pattern of warm and cold bands of temperature in x. The mean depth of the layer is now 15.21 meters $\pm$ 2.50 meters, while that for S2 is 15.04 meters. The temperature variation in x as seen at the surface is now .012°C.

The structure of temperature and layer depth profile has been further accented by hour eighteen. The layer has continued

to deepen, and the fluctuation in x increased. The banding of the in layer temperature pattern in x has become more defined.

After twenty-four hours a layer has been produced that has a depth of 26.14 m, $\pm$ 3.3 m. The surface temperature pattern in x is quite clearly defined, though the variation in temperature is only .015°C.

5. Case V (Superimposed Waves) (Figure 51, 52 and 53)

Since oceanic internal waves are almost never simple sinusoids, one more progression is considered. Spectral analysis of the MILE data (Figure 10) at station P (55° N) shows the dominant wave field to be the semi-diurnal tide superimposed by, at least, the 6-7 hour harmonic of the tidal wave. Internal wave theory indicates that the period of the internal waves must be less than or equal to the inertial period. North of approximately 30° N, no diurnal internal waves may propagate, and therefore, they are not seen in the MILE data. South of this, however, diurnal and semi-diurnal tidal period waves may propagate. Therefore, since previous discussions have been concerned with diurnal and semi-diurnal waves, and there is justification for their presence, these waves will be superimposed to form a slightly more complicated wave system.

The combined wave is directed through the two-dimensional ocean which has the initial conditions of S2, from right to left (large kx to small kx). The amplitude of the motion is such that both waves peak at the same amplitude at their peak motions, though one has half the period of the other. Both waves start with an amplitude of vertical motion in phase at time one.

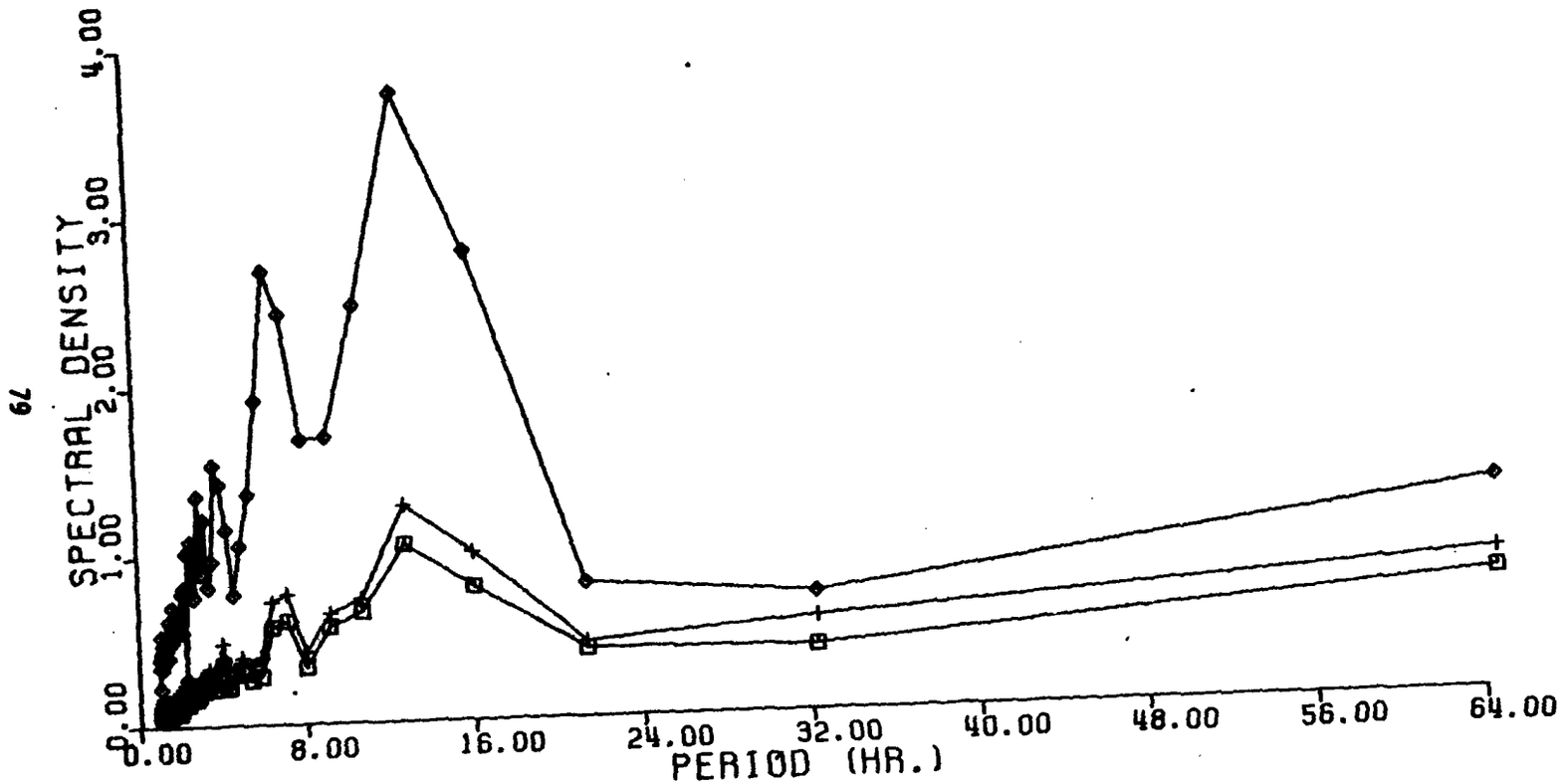

Figure 10. MILE spectral analysis (of temperature variation at 50 m (□), 47 m (+), and 32 m (◇)).

The superimposed waves reflect all of the interactions discussed in the previous sections. Further, this simple addition of two waveforms has developed several new features. The new features can be traced in their development from hour one through hour twenty-four, where they become most evident. Since this is the case, the discussion will be limited to the case of the two-dimensional ocean at hour twenty-four.

By this time a complex structure has emerged for the two-dimensional ocean, both in temperature and in profile of the layer depth. An ocean has been formed that has a mean layer depth of 26.78 m, but this depth has a variation that is not symmetrical from small to large x. At small x the variation from the mean depth is seen to be a maximum of -5.45 m, while at large x the layer depth varies to a depth deviation from the mean of +7.83 m. An ocean has been formed that has a deep layer at one end, and a shallow layer at the other. Further, a deviation of the surface temperature in the x direction of .042°C is seen. The pattern of the warm and cold bands again is seen, but this also is no longer symmetrical. The temperature pattern, as seen at the surface, is a cold band beginning at small kx, progressing through a weak gradient to a warm band centered near kx = 15. A strong gradient is then encountered leading to a cold band centered about kx = 21. Through the introduction of a simple two wave system, an extremely diverse ocean has been produced.

Shifting the phase relationships of the two internal waves, and running the model again, resulted in similar patterns. Positions of the temperature maxima and minima in the layer, and the position of the depth variations shift, but their relative positions are maintained.

The temperature variation in the x direction as seen at the surface does not change with the phase changes.

IV. CONCLUSIONS AND RECOMMENDATIONS

The analysis of the mixing response to the prescribed vertical motion shows that vertical advection can be successfully introduced into this one-dimensional mixed layer model without numerical difficulties. This is important in that it indicates that a single station forecasting model can be altered to include the variability of long internal wave motion. This step is the first of a progressive development of a single station forecasting model that may in the future include other local advective effects.

Using an ensemble of one-dimensional stations, a two-dimensional mixing response to prescribed internal wave motion was simulated. Although the initial temperature field (without wave) and the surface boundary conditions were both horizontally homogeneous, a significant wave-induced horizontal structure was created in the $T(x,z)$ field. Both linear and non-linear effects have been demonstrated in the simple single wave and superimposed wave cases. Horizontal variability has been shown, both in mixed layer depth and in mixed layer temperature structure. The mixed layer temperature develops a corrollary structure of alternating warm and cold patches. In the case of the superimposed waves of different frequencies, this patchiness pattern can be complex, and can give rise to horizontal gradients which could be frontogenetic.

There is an important relationship between the phase of internal motion and the cyclical diurnal heat flux boundary condition. This is clearly demonstrated in the numerical experiments in which the phase of the input pulse or wave system has been varied.

In the case of superimposed diurnal and semi-diurnal waves, the horizontal variation in temperature in the mixed layer was about .04°C after only a single diurnal cycle. In the same period, the mixed layer depth varied by about 13 m. The wave dispersion relation for a two layer ocean at 25° N gives a horizontal wave length scale of from 10 to 100 Km, depending upon stratification. This wave-mixing interaction may, therefore, be an important mechanism for the generation of sea surface patchiness as found by Butler (1981).

Further study must be done in this area. Clearly, more complicated waveforms will produce more complex responses. The model should be tested with salinity changes, including evaporation and precipitation. Tests should be conducted on data sets such as those of MILE. Comparison of the mixed layer model results using MILE boundary conditions, with and without vertical advection, as observed in spectrum analysis, should further demonstrate the importance of addition of vertical motion to mixed layer models.

Finally, the wave systems should be tested in an interactive mode with the mixing of the model. Energy exchanges, as prescribed by wave theory and the studies of Linden (1975), and Kantha et al. (1977) should be allowed, and the relative significance of the different mechanism should be evaluated. Internal vertical motion is an important dynamic variable, and should be treated as such in the future of mixed layer modelling.

DAY	HR	H	T	S	TAU	QNET	WDD	DH
1	1	49.5	15.001	34.000	0.50	- 55.7	0.0	0.0
1	2	18.1	15.009	34.000	0.50	-201.5	0.0	0.0
1	3	16.2	15.026	34.000	0.50	-326.8	0.0	0.0
1	4	13.0	15.047	34.000	0.50	-423.0	0.0	0.0
1	5	12.1	15.075	34.000	0.50	-483.5	0.0	0.0
1	6	11.8	15.105	34.000	0.50	-504.2	0.0	0.0
1	7	13.1	15.132	34.000	0.50	-483.7	0.0	0.0
1	8	12.5	15.154	34.000	0.50	-423.5	0.0	0.0
1	9	13.0	15.168	34.000	0.50	-327.5	0.0	0.0
1	10	13.5	15.175	34.000	0.50	-202.4	0.0	0.0
1	11	14.2	15.172	34.000	0.50	- 56.6	0.0	0.0
1	12	15.0	15.160	34.000	0.50	99.9	0.0	0.0
1	13	15.9	15.149	34.000	0.50	100.8	0.0	0.0
1	14	16.7	15.139	34.000	0.50	100.8	0.0	0.0
1	15	17.5	15.129	34.000	0.50	100.8	0.0	0.0
1	16	18.4	15.120	34.000	0.50	100.8	0.0	0.0
1	17	19.2	15.112	34.000	0.50	100.8	0.0	0.0
1	18	20.0	15.104	34.000	0.50	100.8	0.0	0.0
1	19	20.9	15.097	34.000	0.50	100.8	0.0	0.0
1	20	21.8	15.090	34.000	0.50	100.8	0.0	0.0
1	21	22.7	15.083	34.000	0.50	100.8	0.0	0.0
1	22	23.6	15.077	34.000	0.50	100.8	0.0	0.0
1	23	24.6	15.071	34.000	0.50	100.8	0.0	0.0
1	24	25.7	15.066	34.000	0.50	100.8	0.0	0.0
2	1	26.2	15.066	34.000	0.50	- 55.7	0.0	0.0
2	2	22.4	15.073	34.000	0.50	-201.5	0.0	0.0
2	3	15.1	15.089	34.000	0.50	-326.8	0.0	0.0
2	4	13.2	15.112	34.000	0.50	-423.0	0.0	0.0
2	5	12.0	15.140	34.000	0.50	-483.5	0.0	0.0
2	6	11.7	15.169	34.000	0.50	-504.2	0.0	0.0
2	7	12.0	15.197	34.000	0.50	-483.7	0.0	0.0
2	8	12.4	15.219	34.000	0.50	-423.5	0.0	0.0
2	9	12.9	15.234	34.000	0.50	-327.5	0.0	0.0
2	10	13.4	15.240	34.000	0.50	-202.4	0.0	0.0
2	11	14.1	15.237	34.000	0.50	- 56.6	0.0	0.0
2	12	14.9	15.225	34.000	0.50	99.9	0.0	0.0
2	13	15.7	15.214	34.000	0.50	100.8	0.0	0.0
2	14	16.5	15.203	34.000	0.50	100.8	0.0	0.0
2	15	17.4	15.194	34.000	0.50	100.8	0.0	0.0
2	16	18.2	15.185	34.000	0.50	100.8	0.0	0.0
2	17	19.1	15.177	34.000	0.50	100.8	0.0	0.0
2	18	20.0	15.169	34.000	0.50	100.8	0.0	0.0
2	19	20.9	15.161	34.000	0.50	100.8	0.0	0.0
2	20	21.9	15.155	34.000	0.50	100.8	0.0	0.0
2	21	22.8	15.148	34.000	0.50	100.8	0.0	0.0
2	22	23.8	15.142	34.000	0.50	100.8	0.0	0.0
2	23	24.7	15.136	34.000	0.50	100.8	0.0	0.0
2	24	25.6	15.130	34.000	0.50	100.8	0.0	0.0

(a)

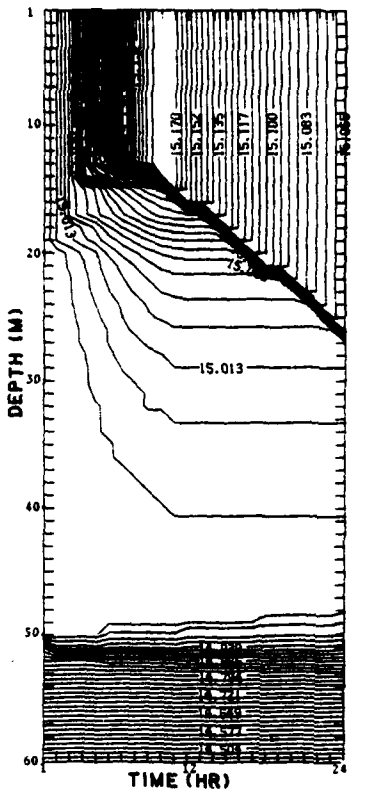

(b)

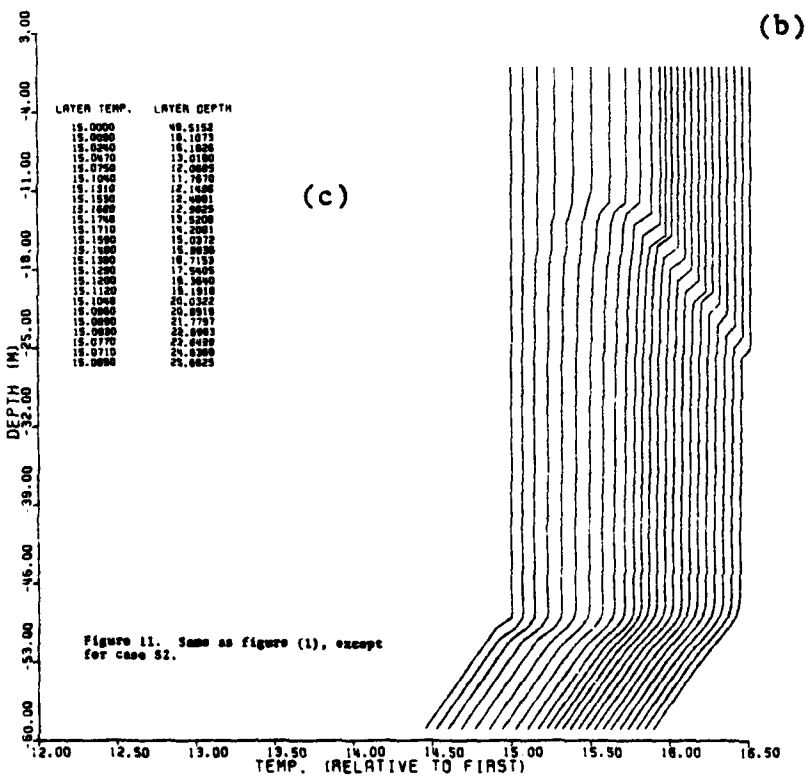

(c)

Figure 11. Same as figure (1), except for case S2.

DAY	HR	K	T	S	TAU	QNET	WDO	DE
1	1	6.5	14.956	34.000	0.50	- 1.5	0.03600	22.981
1	2	7.7	14.940	34.000	0.50	-100.8	0.03600	27.350
1	3	8.7	14.938	34.000	0.50	-184.3	0.03600	30.774
1	4	9.5	14.944	34.000	0.50	-248.4	0.03600	33.644
1	5	10.2	14.954	34.000	0.50	-288.7	0.03600	36.175
1	6	10.9	14.965	34.000	0.50	-302.5	0.03600	38.580
1	7	11.6	14.977	34.000	0.50	-288.9	0.03600	40.890
1	8	12.2	14.986	34.000	0.50	-248.7	0.03600	43.226
1	9	12.9	14.991	34.000	0.50	-184.7	0.03600	45.688
1	10	13.7	14.990	34.000	0.50	-101.3	0.03600	48.284
1	11	14.4	14.984	34.000	0.50	- 4.1	0.03600	51.078
1	12	15.3	14.971	34.000	0.50	100.2	0.03600	54.138
1	13	16.2	14.960	34.000	0.50	100.8	0.03600	57.287
1	14	17.1	14.950	34.000	0.50	100.8	0.03600	60.549
1	15	18.1	14.940	34.000	0.50	100.8	0.03600	63.917
1	16	19.1	14.933	34.000	0.50	100.8	0.03600	67.397
1	17	20.1	14.924	34.000	0.50	100.8	0.03600	70.992
1	18	21.1	14.915	34.000	0.50	100.8	0.03600	74.707
1	19	22.2	14.908	34.000	0.50	100.8	0.03600	78.551
1	20	23.3	14.901	34.000	0.50	100.8	0.03600	82.526
1	21	24.5	14.895	34.000	0.50	100.8	0.03600	86.630
1	22	25.7	14.889	34.000	0.50	100.8	0.03600	90.873
1	23	26.9	14.884	34.000	0.50	100.8	0.03600	95.260
1	24	28.1	14.879	34.000	0.50	100.8	0.03600	99.519
2	1	29.1	14.877	34.000	0.50	- 3.5	0.03600	103.633
2	2	30.4	14.880	34.000	0.50	-100.8	0.03600	107.626
2	3	24.2	14.886	34.000	0.50	-184.3	0.03600	85.396
2	4	20.0	14.896	34.000	0.50	-248.4	0.03600	70.654
2	5	18.5	14.908	34.000	0.50	-288.7	0.03600	65.386
2	6	18.1	14.921	34.000	0.50	-302.5	0.03600	64.099
2	7	19.1	14.933	34.000	0.50	-288.9	0.03600	67.431
2	8	20.3	14.942	34.000	0.50	-248.7	0.03600	71.745
2	9	21.8	14.948	34.000	0.50	-184.7	0.03600	77.107
2	10	23.4	14.950	34.000	0.50	-101.3	0.03600	82.804
2	11	25.3	14.948	34.000	0.50	- 4.1	0.03600	89.514
2	12	27.5	14.943	34.000	0.50	100.2	0.03600	97.279
2	13	29.7	14.938	34.000	0.50	100.8	0.03600	105.191
2	14	32.1	14.934	34.000	0.50	100.8	0.03600	113.383
2	15	34.5	14.930	34.000	0.50	100.8	0.03600	121.934
2	16	37.0	14.926	34.000	0.50	100.8	0.03600	130.806
2	17	39.6	14.923	34.000	0.50	100.8	0.03600	140.036
2	18	42.3	14.920	34.000	0.50	100.8	0.03600	149.572
2	19	45.1	14.917	34.000	0.50	100.8	0.03600	159.512
2	20	48.0	14.915	34.000	0.50	100.8	0.03600	169.789
2	21	51.0	14.912	34.000	0.50	100.8	0.03600	180.441
2	22	54.2	14.910	34.000	0.50	100.8	0.03600	191.488
2	23	57.4	14.908	34.000	0.50	100.8	0.03600	202.906
2	24	60.7	14.906	34.000	0.50	100.8	0.03600	214.586

(a)

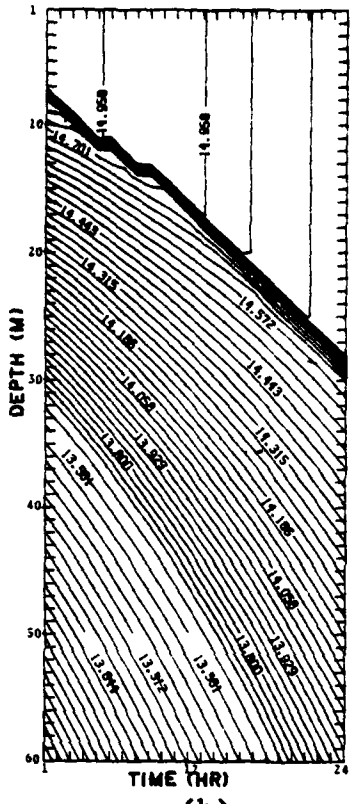

(b)

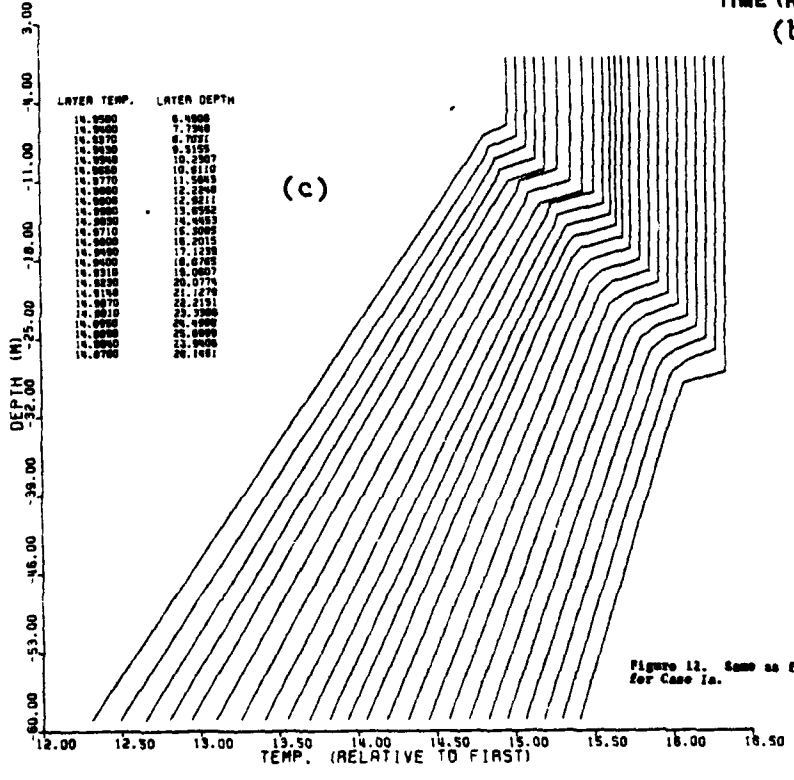

(c)

Figure 12. Same as figure (1), except for Case 1a.

DAY	HR	H	T	S	TAU	QNET	WSQ	DH
1	1	51.3	15.001	34.000	0.50	- 55.7	0.03600	181.500
1	2	18.6	15.009	34.000	0.50	-201.5	0.03600	65.705
1	3	16.6	15.024	34.000	0.50	-326.8	0.03600	58.846
1	4	13.4	15.048	34.000	0.50	-423.0	0.03600	47.351
1	5	12.4	15.076	34.000	0.50	-483.5	0.03600	43.932
1	6	12.1	15.105	34.000	0.50	-504.2	0.03600	42.862
1	7	12.7	15.133	34.000	0.50	-483.7	0.03600	44.885
1	8	13.5	15.155	34.000	0.50	-423.5	0.03600	47.730
1	9	14.4	15.170	34.000	0.50	-327.5	0.03600	51.043
1	10	15.6	15.176	34.000	0.50	-202.4	0.03600	55.035
1	11	16.8	15.175	34.000	0.50	- 56.6	0.03600	59.415
1	12	18.2	15.165	34.000	0.50	99.9	0.03600	64.527
1	13	19.8	15.157	34.000	0.50	100.8	0.03600	69.859
1	14	21.2	15.149	34.000	0.50	100.8	0.03600	75.111
1	15	22.8	15.142	34.000	0.50	100.8	0.03600	80.593
1	16	24.4	15.136	34.000	0.50	100.8	0.03600	86.161
1	17	26.0	15.130	34.000	0.50	100.8	0.03600	91.896
1	18	27.6	15.125	34.000	0.50	100.8	0.03600	97.745
1	19	29.4	15.120	34.000	0.50	100.8	0.03600	103.790
1	20	31.1	15.116	34.000	0.50	100.8	0.03600	110.024
1	21	32.9	15.112	34.000	0.50	100.8	0.03600	116.410
1	22	34.8	15.108	34.000	0.50	100.8	0.03600	122.992
1	23	36.7	15.104	34.000	0.50	100.8	0.03600	129.782
1	24	38.7	15.101	34.000	0.50	100.8	0.03600	136.782
2	1	40.3	15.102	34.000	0.50	- 55.7	0.03600	142.466
2	2	19.9	15.110	34.000	0.50	-201.5	0.03600	70.411
2	3	16.2	15.125	34.000	0.50	-326.8	0.03600	57.316
2	4	13.4	15.148	34.000	0.50	-423.0	0.03600	47.469
2	5	12.4	15.176	34.000	0.50	-483.5	0.03600	43.685
2	6	12.1	15.206	34.000	0.50	-504.2	0.03600	42.702
2	7	12.6	15.234	34.000	0.50	-483.7	0.03600	44.704
2	8	13.5	15.256	34.000	0.50	-423.5	0.03600	47.558
2	9	14.5	15.270	34.000	0.50	-327.5	0.03600	51.119
2	10	15.6	15.277	34.000	0.50	-202.4	0.03600	55.287
2	11	16.9	15.275	34.000	0.50	- 56.6	0.03600	59.629
2	12	18.3	15.266	34.000	0.50	99.9	0.03600	64.707
2	13	19.8	15.258	34.000	0.50	100.8	0.03600	69.993
2	14	21.3	15.250	34.000	0.50	100.8	0.03600	75.215
2	15	22.8	15.243	34.000	0.50	100.8	0.03600	80.664
2	16	24.4	15.237	34.000	0.50	100.8	0.03600	86.134
2	17	26.0	15.231	34.000	0.50	100.8	0.03600	91.828
2	18	27.6	15.226	34.000	0.50	100.8	0.03600	97.623
2	19	29.3	15.221	34.000	0.50	100.8	0.03600	103.616
2	20	31.0	15.217	34.000	0.50	100.8	0.03600	109.788
2	21	32.9	15.213	34.000	0.50	100.8	0.03600	116.216
2	22	34.7	15.209	34.000	0.50	100.8	0.03600	122.785
2	23	36.6	15.205	34.000	0.50	100.8	0.03600	129.540
2	24	38.6	15.202	34.000	0.50	100.8	0.03600	136.504

(a)

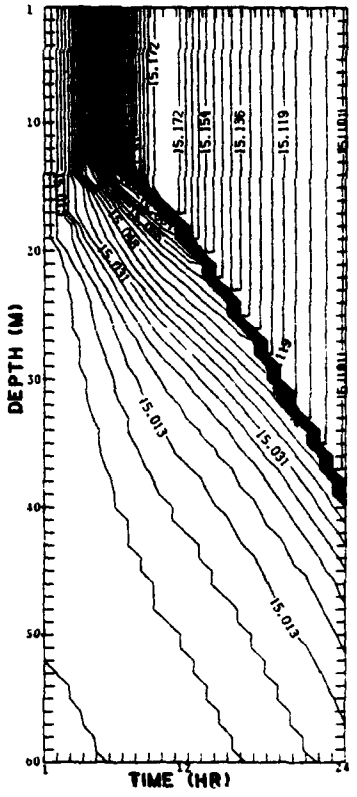

(b)

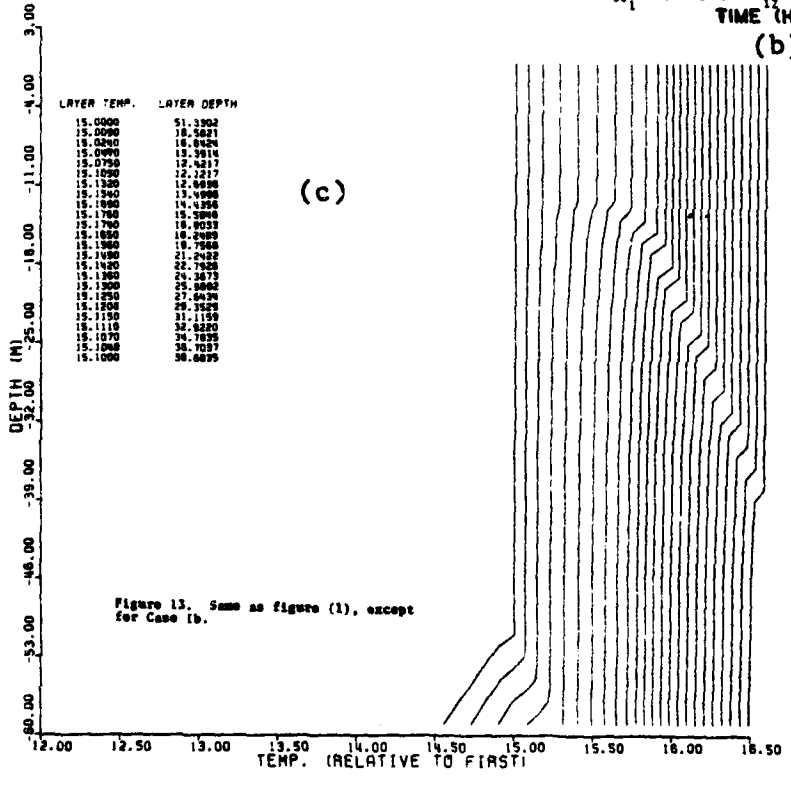

(c)

Figure 13. Same as figure (1), except for Case Ib.

DAY	HR	H	T	S	TAU	QNET	WDO	DH
1	1	6.0	14.956	34.000	0.50	- 3.5	-.03600	- 22.140
1	2	6.9	14.937	34.000	0.50	-100.8	-.03600	- 25.258
1	3	7.3	14.931	34.000	0.50	-184.3	-.03600	- 26.750
1	4	7.6	14.934	34.000	0.50	-248.4	-.03600	- 27.962
1	5	7.8	14.941	34.000	0.50	-288.7	-.03600	- 28.725
1	6	7.9	14.949	34.000	0.50	-302.5	-.03600	- 28.917
1	7	7.9	14.957	34.000	0.50	-288.9	-.03600	- 29.021
1	8	7.9	14.961	34.000	0.50	-248.7	-.03600	- 29.089
1	9	8.0	14.959	34.000	0.50	-184.7	-.03600	- 29.189
1	10	8.0	14.949	34.000	0.50	-101.3	-.03600	- 29.288
1	11	8.0	14.930	34.000	0.50	- 4.1	-.03600	- 29.467
1	12	8.1	14.898	34.000	0.50	100.2	-.03600	- 29.817
1	13	8.3	14.849	34.000	0.50	100.8	-.03600	- 30.262
1	14	8.4	14.842	34.000	0.50	100.8	-.03600	- 30.793
1	15	8.6	14.815	34.000	0.50	100.8	-.03600	- 31.417
1	16	8.7	14.789	34.000	0.50	100.8	-.03600	- 31.996
1	17	8.7	14.763	34.000	0.50	100.8	-.03600	- 31.892
1	18	8.7	14.735	34.000	0.50	100.8	-.03600	- 31.779
1	19	8.7	14.709	34.000	0.50	100.8	-.03600	- 31.733
1	20	8.7	14.683	34.000	0.50	100.8	-.03600	- 31.750
1	21	8.7	14.657	34.000	0.50	100.8	-.03600	- 31.832
1	22	8.6	14.631	34.000	0.50	100.8	-.03600	- 31.625
1	23	8.6	14.605	34.000	0.50	100.8	-.03600	- 31.475
1	24	8.6	14.573	34.000	0.50	100.8	-.03600	- 31.384
2	1	8.5	14.536	34.000	0.50	- 3.5	-.03600	- 31.297
2	2	8.5	14.547	34.000	0.50	-100.8	-.03600	- 31.155
2	3	8.4	14.546	34.000	0.50	-184.3	-.03600	- 30.956
2	4	8.4	14.551	34.000	0.50	-248.4	-.03600	- 30.709
2	5	8.3	14.559	34.000	0.50	-288.7	-.03600	- 30.435
2	6	8.2	14.554	34.000	0.50	-302.5	-.03600	- 30.162
2	7	8.2	14.562	34.000	0.50	-288.9	-.03600	- 29.931
2	8	8.1	14.567	34.000	0.50	-248.7	-.03600	- 29.802
2	9	8.1	14.565	34.000	0.50	-184.7	-.03600	- 29.745
2	10	8.1	14.555	34.000	0.50	-101.3	-.03600	- 29.808
2	11	8.2	14.535	34.000	0.50	- 4.1	-.03600	- 30.018
2	12	8.3	14.477	34.000	0.50	100.2	-.03600	- 30.407
2	13	8.5	14.449	34.000	0.50	100.8	-.03600	- 31.019
2	14	8.7	14.422	34.000	0.50	100.8	-.03600	- 31.729
2	15	8.7	14.396	34.000	0.50	100.8	-.03600	- 31.972
2	16	8.5	14.369	34.000	0.50	100.8	-.03600	- 31.256
2	17	8.3	14.341	34.000	0.50	100.8	-.03600	- 30.583
2	18	8.2	14.304	34.000	0.50	100.8	-.03600	- 29.953
2	19	8.0	14.274	34.000	0.50	100.8	-.03600	- 29.370
2	20	7.9	14.243	34.000	0.50	100.8	-.03600	- 28.828
2	21	7.7	14.212	34.000	0.50	100.8	-.03600	- 28.333
2	22	7.6	14.179	34.000	0.50	100.8	-.03600	- 27.792
2	23	7.4	14.146	34.000	0.50	100.8	-.03600	- 27.302
2	24	7.3	14.095	34.000	0.50	100.8	-.03600	- 26.852

(a)

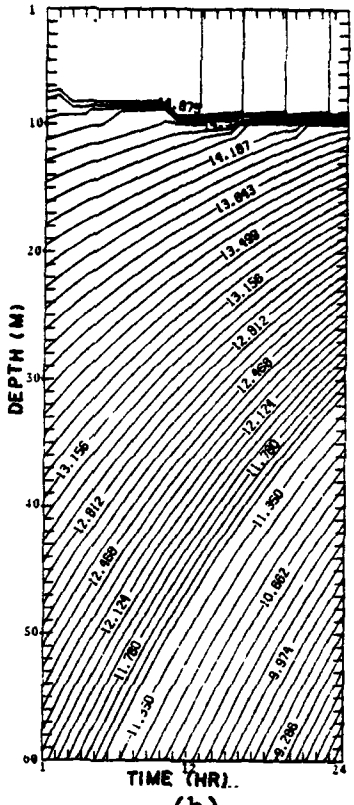

(b)

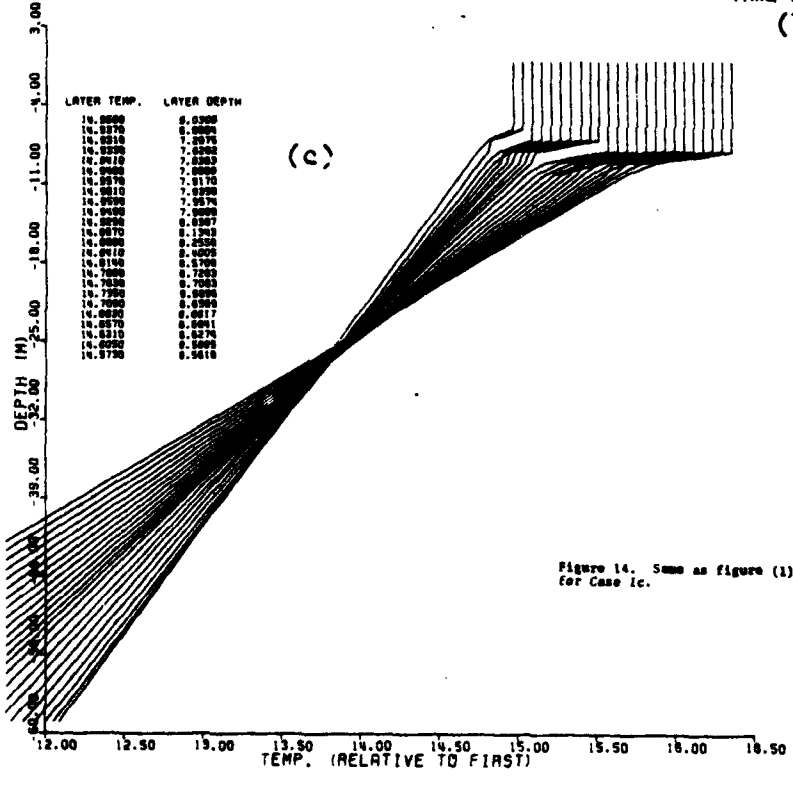

(c)

Figure 14. Same as figure (1), except for Case 1c.

DAY	HR	N	T	S	TAU	QNET	WDO	DR
1	1	47.8	15.001	34.000	0.50	- 55.7	-.03600	-175.086
1	2	17.6	15.000	34.000	0.50	-301.5	-.03600	- 64.667
1	3	15.7	15.024	34.000	0.50	-326.8	-.03600	- 57.600
1	4	12.7	15.047	34.000	0.50	-421.0	-.03600	- 46.385
1	5	11.7	15.075	34.000	0.50	-483.5	-.03600	- 42.818
1	6	11.4	15.104	34.000	0.50	-504.2	-.03600	- 41.864
1	7	11.3	15.131	34.000	0.50	-483.7	-.03600	- 41.478
1	8	11.4	15.154	34.000	0.50	-423.5	-.03600	- 41.627
1	9	11.5	15.168	34.000	0.50	-327.5	-.03600	- 42.236
1	10	11.8	15.174	34.000	0.50	-202.4	-.03600	- 43.128
1	11	12.0	15.168	34.000	0.50	- 56.6	-.03600	- 44.127
1	12	12.5	15.154	34.000	0.50	99.9	-.03600	- 45.777
1	13	13.0	15.139	34.000	0.50	100.8	-.03600	- 47.505
1	14	13.4	15.126	34.000	0.50	100.8	-.03600	- 49.176
1	15	13.9	15.113	34.000	0.50	100.8	-.03600	- 51.027
1	16	14.5	15.101	34.000	0.50	100.8	-.03600	- 52.978
1	17	15.0	15.090	34.000	0.50	100.8	-.03600	- 55.150
1	18	15.7	15.079	34.000	0.50	100.8	-.03600	- 57.549
1	19	16.4	15.069	34.000	0.50	100.8	-.03600	- 60.126
1	20	17.2	15.060	34.000	0.50	100.8	-.03600	- 62.981
1	21	18.1	15.051	34.000	0.50	100.8	-.03600	- 66.262
1	22	19.0	15.043	34.000	0.50	100.8	-.03600	- 69.803
1	23	19.7	15.035	34.000	0.50	100.8	-.03600	- 72.196
1	24	19.7	15.026	34.000	0.50	100.8	-.03600	- 72.084
2	1	19.1	15.026	34.000	0.50	- 55.7	-.03600	- 70.858
2	2	18.7	15.033	34.000	0.50	-301.5	-.03600	- 68.722
2	3	15.4	15.048	34.000	0.50	-326.8	-.03600	- 56.584
2	4	12.7	15.071	34.000	0.50	-421.0	-.03600	- 46.598
2	5	11.7	15.099	34.000	0.50	-483.7	-.03600	- 42.853
2	6	11.4	15.128	34.000	0.50	-504.2	-.03600	- 41.856
2	7	11.3	15.155	34.000	0.50	-483.7	-.03600	- 41.494
2	8	11.4	15.178	34.000	0.50	-423.5	-.03600	- 41.671
2	9	11.5	15.193	34.000	0.50	-327.5	-.03600	- 42.301
2	10	11.8	15.198	34.000	0.50	-202.4	-.03600	- 43.077
2	11	11.9	15.193	34.000	0.50	- 56.6	-.03600	- 43.472
2	12	11.9	15.176	34.000	0.50	99.9	-.03600	- 43.770
2	13	11.9	15.159	34.000	0.50	100.8	-.03600	- 43.658
2	14	11.8	15.143	34.000	0.50	100.8	-.03600	- 43.310
2	15	11.7	15.126	34.000	0.50	100.8	-.03600	- 42.844
2	16	11.5	15.110	34.000	0.50	100.8	-.03600	- 42.310
2	17	11.4	15.093	34.000	0.50	100.8	-.03600	- 41.845
2	18	11.3	15.067	34.000	0.50	100.8	-.03600	- 41.455
2	19	11.2	15.050	34.000	0.50	100.8	-.03600	- 41.171
2	20	11.2	15.033	34.000	0.50	100.8	-.03600	- 40.969
2	21	11.1	15.015	34.000	0.50	100.8	-.03600	- 40.850
2	22	11.1	14.998	34.000	0.50	100.8	-.03600	- 40.819
2	23	11.2	14.980	34.000	0.50	100.8	-.03600	- 40.881
2	24	11.2	14.935	34.000	0.50	100.8	-.03600	- 41.042

(a)

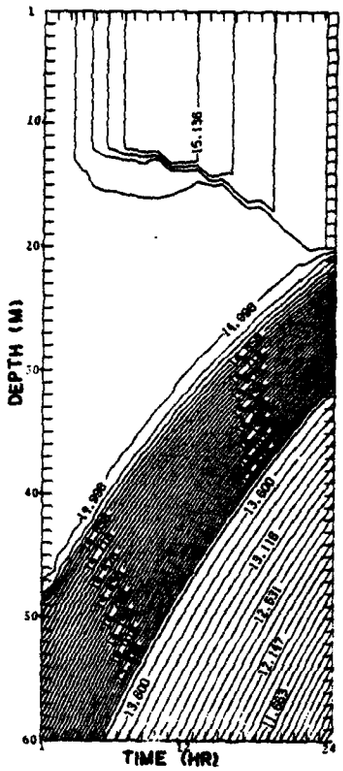

(b)

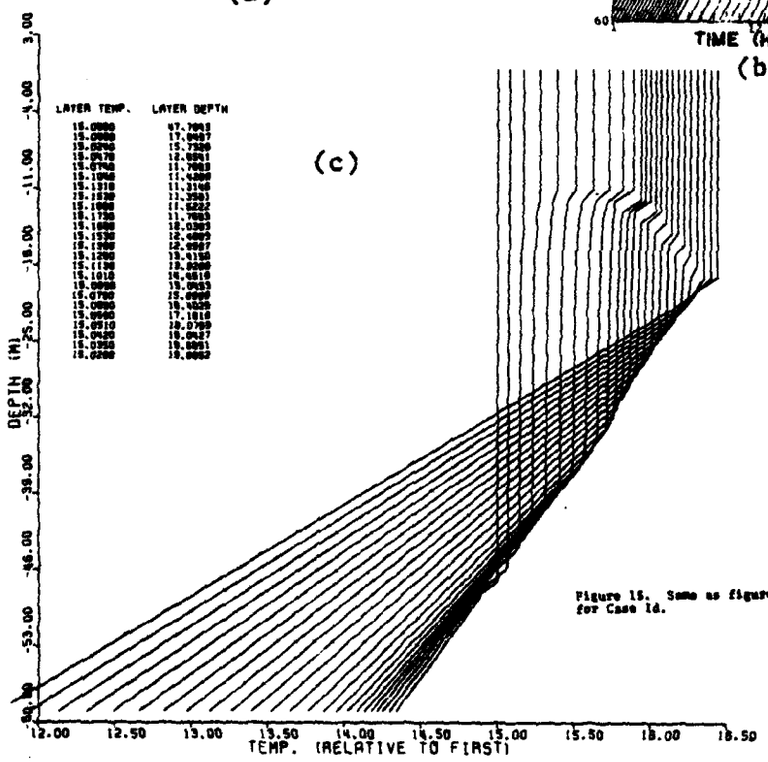

(c)

Figure 15. Same as figure (1), except for Case 1d.

DAY	HR	H	T	S	TAU	QUST	WDD	DS
1	1	6.3	14.956	34.000	0.50	- 1.5	0.0	0.0
1	2	7.3	14.939	34.000	0.50	-100.8	0.0	0.0
1	3	8.0	14.935	34.000	0.50	-184.3	0.0	0.0
1	4	8.5	14.930	34.000	0.50	-248.4	0.0	0.0
1	5	8.9	14.940	34.000	0.50	-288.7	0.0	0.0
1	6	9.2	14.958	34.000	0.50	-302.5	0.0	0.0
1	7	9.5	14.969	34.000	0.50	-288.9	0.0	0.0
1	8	9.8	14.976	34.000	0.50	-248.7	0.0	0.0
1	9	10.1	14.978	34.000	0.50	-184.7	0.0	0.0
1	10	10.4	14.974	34.000	0.50	-101.4	0.0	0.0
1	11	10.7	14.963	34.000	0.50	- 4.1	0.0	0.0
1	12	11.1	14.943	34.000	0.50	100.2	0.0	0.0
1	13	11.5	14.926	34.000	0.50	100.8	0.00932	10.704
1	14	12.1	14.909	34.000	0.50	100.8	0.01800	21.570
1	15	12.7	14.883	34.000	0.50	100.8	0.02546	32.065
1	16	13.5	14.879	34.000	0.50	100.8	0.03118	41.401
1	17	14.3	14.866	34.000	0.50	100.8	0.03477	48.730
1	18	15.1	14.852	34.000	0.50	100.8	0.03600	53.293
1	19	15.9	14.841	34.000	0.50	100.8	0.03477	54.315
1	20	16.7	14.831	34.000	0.50	100.8	0.03118	51.183
1	21	17.3	14.821	34.000	0.50	100.8	0.02546	43.605
1	22	17.9	14.811	34.000	0.50	100.8	0.01800	31.960
1	23	18.3	14.803	34.000	0.50	100.8	0.00932	15.987
1	24	18.5	14.793	34.000	0.50	100.8	0.0	0.0
2	1	18.7	14.798	34.000	0.50	- 1.5	0.0	0.0
2	2	18.9	14.792	34.000	0.50	-100.8	0.0	0.0
2	3	18.9	14.798	34.000	0.50	-184.3	0.0	0.0
2	4	19.0	14.807	34.000	0.50	-248.4	0.0	0.0
2	5	18.2	14.819	34.000	0.50	-288.7	0.0	0.0
2	6	17.6	14.832	34.000	0.50	-302.5	0.0	0.0
2	7	18.0	14.844	34.000	0.50	-288.9	0.0	0.0
2	8	18.2	14.853	34.000	0.50	-248.7	0.0	0.0
2	9	18.4	14.859	34.000	0.50	-184.7	0.0	0.0
2	10	18.6	14.861	34.000	0.50	-101.4	0.0	0.0
2	11	19.1	14.857	34.000	0.50	- 4.1	0.0	0.0
2	12	19.3	14.848	34.000	0.50	100.2	0.0	0.0
2	13	19.7	14.840	34.000	0.50	100.8	0.00932	18.275
2	14	20.3	14.832	34.000	0.50	100.8	0.01800	36.187
2	15	21.0	14.824	34.000	0.50	100.8	0.02546	52.868
2	16	21.9	14.817	34.000	0.50	100.8	0.03118	67.293
2	17	22.9	14.811	34.000	0.50	100.8	0.03477	78.276
2	18	23.9	14.803	34.000	0.50	100.8	0.03600	84.619
2	19	25.0	14.797	34.000	0.50	100.8	0.03477	85.298
2	20	25.9	14.792	34.000	0.50	100.8	0.03118	79.363
2	21	26.8	14.786	34.000	0.50	100.8	0.02546	67.239
2	22	27.4	14.781	34.000	0.50	100.8	0.01800	48.873
2	23	27.8	14.776	34.000	0.50	100.8	0.00932	25.790
2	24	28.0	14.771	34.000	0.50	100.8	0.0	0.0

(a)

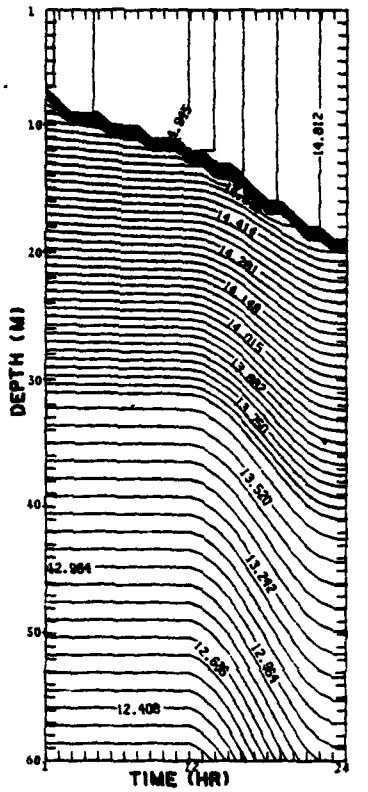

(b)

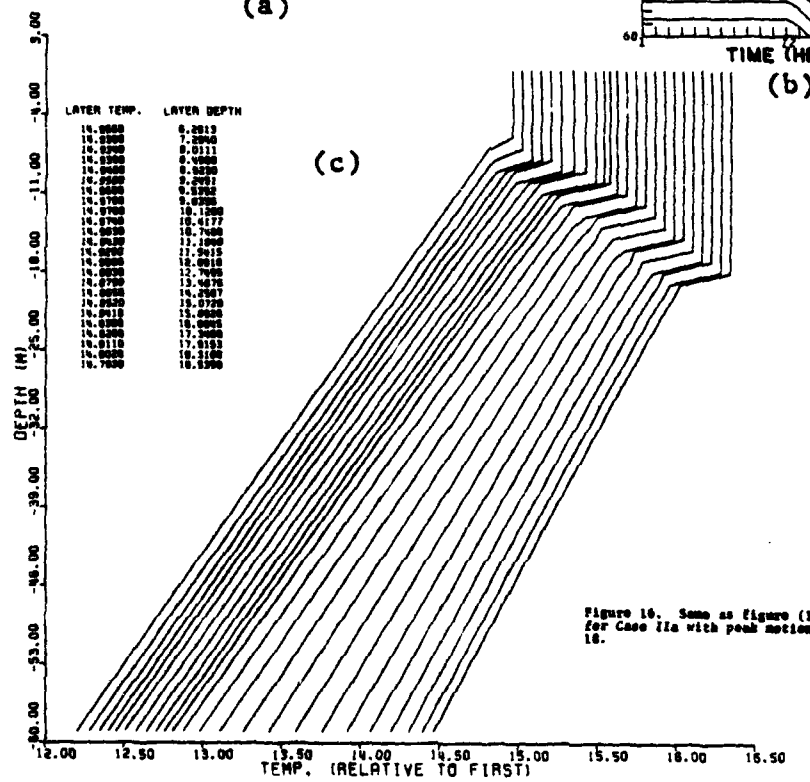

(c)

Figure 16. Same as figure (1), except for Case IIa with peak motion at hour 18.

DAY	HR	H	T	S	TAU	QNET	WDO	DH
1	1	6.5	14.956	34.000	0.50	- 3.8	0.03477	22.156
1	2	7.7	14.948	34.000	0.50	-100.8	0.03118	23.607
1	3	8.6	14.938	34.000	0.50	-184.2	0.02846	31.546
1	4	9.2	14.943	34.000	0.50	-248.4	0.01800	18.469
1	5	9.7	14.954	34.000	0.50	-288.7	0.00932	8.979
1	6	10.0	14.964	34.000	0.50	-302.5	0.0	0.0
1	7	10.3	14.975	34.000	0.50	-288.7	0.0	0.0
1	8	10.5	14.984	34.000	0.50	-248.7	0.0	0.0
1	9	10.8	14.987	34.000	0.50	-184.7	0.0	0.0
1	10	11.1	14.984	34.000	0.50	-101.1	0.0	0.0
1	11	11.4	14.974	34.000	0.50	- 4.1	0.0	0.0
1	12	11.8	14.956	34.000	0.50	100.2	0.0	0.0
1	13	12.2	14.940	34.000	0.50	100.8	0.0	0.0
1	14	12.5	14.924	34.000	0.50	100.8	0.0	0.0
1	15	12.8	14.909	34.000	0.50	100.8	0.0	0.0
1	16	13.1	14.895	34.000	0.50	100.8	0.0	0.0
1	17	13.4	14.881	34.000	0.50	100.8	0.0	0.0
1	18	13.8	14.867	34.000	0.50	100.8	0.0	0.0
1	19	14.2	14.854	34.000	0.50	100.8	0.00932	13.167
1	20	14.7	14.841	34.000	0.50	100.8	0.01800	26.290
1	21	15.4	14.830	34.000	0.50	100.8	0.02846	38.712
1	22	16.2	14.819	34.000	0.50	100.8	0.03118	49.581
1	23	17.0	14.808	34.000	0.50	100.8	0.03477	58.067
1	24	17.9	14.798	34.000	0.50	100.8	0.03600	63.132
2	1	18.7	14.795	34.000	0.50	- 3.8	0.03477	63.842
2	2	19.4	14.796	34.000	0.50	-100.8	0.03118	59.561
2	3	20.0	14.802	34.000	0.50	-184.2	0.02846	50.219
2	4	20.4	14.812	34.000	0.50	-248.4	0.01800	36.313
2	5	20.0	14.824	34.000	0.50	-288.7	0.00932	16.678
2	6	17.7	14.837	34.000	0.50	-302.5	0.0	0.0
2	7	18.2	14.848	34.000	0.50	-288.9	0.0	0.0
2	8	18.8	14.858	34.000	0.50	-248.7	0.0	0.0
2	9	19.3	14.864	34.000	0.50	-184.7	0.0	0.0
2	10	19.8	14.865	34.000	0.50	-101.1	0.0	0.0
2	11	20.2	14.863	34.000	0.50	- 4.1	0.0	0.0
2	12	20.5	14.853	34.000	0.50	100.2	0.0	0.0
2	13	20.8	14.846	34.000	0.50	100.8	0.0	0.0
2	14	21.1	14.839	34.000	0.50	100.8	0.0	0.0
2	15	21.3	14.831	34.000	0.50	100.8	0.0	0.0
2	16	21.5	14.824	34.000	0.50	100.8	0.0	0.0
2	17	21.7	14.818	34.000	0.50	100.8	0.0	0.0
2	18	21.9	14.809	34.000	0.50	100.8	0.0	0.0
2	19	22.2	14.802	34.000	0.50	100.8	0.00932	30.705
2	20	22.9	14.796	34.000	0.50	100.8	0.01800	48.866
2	21	23.7	14.790	34.000	0.50	100.8	0.02846	59.506
2	22	24.6	14.783	34.000	0.50	100.8	0.03118	75.477
2	23	25.6	14.778	34.000	0.50	100.8	0.03477	87.570
2	24	26.7	14.772	34.000	0.50	100.8	0.03600	94.494

(a)

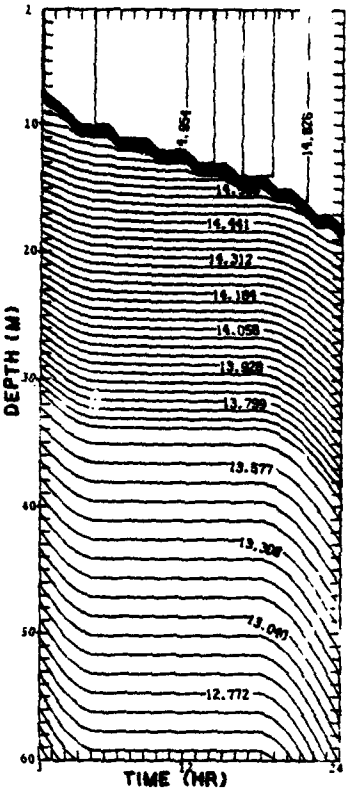

(b)

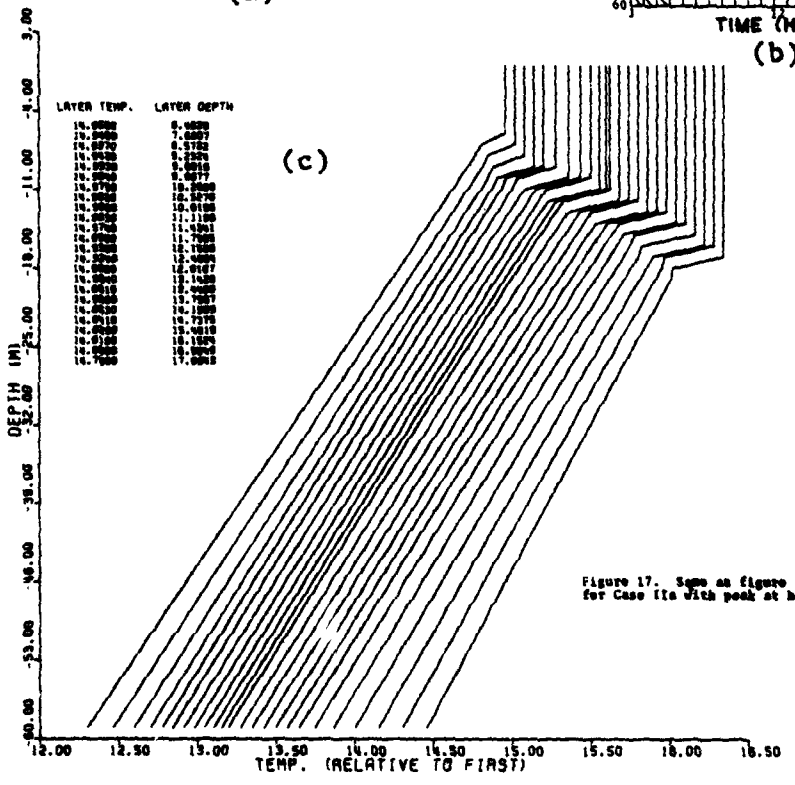

Figure 17. Same as figure (1), except for Case IIa with peak at hour 24.

DAY	HR	H	T	S	TAU	QFRT	WDO	DH
1	1	6.4	14.936	34.000	0.50	- 3.5	0.01800	11.371
1	2	7.6	14.940	34.000	0.50	-100.8	0.02546	18.896
1	3	8.5	14.937	34.000	0.50	-184.3	0.03118	26.072
1	4	9.3	14.942	34.000	0.50	-248.4	0.03477	31.702
1	5	10.1	14.953	34.000	0.50	-288.7	0.03600	35.360
1	6	10.8	14.963	34.000	0.50	-302.5	0.03477	36.784
1	7	11.4	14.974	34.000	0.50	-288.8	0.03118	36.961
1	8	11.9	14.983	34.000	0.50	-248.7	0.02546	35.977
1	9	12.4	14.988	34.000	0.50	-184.7	0.01800	33.893
1	10	12.8	14.986	34.000	0.50	-101.3	0.00932	31.037
1	11	13.1	14.979	34.000	0.50	- 4.1	0.0	0.0
1	12	13.4	14.964	34.000	0.50	100.2	0.0	0.0
1	13	13.7	14.951	34.000	0.50	100.8	0.0	0.0
1	14	14.0	14.938	34.000	0.50	100.8	0.0	0.0
1	15	14.3	14.924	34.000	0.50	100.8	0.0	0.0
1	16	14.6	14.913	34.000	0.50	100.8	0.0	0.0
1	17	15.0	14.902	34.000	0.50	100.8	0.0	0.0
1	18	15.2	14.888	34.000	0.50	100.8	0.0	0.0
1	19	15.5	14.878	34.000	0.50	100.8	0.0	0.0
1	20	15.8	14.867	34.000	0.50	100.8	0.0	0.0
1	21	16.1	14.857	34.000	0.50	100.8	0.0	0.0
1	22	16.3	14.847	34.000	0.50	100.8	0.0	0.0
1	23	16.6	14.837	34.000	0.50	100.8	0.0	0.0
1	24	17.0	14.826	34.000	0.50	100.8	0.00932	15.804
2	1	17.6	14.822	34.000	0.50	- 3.5	0.01800	31.355
2	2	18.2	14.823	34.000	0.50	-100.8	0.02546	45.744
2	3	18.9	14.829	34.000	0.50	-184.1	0.03118	57.962
2	4	19.6	14.838	34.000	0.50	-248.4	0.03477	66.985
2	5	20.7	14.851	34.000	0.50	-288.7	0.03600	69.982
2	6	20.1	14.864	34.000	0.50	-302.5	0.03477	61.851
2	7	19.0	14.876	34.000	0.50	-288.9	0.03118	58.628
2	8	20.1	14.885	34.000	0.50	-248.7	0.02546	50.426
2	9	21.2	14.891	34.000	0.50	-184.7	0.01800	37.889
2	10	22.3	14.893	34.000	0.50	-101.3	0.00932	20.646
2	11	22.5	14.891	34.000	0.50	- 4.1	0.0	0.0
2	12	22.9	14.883	34.000	0.50	100.2	0.0	0.0
2	13	23.2	14.876	34.000	0.50	100.8	0.0	0.0
2	14	23.4	14.870	34.000	0.50	100.8	0.0	0.0
2	15	23.7	14.864	34.000	0.50	100.8	0.0	0.0
2	16	23.9	14.858	34.000	0.50	100.8	0.0	0.0
2	17	24.2	14.852	34.000	0.50	100.8	0.0	0.0
2	18	24.3	14.845	34.000	0.50	100.8	0.0	0.0
2	19	24.5	14.840	34.000	0.50	100.8	0.0	0.0
2	20	24.7	14.834	34.000	0.50	100.8	0.0	0.0
2	21	24.9	14.828	34.000	0.50	100.8	0.0	0.0
2	22	25.1	14.822	34.000	0.50	100.8	0.0	0.0
2	23	25.1	14.817	34.000	0.50	100.8	0.0	0.0
2	24	25.7	14.811	34.000	0.50	100.8	0.0	0.0

(a)

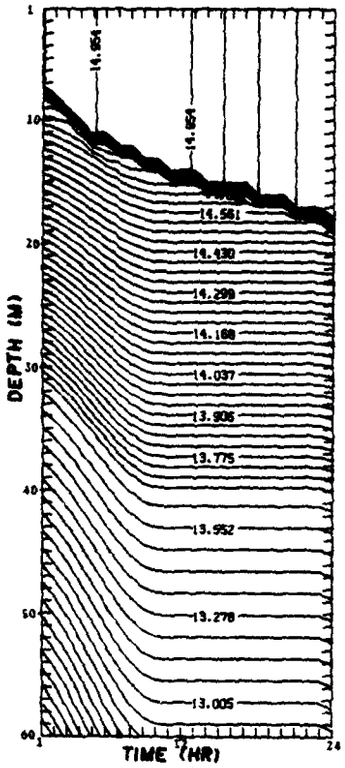

(b)

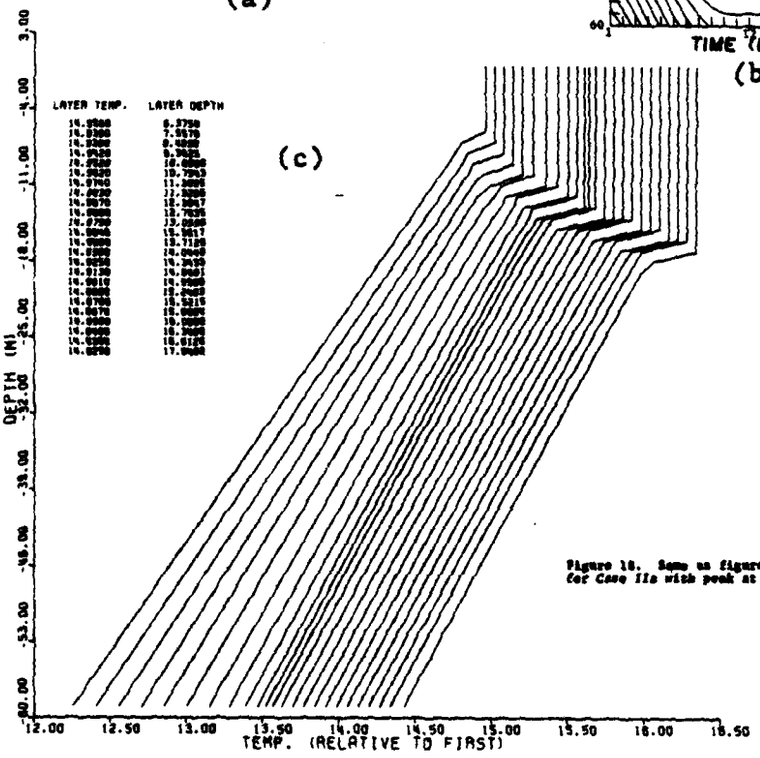

(c)

Figure 18. Same as figure (1), except for Case IIa with peak at hour 5.

DAY	HR	H	T	S	TAU	QNET	WSB	RH
1	1	49.5	15.081	34.000	0.50	- 55.7	0.0	0.0
1	2	18.1	15.009	34.000	0.50	-201.5	0.0	0.0
1	3	16.2	15.036	34.000	0.50	-326.8	0.0	0.0
1	4	13.0	15.067	34.000	0.50	-423.0	0.0	0.0
1	5	12.1	15.075	34.000	0.50	-483.5	0.0	0.0
1	6	11.8	15.105	34.000	0.50	-504.2	0.0	0.0
1	7	12.1	15.132	34.000	0.50	-483.7	0.0	0.0
1	8	12.5	15.154	34.000	0.50	-423.5	0.0	0.0
1	9	13.0	15.168	34.000	0.50	-327.5	0.0	0.0
1	10	13.5	15.175	34.000	0.50	-202.4	0.0	0.0
1	11	14.2	15.172	34.000	0.50	- 56.6	0.0	0.0
1	12	15.0	15.168	34.000	0.50	99.9	0.0	0.0
1	13	16.0	15.169	34.000	0.50	100.8	0.00932	14.969
1	14	17.2	15.139	34.000	0.50	100.8	0.01800	30.730
1	15	18.6	15.130	34.000	0.50	100.8	0.02546	46.786
1	16	20.0	15.122	34.000	0.50	100.8	0.03218	61.336
1	17	21.5	15.114	34.000	0.50	100.8	0.03477	73.399
1	18	23.1	15.107	34.000	0.50	100.8	0.03606	81.528
1	19	24.7	15.101	34.000	0.50	100.8	0.03477	86.247
1	20	26.2	15.096	34.000	0.50	100.8	0.03118	88.443
1	21	27.7	15.090	34.000	0.50	100.8	0.02546	89.511
1	22	28.9	15.086	34.000	0.50	100.8	0.01800	91.613
1	23	30.0	15.081	34.000	0.50	100.8	0.00932	27.799
1	24	30.8	15.077	34.000	0.50	100.8	0.0	0.0
2	1	31.1	15.077	34.000	0.50	- 55.7	0.0	0.0
2	2	21.0	15.088	34.000	0.50	-201.5	0.0	0.0
2	3	15.4	15.101	34.000	0.50	-326.8	0.0	0.0
2	4	13.1	15.123	34.000	0.50	-423.0	0.0	0.0
2	5	12.0	15.152	34.000	0.50	-483.5	0.0	0.0
2	6	11.7	15.181	34.000	0.50	-504.2	0.0	0.0
2	7	12.0	15.208	34.000	0.50	-483.7	0.0	0.0
2	8	12.4	15.231	34.000	0.50	-423.5	0.0	0.0
2	9	12.9	15.248	34.000	0.50	-327.5	0.0	0.0
2	10	13.4	15.251	34.000	0.50	-202.4	0.0	0.0
2	11	14.1	15.248	34.000	0.50	- 56.6	0.0	0.0
2	12	14.9	15.238	34.000	0.50	99.9	0.0	0.0
2	13	15.9	15.225	34.000	0.50	100.8	0.00932	14.752
2	14	17.0	15.215	34.000	0.50	100.8	0.01800	30.258
2	15	18.1	15.206	34.000	0.50	100.8	0.02546	46.032
2	16	19.4	15.198	34.000	0.50	100.8	0.03118	60.690
2	17	21.1	15.190	34.000	0.50	100.8	0.03477	72.794
2	18	22.9	15.183	34.000	0.50	100.8	0.03606	81.054
2	19	24.6	15.177	34.000	0.50	100.8	0.03477	83.923
2	20	26.2	15.172	34.000	0.50	100.8	0.03118	80.282
2	21	27.6	15.166	34.000	0.50	100.8	0.02546	69.677
2	22	28.9	15.162	34.000	0.50	100.8	0.01800	51.644
2	23	30.0	15.157	34.000	0.50	100.8	0.00932	27.833
2	24	30.8	15.153	34.000	0.50	100.8	0.0	0.0

(a)

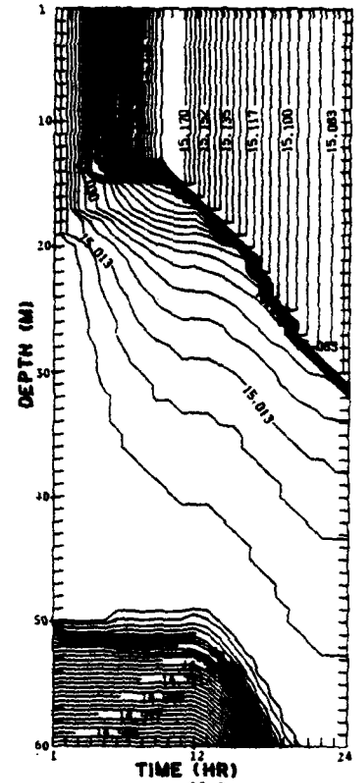

(b)

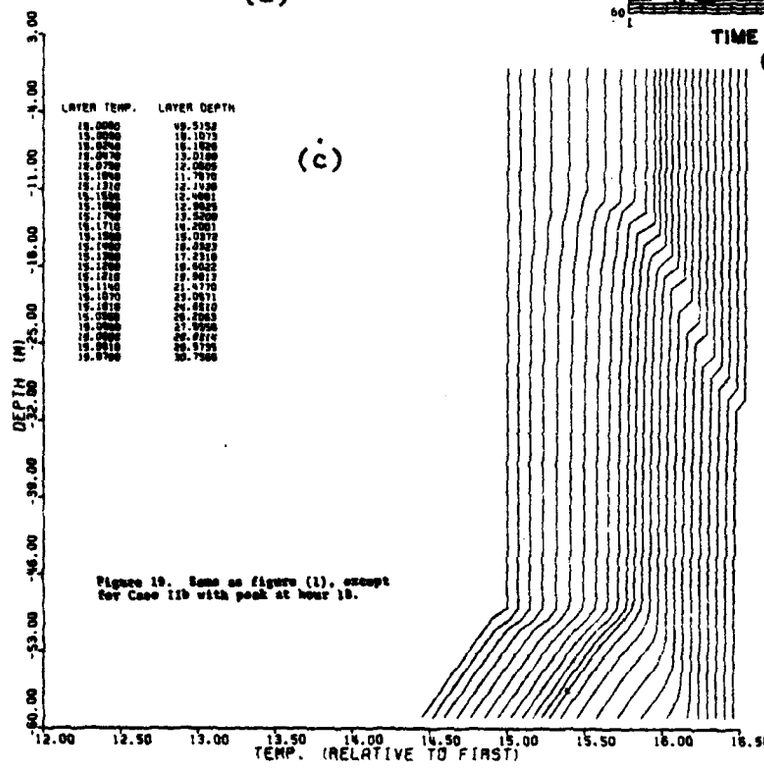

(c)

Figure 19. Same as figure (1), except for Case IIb with peak at hour 18.

DAY	HR	H	T	S	TAU	QNET	WND	DE
1	1	51.3	15.001	34.000	0.50	- 55.7	0.03477	175.207
1	2	18.5	15.089	34.000	0.50	-201.5	0.03118	56.784
1	3	16.5	15.024	34.000	0.50	-326.8	0.02546	61.448
1	4	13.2	15.048	34.000	0.50	-423.0	0.01800	23.522
1	5	12.1	15.076	34.000	0.50	-483.5	0.00932	11.257
1	6	11.8	15.101	34.000	0.50	-504.2	0.0	0.0
1	7	12.1	15.132	34.000	0.50	-483.7	0.0	0.0
1	8	12.5	15.184	34.000	0.50	-423.5	0.0	0.0
1	9	13.0	15.169	34.000	0.50	-327.5	0.0	0.0
1	10	12.6	15.175	34.000	0.50	-202.4	0.0	0.0
1	11	14.2	15.171	34.000	0.50	- 56.6	0.0	0.0
1	12	15.1	15.160	34.000	0.50	99.9	0.0	0.0
1	13	15.9	15.169	34.000	0.50	100.8	0.0	0.0
1	14	16.8	15.139	34.000	0.50	100.8	0.0	0.0
1	15	17.6	15.130	34.000	0.50	100.8	0.0	0.0
1	16	18.5	15.121	34.000	0.50	100.8	0.0	0.0
1	17	19.3	15.113	34.000	0.50	100.8	0.0	0.0
1	18	20.2	15.105	34.000	0.50	100.8	0.0	0.0
1	19	21.3	15.096	34.000	0.50	100.8	0.00932	19.714
1	20	22.5	15.091	34.000	0.50	100.8	0.01800	48.192
1	21	24.0	15.085	34.000	0.50	100.8	0.02546	60.364
1	22	25.7	15.079	34.000	0.50	100.8	0.03118	78.928
1	23	27.6	15.074	34.000	0.50	100.8	0.03477	94.207
1	24	29.5	15.069	34.000	0.50	100.8	0.03600	104.306
2	1	31.0	15.070	34.000	0.50	- 55.7	0.03477	106.008
2	2	21.7	15.077	34.000	0.50	-201.5	0.03118	68.710
2	3	15.6	15.093	34.000	0.50	-326.8	0.02546	39.216
2	4	13.3	15.116	34.000	0.50	-423.0	0.01800	23.782
2	5	12.1	15.144	34.000	0.50	-483.5	0.00932	11.182
2	6	11.7	15.173	34.000	0.50	-504.2	0.0	0.0
2	7	12.0	15.201	34.000	0.50	-483.7	0.0	0.0
2	8	12.4	15.223	34.000	0.50	-423.5	0.0	0.0
2	9	12.9	15.238	34.000	0.50	-327.5	0.0	0.0
2	10	13.5	15.244	34.000	0.50	-202.4	0.0	0.0
2	11	14.2	15.241	34.000	0.50	- 56.6	0.0	0.0
2	12	15.0	15.229	34.000	0.50	99.9	0.0	0.0
2	13	15.8	15.218	34.000	0.50	100.8	0.0	0.0
2	14	16.7	15.208	34.000	0.50	100.8	0.0	0.0
2	15	17.5	15.198	34.000	0.50	100.8	0.0	0.0
2	16	18.3	15.189	34.000	0.50	100.8	0.0	0.0
2	17	19.2	15.181	34.000	0.50	100.8	0.0	0.0
2	18	20.1	15.173	34.000	0.50	100.8	0.0	0.0
2	19	21.2	15.166	34.000	0.50	100.8	0.00932	19.677
2	20	22.5	15.159	34.000	0.50	100.8	0.01800	48.216
2	21	24.1	15.153	34.000	0.50	100.8	0.02546	60.511
2	22	25.8	15.147	34.000	0.50	100.8	0.03118	79.246
2	23	27.7	15.142	34.000	0.50	100.8	0.03477	94.597
2	24	29.6	15.137	34.000	0.50	100.8	0.03600	104.837

(a)

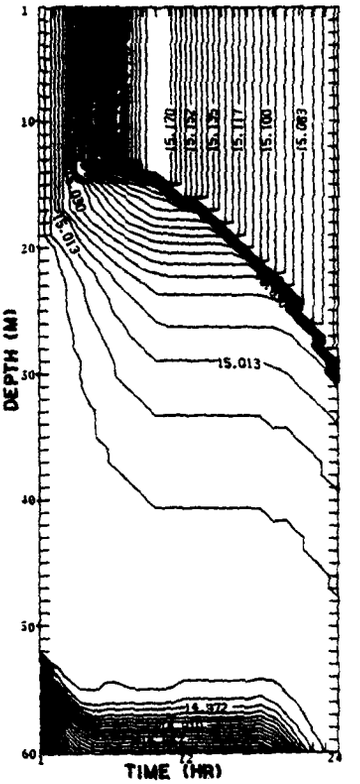

(b)

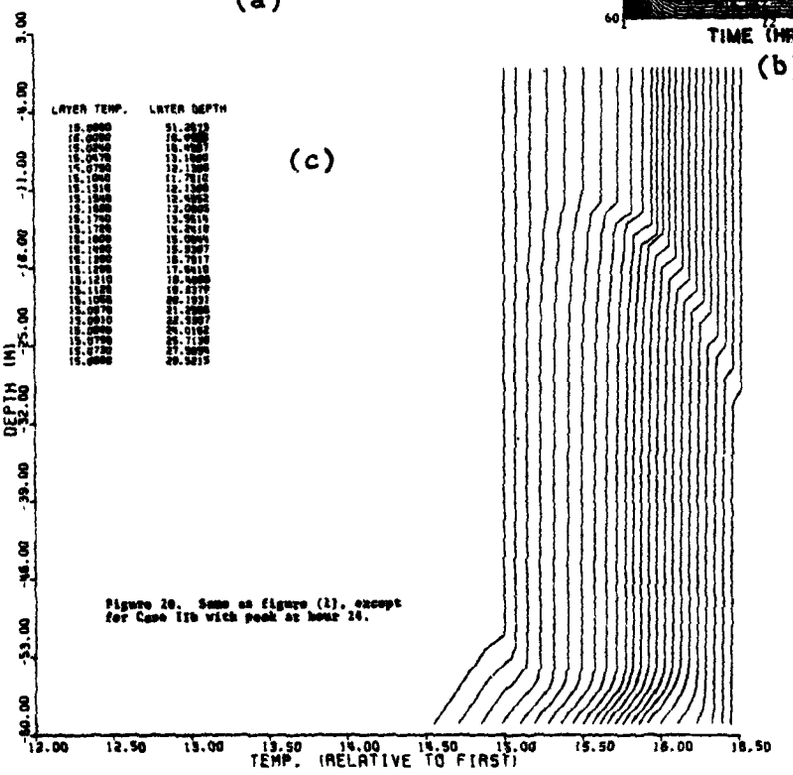

(c)

Figure 20. Same as figure (1), except for Case IIb with peak at hour 24.

DAY	HR	H	T	S	TAU	QNET	WND	DH
1	1	30.4	15.001	34.000	0.50	- 55.7	0.01800	89.930
1	2	18.5	15.000	34.000	0.50	-201.5	0.02546	46.448
1	3	16.6	15.024	34.000	0.50	-326.8	0.03118	50.926
1	4	13.4	15.048	34.000	0.50	-423.0	0.03477	45.750
1	5	12.4	15.076	34.000	0.50	-483.5	0.03600	43.936
1	6	12.1	15.105	34.000	0.50	-504.2	0.03477	41.376
1	7	12.6	15.133	34.000	0.50	-483.7	0.03118	38.787
1	8	13.3	15.155	34.000	0.50	-423.5	0.02546	33.483
1	9	14.1	15.169	34.000	0.50	-327.5	0.01800	25.150
1	10	14.9	15.176	34.000	0.50	-202.4	0.00932	13.852
1	11	15.6	15.174	34.000	0.50	- 56.6	0.0	0.0
1	12	16.5	15.163	34.000	0.50	99.9	0.0	0.0
1	13	17.3	15.156	34.000	0.50	100.8	0.0	0.0
1	14	18.1	15.148	34.000	0.50	100.8	0.0	0.0
1	15	18.9	15.136	34.000	0.50	100.8	0.0	0.0
1	16	19.7	15.128	34.000	0.50	100.8	0.0	0.0
1	17	20.5	15.121	34.000	0.50	100.8	0.0	0.0
1	18	21.4	15.114	34.000	0.50	100.8	0.0	0.0
1	19	22.2	15.107	34.000	0.50	100.8	0.0	0.0
1	20	23.0	15.100	34.000	0.50	100.8	0.0	0.0
1	21	23.9	15.094	34.000	0.50	100.8	0.0	0.0
1	22	24.7	15.089	34.000	0.50	100.8	0.0	0.0
1	23	25.6	15.083	34.000	0.50	100.8	0.0	0.0
1	24	26.7	15.078	34.000	0.50	100.8	0.00932	24.743
2	1	27.6	15.078	34.000	0.50	- 55.7	0.01800	49.312
2	2	22.6	15.085	34.000	0.50	-201.5	0.02546	56.700
2	3	15.5	15.101	34.000	0.50	-326.8	0.03118	47.578
2	4	13.6	15.124	34.000	0.50	-423.0	0.03477	46.611
2	5	12.3	15.152	34.000	0.50	-483.5	0.03600	43.595
2	6	12.1	15.182	34.000	0.50	-504.2	0.03477	41.268
2	7	12.5	15.210	34.000	0.50	-483.7	0.03118	38.260
2	8	13.2	15.232	34.000	0.50	-423.5	0.02546	33.120
2	9	14.0	15.247	34.000	0.50	-327.5	0.01800	24.907
2	10	14.7	15.253	34.000	0.50	-202.4	0.00932	13.616
2	11	15.4	15.251	34.000	0.50	- 56.6	0.0	0.0
2	12	16.2	15.241	34.000	0.50	99.9	0.0	0.0
2	13	17.1	15.231	34.000	0.50	100.8	0.0	0.0
2	14	17.9	15.222	34.000	0.50	100.8	0.0	0.0
2	15	18.7	15.213	34.000	0.50	100.8	0.0	0.0
2	16	19.5	15.205	34.000	0.50	100.8	0.0	0.0
2	17	20.3	15.197	34.000	0.50	100.8	0.0	0.0
2	18	21.1	15.190	34.000	0.50	100.8	0.0	0.0
2	19	22.0	15.183	34.000	0.50	100.8	0.0	0.0
2	20	22.8	15.177	34.000	0.50	100.8	0.0	0.0
2	21	23.7	15.171	34.000	0.50	100.8	0.0	0.0
2	22	24.6	15.165	34.000	0.50	100.8	0.0	0.0
2	23	25.5	15.159	34.000	0.50	100.8	0.0	0.0
2	24	26.7	15.154	34.000	0.50	100.8	0.00932	24.791

(a)

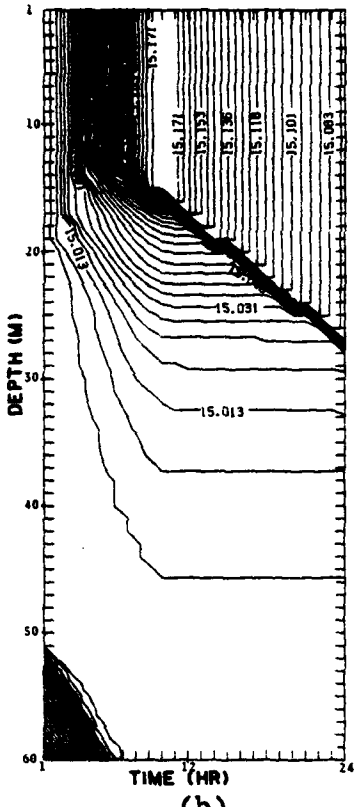

(b)

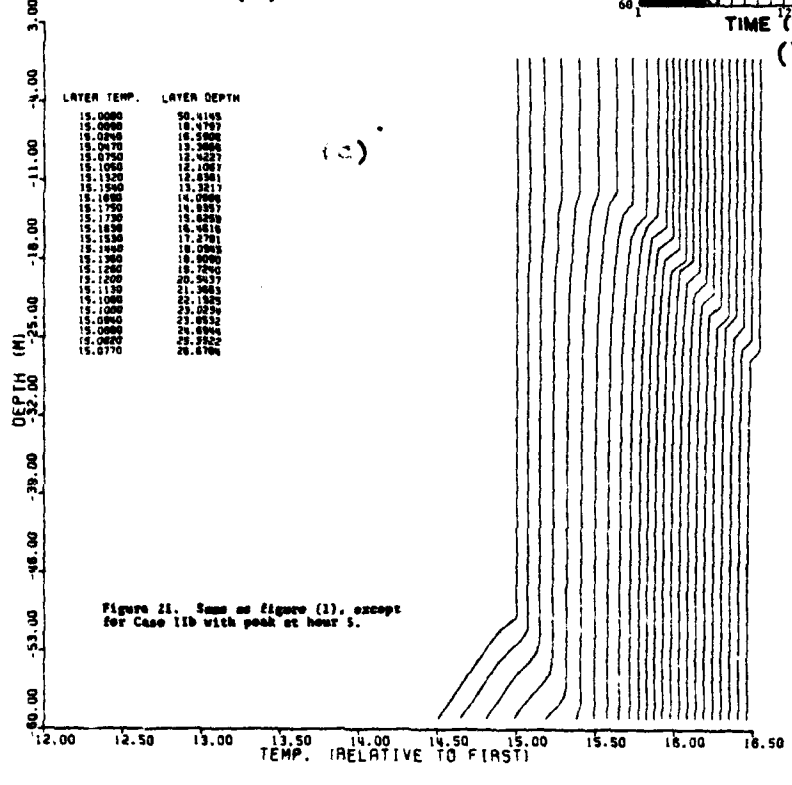

(c)

Figure 21. Same as figure (1), except for Case IIb with peak at hour 5.

DAY	HR	H	T	S	TAU	QNET	WDD	QE
1	1	6.0	14.954	34.000	0.50	- 3.5	-.03477	-21.398
1	2	6.9	14.937	34.000	0.50	-100.8	-.03118	-21.939
1	3	7.4	14.932	34.000	0.50	-184.3	-.02546	-19.111
1	4	7.9	14.934	34.000	0.50	-248.4	-.01800	-14.295
1	5	8.2	14.943	34.000	0.50	-288.7	-.00932	- 7.661
1	6	8.5	14.950	34.000	0.50	-302.5	0.0	0.0
1	7	8.9	14.960	34.000	0.50	-288.9	0.0	0.0
1	8	9.2	14.966	34.000	0.50	-248.7	0.0	0.0
1	9	9.5	14.967	34.000	0.50	-184.7	0.0	0.0
1	10	9.8	14.962	34.000	0.50	-101.3	0.0	0.0
1	11	10.1	14.949	34.000	0.50	- 4.1	0.0	0.0
1	12	10.4	14.927	34.000	0.50	100.2	0.0	0.0
1	13	10.8	14.900	34.000	0.50	100.8	0.0	0.0
1	14	11.1	14.869	34.000	0.50	100.8	0.0	0.0
1	15	11.4	14.871	34.000	0.50	100.8	0.0	0.0
1	16	11.7	14.854	34.000	0.50	100.8	0.0	0.0
1	17	12.0	14.838	34.000	0.50	100.8	0.0	0.0
1	18	12.3	14.821	34.000	0.50	100.8	0.0	0.0
1	19	12.5	14.806	34.000	0.50	100.8	-.00932	-11.687
1	20	12.5	14.791	34.000	0.50	100.8	-.01800	-22.791
1	21	12.5	14.776	34.000	0.50	100.8	-.02546	-32.299
1	22	12.4	14.761	34.000	0.50	100.8	-.03118	-39.426
1	23	12.3	14.746	34.000	0.50	100.8	-.03477	-43.687
1	24	12.2	14.727	34.000	0.50	100.8	-.03600	-44.903
2	1	12.2	14.719	34.000	0.50	- 3.5	-.03477	-43.006
2	2	12.1	14.717	34.000	0.50	-100.8	-.03118	-38.216
2	3	12.0	14.721	34.000	0.50	-184.3	-.02546	-30.974
2	4	12.0	14.730	34.000	0.50	-248.4	-.01800	-21.820
2	5	12.1	14.742	34.000	0.50	-288.7	-.00932	-11.317
2	6	12.3	14.749	34.000	0.50	-302.5	0.0	0.0
2	7	12.4	14.761	34.000	0.50	-288.9	0.0	0.0
2	8	12.6	14.770	34.000	0.50	-248.7	0.0	0.0
2	9	12.8	14.774	34.000	0.50	-184.7	0.0	0.0
2	10	13.0	14.774	34.000	0.50	-101.3	0.0	0.0
2	11	13.2	14.766	34.000	0.50	- 4.1	0.0	0.0
2	12	13.4	14.750	34.000	0.50	100.2	0.0	0.0
2	13	13.6	14.736	34.000	0.50	100.8	0.0	0.0
2	14	13.7	14.723	34.000	0.50	100.8	0.0	0.0
2	15	13.9	14.710	34.000	0.50	100.8	0.0	0.0
2	16	14.1	14.697	34.000	0.50	100.8	0.0	0.0
2	17	14.2	14.684	34.000	0.50	100.8	0.0	0.0
2	18	14.4	14.670	34.000	0.50	100.8	0.0	0.0
2	19	14.4	14.658	34.000	0.50	100.8	-.00932	-13.497
2	20	14.3	14.645	34.000	0.50	100.8	-.01800	-26.005
2	21	14.1	14.633	34.000	0.50	100.8	-.02546	-36.198
2	22	13.8	14.620	34.000	0.50	100.8	-.03118	-43.655
2	23	13.5	14.607	34.000	0.50	100.8	-.03477	-47.921
2	24	13.2	14.592	34.000	0.50	100.8	-.03600	-48.452

(a)

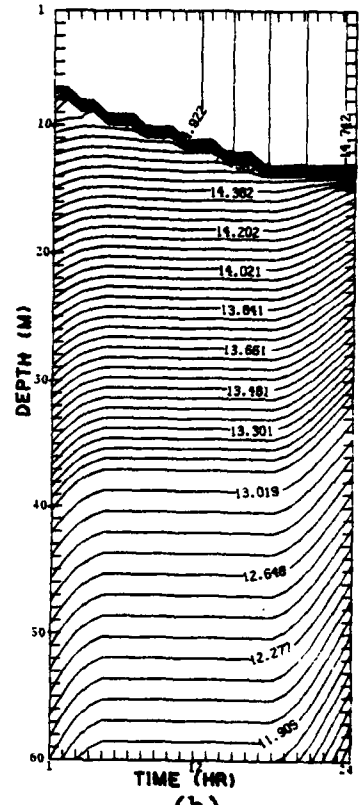

(b)

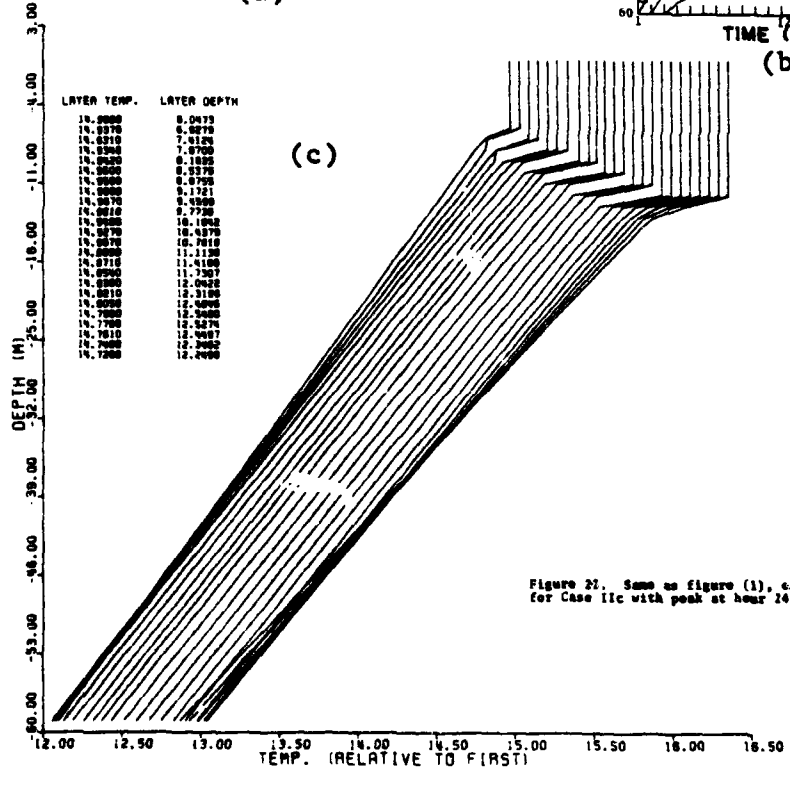

Figure 21. Same as figure (1), except for Case IIc with peak at hour 14.

AD-A120 396 NAVAL POSTGRADUATE SCHOOL MONTEREY CA F/G 8/3
OCEANIC MIXED LAYER RESPONSE TO TIDAL PERIOD INTERNAL WAVE MOTI--ETC(U)
JUN 82 R J BURGER

UNCLASSIFIED NL

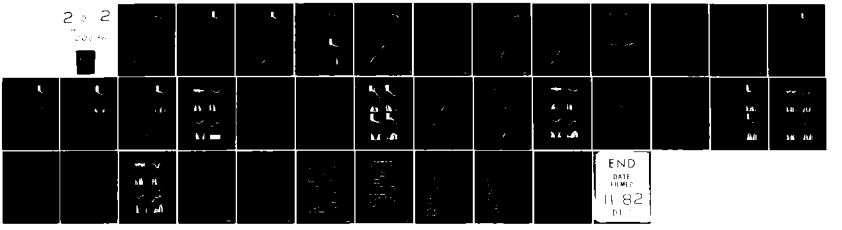

DAY	HR	Z	T	S	TAU	QUEST	WDO	DO
1	1	6.1	14.956	34.000	0.50	- 3.5	-.01800	-11.170
1	2	7.0	14.938	34.000	0.50	-100.8	-.02546	-18.121
1	3	7.5	14.933	34.000	0.50	-184.3	-.03118	-23.828
1	4	7.8	14.936	34.000	0.50	-248.4	-.03477	-27.773
1	5	8.0	14.944	34.000	0.50	-288.7	-.03600	-29.128
1	6	8.0	14.952	34.000	0.50	-302.5	-.03477	-28.357
1	7	8.1	14.960	34.000	0.50	-288.9	-.03118	-25.696
1	8	8.2	14.965	34.000	0.50	-248.7	-.02546	-21.259
1	9	8.5	14.964	34.000	0.50	-184.7	-.01800	-15.307
1	10	8.8	14.956	34.000	0.50	-101.3	-.00932	- 8.241
1	11	9.2	14.940	34.000	0.50	- 4.1	0.0	0.0
1	12	9.5	14.914	34.000	0.50	100.2	0.0	0.0
1	13	9.9	14.888	34.000	0.50	100.8	0.0	0.0
1	14	10.2	14.871	34.000	0.50	100.8	0.0	0.0
1	15	10.5	14.851	34.000	0.50	100.8	0.0	0.0
1	16	10.8	14.831	34.000	0.50	100.8	0.0	0.0
1	17	11.1	14.813	34.000	0.50	100.8	0.0	0.0
1	18	11.4	14.793	34.000	0.50	100.8	0.0	0.0
1	19	11.7	14.776	34.000	0.50	100.8	0.0	0.0
1	20	11.9	14.760	34.000	0.50	100.8	0.0	0.0
1	21	12.2	14.744	34.000	0.50	100.8	0.0	0.0
1	22	12.4	14.728	34.000	0.50	100.8	0.0	0.0
1	23	12.7	14.713	34.000	0.50	100.8	0.0	0.0
1	24	12.8	14.696	34.000	0.50	100.8	-.00932	-12.035
2	1	12.8	14.689	34.000	0.50	- 3.5	-.01800	-23.311
2	2	12.7	14.688	34.000	0.50	-100.8	-.02546	-32.680
2	3	12.4	14.693	34.000	0.50	-184.3	-.03118	-39.327
2	4	12.1	14.702	34.000	0.50	-248.4	-.03477	-42.847
2	5	11.8	14.714	34.000	0.50	-288.7	-.03600	-43.202
2	6	11.5	14.725	34.000	0.50	-302.5	-.03477	-40.651
2	7	11.3	14.737	34.000	0.50	-288.9	-.03118	-35.629
2	8	11.1	14.745	34.000	0.50	-248.7	-.02546	-28.620
2	9	11.1	14.749	34.000	0.50	-184.7	-.01800	-20.084
2	10	11.1	14.746	34.000	0.50	-101.3	-.00932	-10.427
2	11	11.4	14.736	34.000	0.50	- 4.1	0.0	0.0
2	12	11.6	14.713	34.000	0.50	100.2	0.0	0.0
2	13	11.8	14.696	34.000	0.50	100.8	0.0	0.0
2	14	12.1	14.680	34.000	0.50	100.8	0.0	0.0
2	15	12.3	14.664	34.000	0.50	100.8	0.0	0.0
2	16	12.4	14.648	34.000	0.50	100.8	0.0	0.0
2	17	12.6	14.633	34.000	0.50	100.8	0.0	0.0
2	18	12.8	14.615	34.000	0.50	100.8	0.0	0.0
2	19	13.0	14.600	34.000	0.50	100.8	0.0	0.0
2	20	13.2	14.586	34.000	0.50	100.8	0.0	0.0
2	21	13.3	14.572	34.000	0.50	100.8	0.0	0.0
2	22	13.5	14.558	34.000	0.50	100.8	0.0	0.0
2	23	13.7	14.544	34.000	0.50	100.8	0.0	0.0
2	24	13.7	14.528	34.000	0.50	100.8	-.00932	-12.033

(a)

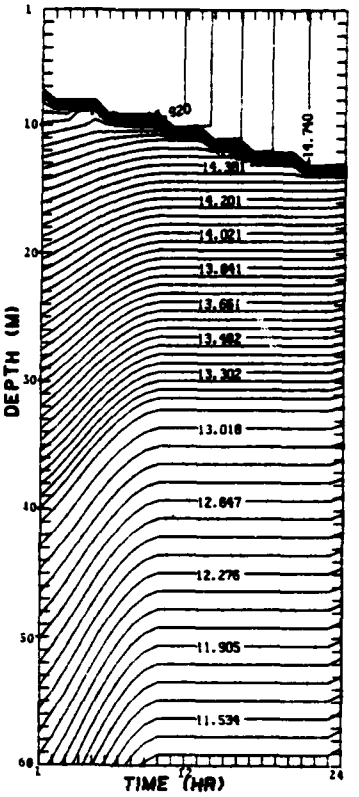

(b)

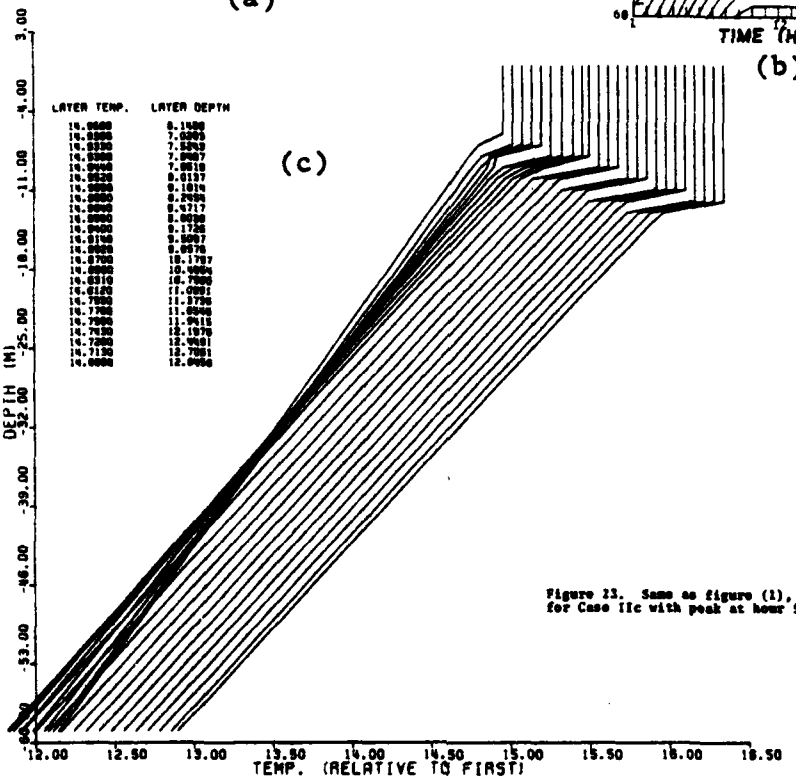

(c)

Figure 23. Same as figure (1), except for Case IIc with peak at hour 5.

DAY	HR	K	T	S	TAU	QNET	WDD	DE
1	1	47.8	15.001	34.000	0.50	- 55.7	-.03477	-169.223
1	2	17.7	15.009	34.000	0.50	-201.5	-.03118	- 56.143
1	3	15.9	15.024	34.000	0.50	-326.8	-.02546	- 40.938
1	4	12.9	15.047	34.000	0.50	-423.0	-.01800	- 23.364
1	5	12.0	15.075	34.000	0.50	-483.5	-.00932	- 11.218
1	6	11.8	15.106	34.000	0.50	-504.2	-.00000	- 0.000
1	7	12.1	15.131	34.000	0.50	-483.7	0.0	0.0
1	8	12.5	15.153	34.000	0.50	-423.5	0.0	0.0
1	9	12.9	15.168	34.000	0.50	-327.5	0.0	0.0
1	10	13.5	15.174	34.000	0.50	-202.4	0.0	0.0
1	11	14.1	15.171	34.000	0.50	- 56.6	0.0	0.0
1	12	15.0	15.159	34.000	0.50	99.9	0.0	0.0
1	13	15.8	15.148	34.000	0.50	100.8	0.0	0.0
1	14	16.6	15.138	34.000	0.50	100.8	0.0	0.0
1	15	17.4	15.128	34.000	0.50	100.8	0.0	0.0
1	16	18.2	15.119	34.000	0.50	100.8	0.0	0.0
1	17	19.0	15.111	34.000	0.50	100.8	0.0	0.0
1	18	19.9	15.103	34.000	0.50	100.8	0.0	0.0
1	19	20.6	15.095	34.000	0.50	100.8	-.00932	- 19.256
1	20	21.1	15.088	34.000	0.50	100.8	-.01800	- 38.331
1	21	21.5	15.082	34.000	0.50	100.8	-.02546	- 55.477
1	22	21.8	15.075	34.000	0.50	100.8	-.03118	- 69.136
1	23	22.1	15.068	34.000	0.50	100.8	-.03477	- 78.296
1	24	22.5	15.062	34.000	0.50	100.8	-.03600	- 82.402
2	1	22.4	15.062	34.000	0.50	- 55.7	-.03477	- 79.400
2	2	21.9	15.069	34.000	0.50	-201.5	-.03118	- 69.231
2	3	14.8	15.085	34.000	0.50	-326.8	-.02546	- 38.163
2	4	13.0	15.108	34.000	0.50	-423.0	-.01800	- 23.687
2	5	11.9	15.136	34.000	0.50	-483.5	-.00932	- 11.136
2	6	11.8	15.165	34.000	0.50	-504.2	-.00000	- 0.000
2	7	12.1	15.192	34.000	0.50	-483.7	0.0	0.0
2	8	12.4	15.214	34.000	0.50	-423.7	0.0	0.0
2	9	12.9	15.229	34.000	0.50	-327.5	0.0	0.0
2	10	13.4	15.235	34.000	0.50	-202.4	0.0	0.0
2	11	14.1	15.232	34.000	0.50	- 56.6	0.0	0.0
2	12	14.9	15.220	34.000	0.50	99.9	0.0	0.0
2	13	15.7	15.209	34.000	0.50	100.8	0.0	0.0
2	14	16.5	15.199	34.000	0.50	100.8	0.0	0.0
2	15	17.3	15.189	34.000	0.50	100.8	0.0	0.0
2	16	18.2	15.180	34.000	0.50	100.8	0.0	0.0
2	17	19.0	15.172	34.000	0.50	100.8	0.0	0.0
2	18	19.8	15.163	34.000	0.50	100.8	0.0	0.0
2	19	20.4	15.156	34.000	0.50	100.8	-.00932	- 19.065
2	20	20.7	15.149	34.000	0.50	100.8	-.01800	- 37.614
2	21	20.8	15.142	34.000	0.50	100.8	-.02546	- 53.606
2	22	20.8	15.136	34.000	0.50	100.8	-.03118	- 63.729
2	23	20.7	15.127	34.000	0.50	100.8	-.03477	- 73.101
2	24	20.6	15.120	34.000	0.50	100.8	-.03600	- 75.372

(a)

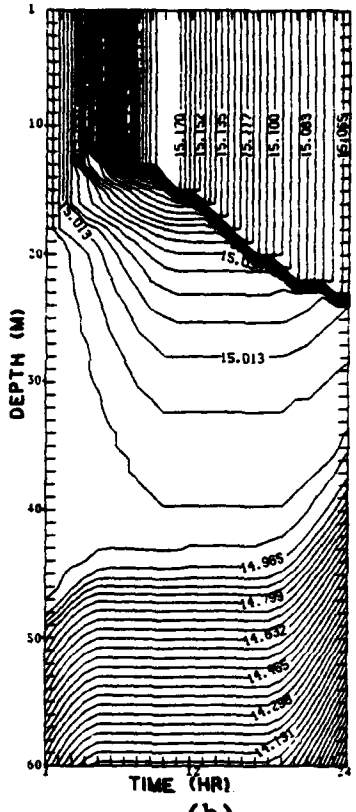

(b)

LAYER TEMP.	LAYER DEPTH
15.0000	47.6230
15.0088	17.7267
15.0848	15.8778
15.0170	12.8821
15.0790	11.9836
15.1068	11.7827
15.1310	12.1353
15.1530	12.4811
15.1908	12.8968
15.1768	13.4766
15.1710	14.1482
15.1590	14.8758
15.1488	15.7987
15.1378	16.5872
15.1288	17.4042
15.1198	18.2178
15.1100	19.0480
15.1020	19.8626
15.0950	20.5737
15.0888	21.1040
15.0810	21.5179
15.0748	21.8317
15.0688	22.1271
15.0620	22.4080

(c)

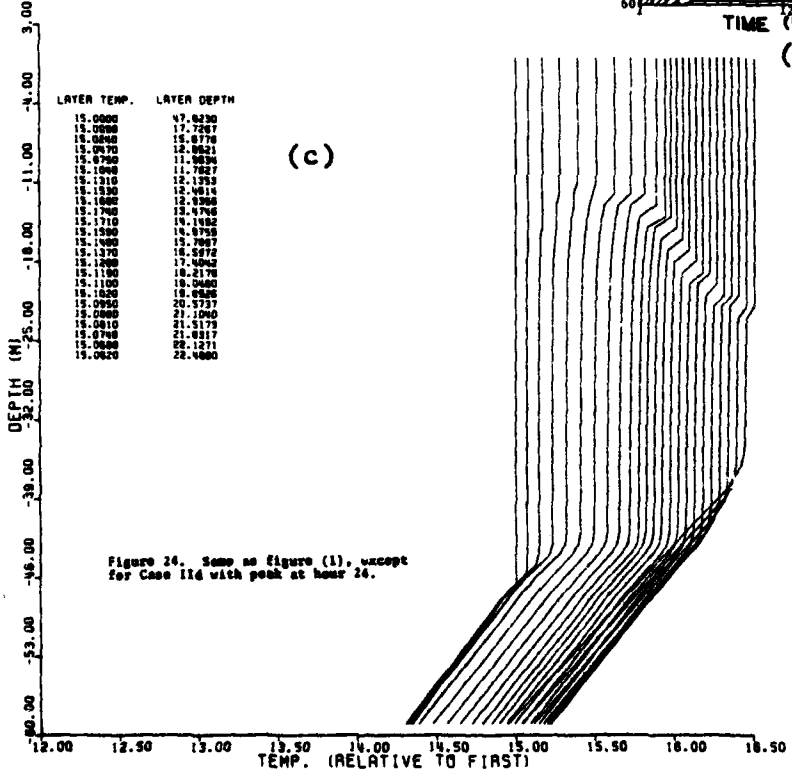

Figure 24. Same as figure (1), except for Case IId with peak at hour 24.

DAY	HR	K	T	S	TAU	QNET	UDD	DB
1	1	40.6	15.001	34.000	0.50	- 55.7	-.01800	-88.332
1	2	17.7	15.009	34.000	0.50	-201.5	-.02546	-45.748
1	3	15.8	15.024	34.000	0.50	-326.8	-.03118	-49.982
1	4	12.7	15.047	34.000	0.50	-423.0	-.03477	-44.793
1	5	11.7	15.075	34.000	0.50	-483.5	-.03600	-42.914
1	6	11.4	15.104	34.000	0.50	-504.2	-.03477	-40.463
1	7	11.4	15.131	34.000	0.50	-483.7	-.03118	-36.036
1	8	11.5	15.154	34.000	0.50	-423.5	-.02546	-29.723
1	9	11.9	15.168	34.000	0.50	-327.5	-.01800	-21.547
1	10	12.3	15.174	34.000	0.50	-202.4	-.00932	-11.538
1	11	13.0	15.170	34.000	0.50	- 56.6	0.0	0.0
1	12	13.9	15.156	34.000	0.50	99.9	0.0	0.0
1	13	14.7	15.144	34.000	0.50	100.8	0.0	0.0
1	14	15.5	15.133	34.000	0.50	100.8	0.0	0.0
1	15	16.4	15.122	34.000	0.50	100.8	0.0	0.0
1	16	17.3	15.113	34.000	0.50	100.8	0.0	0.0
1	17	18.2	15.104	34.000	0.50	100.8	0.0	0.0
1	18	19.1	15.095	34.000	0.50	100.8	0.0	0.0
1	19	20.1	15.087	34.000	0.50	100.8	0.0	0.0
1	20	21.1	15.080	34.000	0.50	100.8	0.0	0.0
1	21	22.1	15.073	34.000	0.50	100.8	0.0	0.0
1	22	23.2	15.067	34.000	0.50	100.8	0.0	0.0
1	23	24.3	15.061	34.000	0.50	100.8	0.0	0.0
1	24	25.2	15.055	34.000	0.50	100.8	-.00932	-23.635
2	1	25.5	15.056	34.000	0.50	- 55.7	-.01800	-46.285
2	2	22.1	15.063	34.000	0.50	-201.5	-.02546	-57.014
2	3	14.7	15.079	34.000	0.50	-326.8	-.03118	-46.435
2	4	12.9	15.101	34.000	0.50	-423.0	-.03477	-45.491
2	5	11.6	15.129	34.000	0.50	-483.5	-.03600	-42.599
2	6	11.2	15.159	34.000	0.50	-504.2	-.03477	-39.717
2	7	11.3	15.186	34.000	0.50	-483.7	-.03118	-35.651
2	8	11.5	15.209	34.000	0.50	-423.5	-.02546	-29.523
2	9	11.8	15.223	34.000	0.50	-327.5	-.01800	-21.473
2	10	12.3	15.229	34.000	0.50	-202.4	-.00932	-11.486
2	11	13.0	15.225	34.000	0.50	- 56.6	0.0	0.0
2	12	13.8	15.211	34.000	0.50	99.9	0.0	0.0
2	13	14.6	15.199	34.000	0.50	100.8	0.0	0.0
2	14	15.5	15.187	34.000	0.50	100.8	0.0	0.0
2	15	16.4	15.177	34.000	0.50	100.8	0.0	0.0
2	16	17.3	15.167	34.000	0.50	100.8	0.0	0.0
2	17	18.2	15.158	34.000	0.50	100.8	0.0	0.0
2	18	19.0	15.150	34.000	0.50	100.8	0.0	0.0
2	19	19.7	15.142	34.000	0.50	100.8	0.0	0.0
2	20	20.5	15.134	34.000	0.50	100.8	0.0	0.0
2	21	21.1	15.127	34.000	0.50	100.8	0.0	0.0
2	22	21.8	15.120	34.000	0.50	100.8	0.0	0.0
2	23	22.5	15.113	34.000	0.50	100.8	0.0	0.0
2	24	22.9	15.107	34.000	0.50	100.8	-.00932	-21.475

(a)

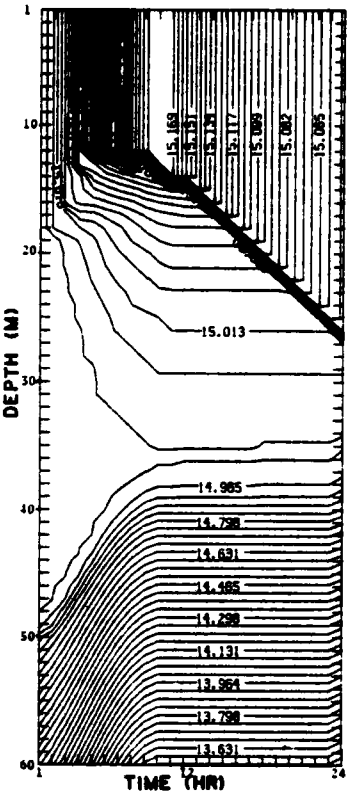

(b)

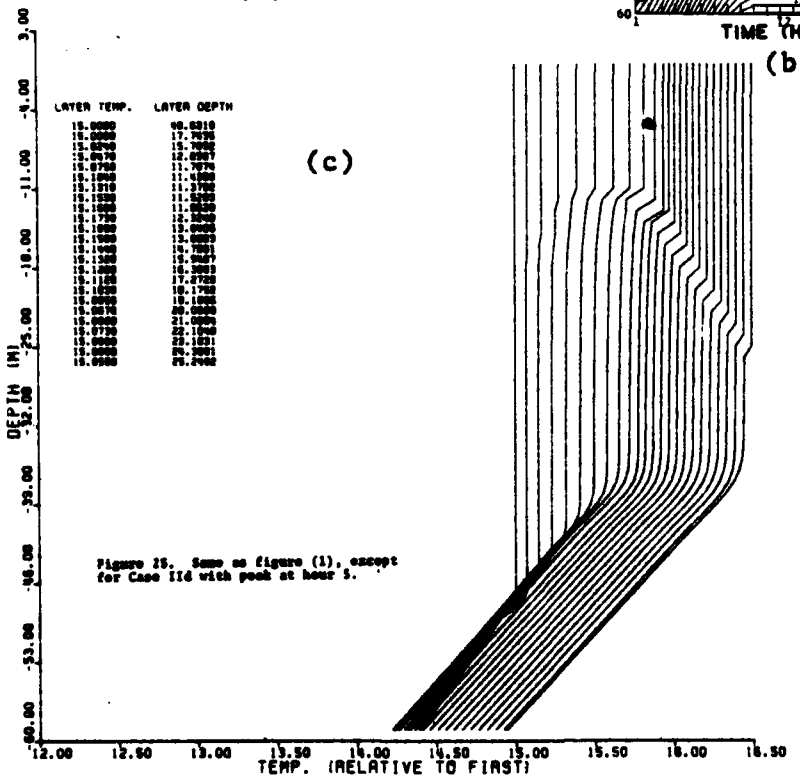

(c)

Figure 25. Same as figure (1), except for Case IId with peak at hour 5.

DAY	HR	H	T	S	TAU	QNET	WDD	DH
1	1	6.3	14.956	34.000	0.50	- 3.5	0.0	0.0
1	2	7.3	14.939	34.000	0.50	-100.8	0.0	0.0
1	3	8.0	14.935	34.000	0.50	-184.3	0.0	0.0
1	4	8.5	14.939	34.000	0.50	-248.4	0.0	0.0
1	5	8.9	14.949	34.000	0.50	-288.7	0.0	0.0
1	6	9.2	14.958	34.000	0.50	-302.5	0.0	0.0
1	7	9.5	14.969	34.000	0.50	-288.9	0.0	0.0
1	8	9.8	14.976	34.000	0.50	-248.7	0.0	0.0
1	9	10.1	14.978	34.000	0.50	-184.7	0.0	0.0
1	10	10.4	14.974	34.000	0.50	-101.3	0.0	0.0
1	11	10.7	14.963	34.000	0.50	- 4.1	0.0	0.0
1	12	11.1	14.943	34.000	0.50	100.2	0.0	0.0
1	13	11.3	14.926	34.000	0.50	100.8	-.00932	-10.604
1	14	11.5	14.909	34.000	0.50	100.8	-.01800	-20.816
1	15	11.5	14.892	34.000	0.50	100.8	-.02546	-29.699
1	16	11.5	14.875	34.000	0.50	100.8	-.03118	-36.504
1	17	11.5	14.858	34.000	0.50	100.8	-.03477	-40.743
1	18	11.5	14.837	34.000	0.50	100.8	-.03600	-42.198
1	19	11.6	14.820	34.000	0.50	100.8	-.03477	-40.984
1	20	11.7	14.804	34.000	0.50	100.8	-.03118	-36.911
1	21	11.6	14.787	34.000	0.50	100.8	-.02546	-29.966
1	22	11.7	14.770	34.000	0.50	100.8	-.01800	-21.230
1	23	11.9	14.754	34.000	0.50	100.8	-.00932	-11.108
1	24	12.1	14.737	34.000	0.50	100.8	0.0	0.0
2	1	12.4	14.728	34.000	0.50	- 3.5	0.0	0.0
2	2	12.5	14.727	34.000	0.50	-100.8	0.0	0.0
2	3	12.7	14.731	34.000	0.50	-184.3	0.0	0.0
2	4	12.8	14.741	34.000	0.50	-248.4	0.0	0.0
2	5	12.9	14.753	34.000	0.50	-288.7	0.0	0.0
2	6	13.0	14.765	34.000	0.50	-302.5	0.0	0.0
2	7	13.1	14.777	34.000	0.50	-288.9	0.0	0.0
2	8	13.2	14.786	34.000	0.50	-248.7	0.0	0.0
2	9	13.3	14.791	34.000	0.50	-184.7	0.0	0.0
2	10	13.4	14.790	34.000	0.50	-101.3	0.0	0.0
2	11	13.6	14.784	34.000	0.50	- 4.1	0.0	0.0
2	12	13.8	14.769	34.000	0.50	100.2	0.0	0.0
2	13	13.9	14.755	34.000	0.50	100.8	-.00932	-12.973
2	14	13.8	14.742	34.000	0.50	100.8	-.01800	-25.062
2	15	13.6	14.729	34.000	0.50	100.8	-.02546	-35.120
2	16	13.4	14.716	34.000	0.50	100.8	-.03118	-42.369
2	17	13.1	14.702	34.000	0.50	100.8	-.03477	-46.369
2	18	12.8	14.686	34.000	0.50	100.8	-.03600	-47.034
2	19	12.6	14.671	34.000	0.50	100.8	-.03477	-44.547
2	20	12.4	14.656	34.000	0.50	100.8	-.03118	-39.233
2	21	12.3	14.641	34.000	0.50	100.8	-.02546	-31.443
2	22	12.3	14.625	34.000	0.50	100.8	-.01800	-22.265
2	23	12.4	14.610	34.000	0.50	100.8	-.00932	-11.568
2	24	12.6	14.590	34.000	0.50	100.8	0.0	0.0

(a)

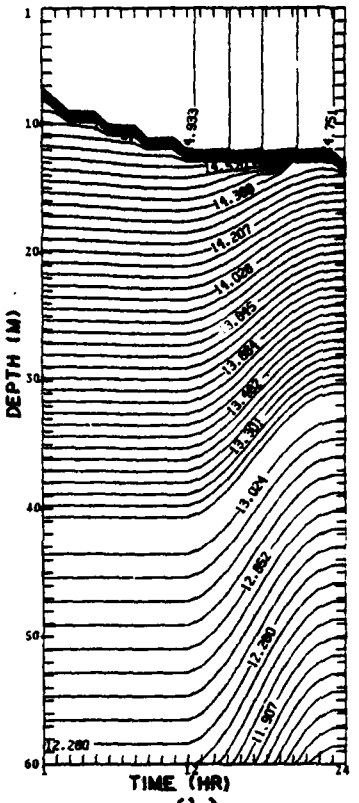

(b)

DAY	HR	H	T	S	TAU	QNET	WDD	DH
1	1	49.5	15.081	34.000	0.50	- 55.7	0.0	0.0
1	2	10.1	15.099	34.000	0.50	-201.5	0.0	0.0
1	3	16.2	15.026	34.000	0.50	-326.8	0.0	0.0
1	4	13.0	15.047	34.000	0.50	-423.0	0.0	0.0
1	5	12.1	15.075	34.000	0.50	-483.5	0.0	0.0
1	6	11.8	15.105	34.000	0.50	-504.2	0.0	0.0
1	7	12.1	15.132	34.000	0.50	-483.5	0.0	0.0
1	8	12.5	15.154	34.000	0.50	-423.5	0.0	0.0
1	9	13.0	15.168	34.000	0.50	-327.5	0.0	0.0
1	10	13.5	15.175	34.000	0.50	-202.4	0.0	0.0
1	11	14.2	15.172	34.000	0.50	- 56.6	0.0	0.0
1	12	15.0	15.166	34.000	0.50	99.9	0.0	0.0
1	13	15.7	15.149	34.000	0.50	100.8	-.00932	-14.731
1	14	16.3	15.138	34.000	0.50	100.8	-.01800	-28.577
1	15	16.7	15.129	34.000	0.50	100.8	-.02546	-41.104
1	16	17.0	15.119	34.000	0.50	100.8	-.03118	-51.910
1	17	17.3	15.110	34.000	0.50	100.8	-.03477	-61.301
1	18	17.6	15.101	34.000	0.50	100.8	-.03600	-64.696
1	19	18.0	15.092	34.000	0.50	100.8	-.03477	-63.643
1	20	18.4	15.084	34.000	0.50	100.8	-.03118	-58.407
1	21	19.1	15.078	34.000	0.50	100.8	-.02546	-49.130
1	22	19.9	15.068	34.000	0.50	100.8	-.01800	-36.125
1	23	20.9	15.061	34.000	0.50	100.8	-.00932	-19.604
1	24	22.3	15.054	34.000	0.50	100.8	-.00000	-00.001
2	1	23.1	15.054	34.000	0.50	- 55.7	0.0	0.0
2	2	23.1	15.061	34.000	0.50	-201.5	0.0	0.0
2	3	24.9	15.077	34.000	0.50	-326.8	0.0	0.0
2	4	13.3	15.100	34.000	0.50	-423.0	0.0	0.0
2	5	12.0	15.128	34.000	0.50	-483.5	0.0	0.0
2	6	11.7	15.157	34.000	0.50	-504.2	0.0	0.0
2	7	12.1	15.184	34.000	0.50	-483.5	0.0	0.0
2	8	12.4	15.206	34.000	0.50	-423.5	0.0	0.0
2	9	12.9	15.221	34.000	0.50	-327.5	0.0	0.0
2	10	13.5	15.227	34.000	0.50	-202.4	0.0	0.0
2	11	14.2	15.224	34.000	0.50	- 56.6	0.0	0.0
2	12	15.0	15.212	34.000	0.50	99.9	0.0	0.0
2	13	15.6	15.201	34.000	0.50	100.8	-.00932	-14.641
2	14	16.2	15.191	34.000	0.50	100.8	-.01800	-29.389
2	15	16.6	15.181	34.000	0.50	100.8	-.02546	-42.771
2	16	16.9	15.172	34.000	0.50	100.8	-.03118	-51.606
2	17	17.2	15.162	34.000	0.50	100.8	-.03477	-61.038
2	18	17.6	15.153	34.000	0.50	100.8	-.03600	-64.530
2	19	17.9	15.144	34.000	0.50	100.8	-.03477	-63.417
2	20	18.3	15.136	34.000	0.50	100.8	-.03118	-57.717
2	21	18.7	15.128	34.000	0.50	100.8	-.02546	-48.092
2	22	19.1	15.119	34.000	0.50	100.8	-.01800	-34.610
2	23	19.7	15.112	34.000	0.50	100.8	-.00932	-18.390
2	24	20.4	15.104	34.000	0.50	100.8	-.00000	-00.001

(c)

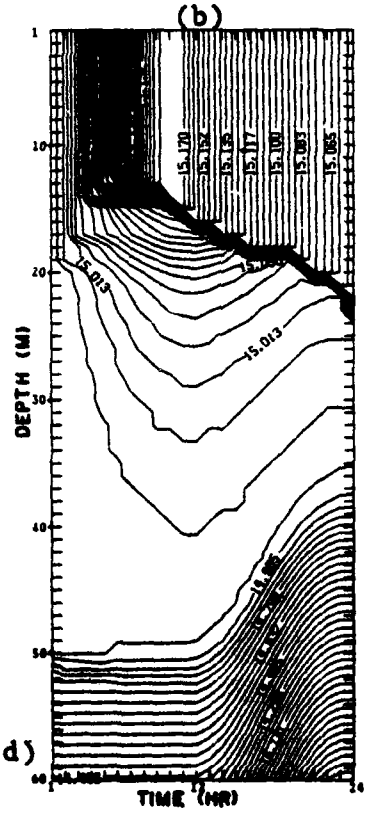

(d)

Figure 26. (a) and (b) same as figure (1), except for Case IIc with peak at hour 18. (c) and (d) same as (a) and (b), except for Case IId.

DAY	HR	H	T	S	TAU	QNET	WDS	DB
1	1	6.3	14.956	34.000	0.50	- 3.5	0.0	0.0
1	2	7.2	14.939	34.000	0.50	-100.8	-.00932	- 6.756
1	3	7.8	14.935	34.000	0.50	-184.3	-.01800	-14.212
1	4	8.1	14.939	34.000	0.50	-248.4	-.02546	-20.986
1	5	8.3	14.947	34.000	0.50	-288.7	-.03118	-26.310
1	6	8.4	14.954	34.000	0.50	-302.5	-.03477	-29.781
1	7	8.5	14.963	34.000	0.50	-288.9	-.03600	-31.198
1	8	8.6	14.969	34.000	0.50	-248.7	-.03477	-30.526
1	9	8.8	14.969	34.000	0.50	-184.7	-.03118	-27.771
1	10	8.8	14.962	34.000	0.50	-101.3	-.02546	-22.787
1	11	9.0	14.966	34.000	0.50	- 4.1	-.01800	-16.328
1	12	9.2	14.920	34.000	0.50	+100.2	-.00932	- 8.652
1	13	9.6	14.896	34.000	0.50	100.8	0.0	0.0
1	14	10.0	14.874	34.000	0.50	100.8	0.00932	9.319
1	15	10.6	14.853	34.000	0.50	100.8	0.01800	18.919
1	16	11.3	14.835	34.000	0.50	100.8	0.02546	28.302
1	17	12.0	14.817	34.000	0.50	100.8	0.03118	36.838
1	18	12.8	14.797	34.000	0.50	100.8	0.03477	43.781
1	19	13.6	14.783	34.000	0.50	100.8	0.03600	48.172
1	20	14.4	14.770	34.000	0.50	100.8	0.03477	49.208
1	21	15.1	14.758	34.000	0.50	100.8	0.03118	46.682
1	22	15.8	14.747	34.000	0.50	100.8	0.02546	39.755
1	23	16.4	14.736	34.000	0.50	100.8	0.01800	29.195
1	24	16.7	14.725	34.000	0.50	100.8	0.00932	15.526
2	1	16.9	14.720	34.000	0.50	- 3.5	0.0	0.0
2	2	16.9	14.722	34.000	0.50	-100.8	-.00932	-15.816
2	3	16.7	14.728	34.000	0.50	-184.3	-.01800	-30.300
2	4	16.3	14.737	34.000	0.50	-248.4	-.02546	-42.078
2	5	15.9	14.749	34.000	0.50	-288.7	-.03118	-50.223
2	6	15.4	14.761	34.000	0.50	-302.5	-.03477	-54.338
2	7	14.9	14.773	34.000	0.50	-288.9	-.03600	-54.494
2	8	14.4	14.783	34.000	0.50	-248.7	-.03477	-51.081
2	9	14.1	14.788	34.000	0.50	-184.7	-.03118	-44.649
2	10	13.9	14.788	34.000	0.50	-101.3	-.02546	-35.798
2	11	13.8	14.782	34.000	0.50	- 4.1	-.01800	-25.074
2	12	13.9	14.768	34.000	0.50	100.2	-.00932	-13.901
2	13	14.1	14.755	34.000	0.50	100.8	0.0	0.0
2	14	14.4	14.742	34.000	0.50	100.8	0.00932	13.323
2	15	14.8	14.730	34.000	0.50	100.8	0.01800	26.414
2	16	15.4	14.718	34.000	0.50	100.8	0.02546	38.631
2	17	16.0	14.707	34.000	0.50	100.8	0.03118	49.224
2	18	16.8	14.695	34.000	0.50	100.8	0.03477	57.351
2	19	17.6	14.685	34.000	0.50	100.8	0.03600	62.131
2	20	18.4	14.675	34.000	0.50	100.8	0.03477	62.760
2	21	19.0	14.667	34.000	0.50	100.8	0.03118	58.667
2	22	19.8	14.659	34.000	0.50	100.8	0.02546	49.687
2	23	20.3	14.651	34.000	0.50	100.8	0.01800	36.190
2	24	20.6	14.642	34.000	0.50	100.8	0.00932	19.137

(a)

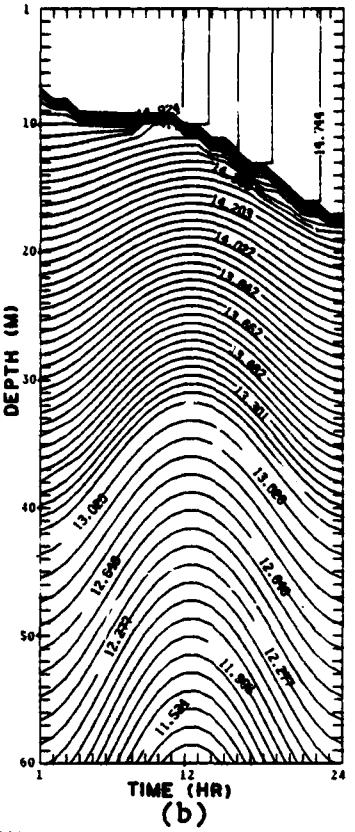

(b)

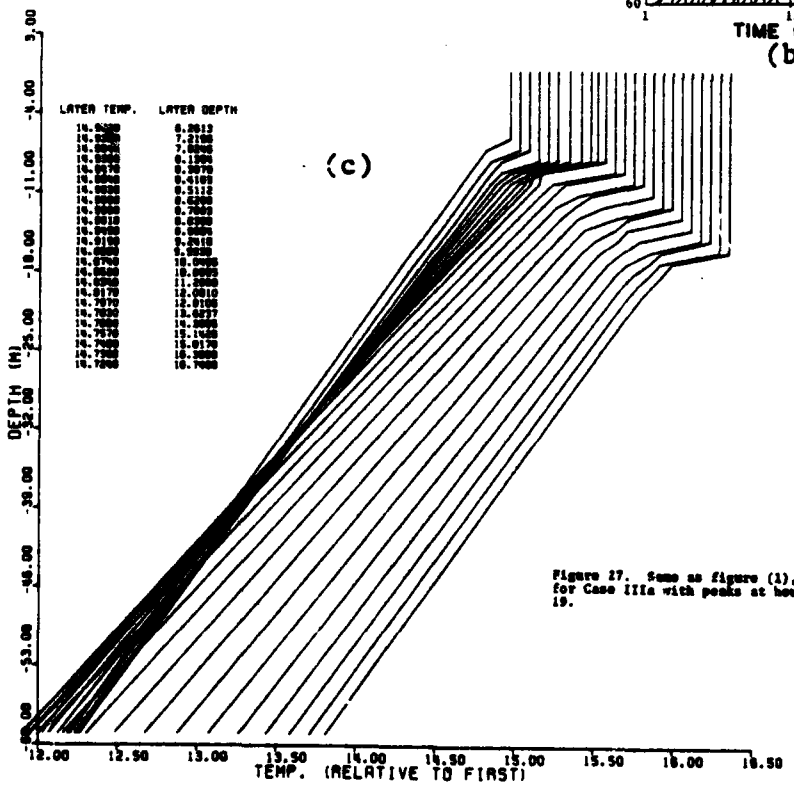

(c)

Figure 27. Same as figure (1), except for Case IIIa with peaks at hours 7 and 19.

DAY	HR	H	T	S	TAU	QNET	WDD	DH
1	1	6.0	14.956	34.000	0.50	- 3.5	-.03600	-22.140
1	2	6.9	14.937	34.000	0.50	-100.8	-.03477	-24.417
1	3	7.3	14.932	34.000	0.50	-184.3	-.03118	-23.270
1	4	7.8	14.934	34.000	0.50	-248.4	-.02546	-20.008
1	5	8.1	14.942	34.000	0.50	-288.7	-.01800	-14.652
1	6	8.3	14.949	34.000	0.50	-302.5	-.00932	- 7.808
1	7	8.7	14.959	34.000	0.50	-288.9	0.0	0.0
1	8	9.1	14.965	34.000	0.50	-248.7	0.00932	8.440
1	9	9.5	14.966	34.000	0.50	-184.7	0.01800	17.029
1	10	10.1	14.960	34.000	0.50	-101.3	0.02546	25.378
1	11	10.7	14.948	34.000	0.50	- 4.1	0.03118	32.978
1	12	11.5	14.928	34.000	0.50	100.2	0.03477	39.220
1	13	12.2	14.911	34.000	0.50	100.8	0.03600	43.180
1	14	13.0	14.896	34.000	0.50	100.8	0.03477	44.276
1	15	13.7	14.882	34.000	0.50	100.8	0.03118	41.902
1	16	14.3	14.869	34.000	0.50	100.8	0.02546	35.893
1	17	14.8	14.857	34.000	0.50	100.8	0.01800	26.626
1	18	15.2	14.844	34.000	0.50	100.8	0.00932	14.111
1	19	15.5	14.833	34.000	0.50	100.8	0.0	0.0
1	20	15.6	14.822	34.000	0.50	100.8	-.00932	-14.562
1	21	15.5	14.811	34.000	0.50	100.8	-.01800	-28.200
1	22	15.4	14.800	34.000	0.50	100.8	-.02546	-39.680
1	23	15.2	14.789	34.000	0.50	100.8	-.03118	-48.077
1	24	14.9	14.776	34.000	0.50	100.8	-.03477	-52.960
2	1	14.6	14.771	34.000	0.50	- 3.5	-.03600	-53.604
2	2	14.3	14.771	34.000	0.50	-100.8	-.03477	-50.564
2	3	14.0	14.776	34.000	0.50	-184.3	-.03118	-44.329
2	4	13.7	14.786	34.000	0.50	-248.4	-.02546	-35.447
2	5	13.6	14.798	34.000	0.50	-288.7	-.01800	-24.685
2	6	13.5	14.810	34.000	0.50	-302.5	-.00932	-12.683
2	7	13.6	14.822	34.000	0.50	-288.9	0.0	0.0
2	8	13.9	14.831	34.000	0.50	-248.7	0.00932	12.864
2	9	14.2	14.837	34.000	0.50	-184.7	0.01800	25.415
2	10	14.8	14.837	34.000	0.50	-101.3	0.02546	37.113
2	11	15.4	14.831	34.000	0.50	- 4.1	0.03118	47.309
2	12	16.2	14.818	34.000	0.50	100.2	0.03477	55.256
2	13	17.0	14.808	34.000	0.50	100.8	0.03600	60.002
2	14	17.8	14.798	34.000	0.50	100.8	0.03477	60.691
2	15	18.5	14.789	34.000	0.50	100.8	0.03118	56.796
2	16	19.2	14.782	34.000	0.50	100.8	0.02546	48.153
2	17	19.7	14.773	34.000	0.50	100.8	0.01800	35.109
2	18	20.0	14.764	34.000	0.50	100.8	0.00932	18.583
2	19	20.2	14.756	34.000	0.50	100.8	0.0	0.0
2	20	20.2	14.749	34.000	0.50	100.8	-.00932	-18.983
2	21	20.0	14.741	34.000	0.50	100.8	-.01800	-36.339
2	22	19.7	14.733	34.000	0.50	100.8	-.02546	-50.746
2	23	19.3	14.725	34.000	0.50	100.8	-.03118	-60.996
2	24	18.8	14.715	34.000	0.50	100.8	-.03477	-66.499

(a)

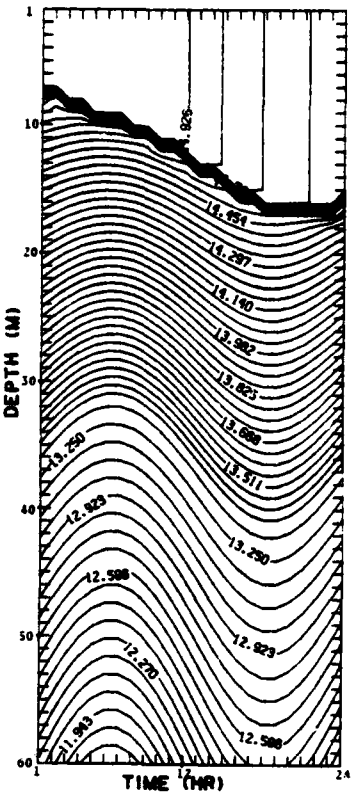

(b)

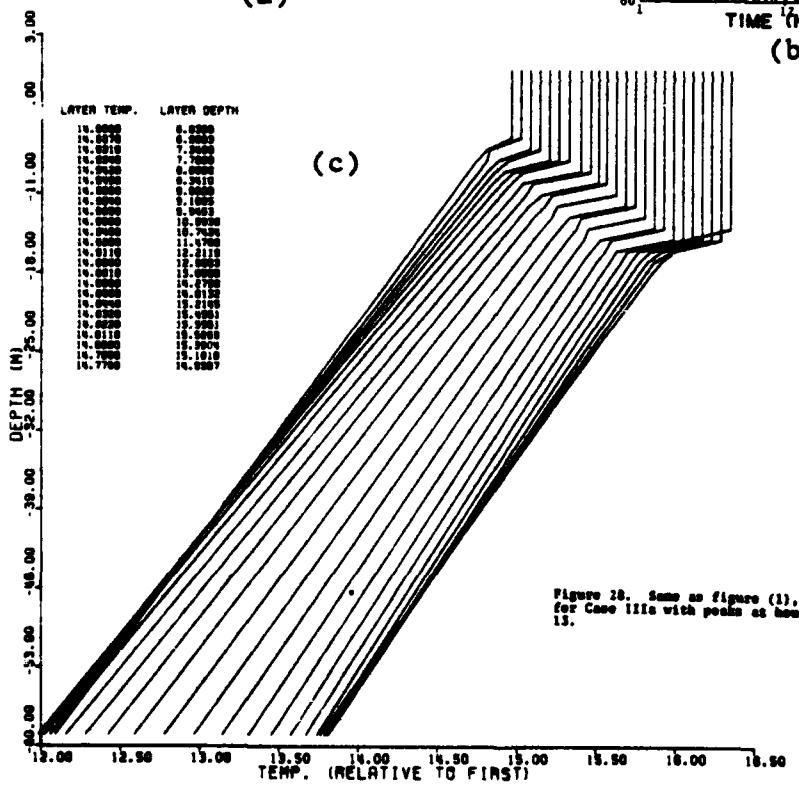

(c)

Figure 28. Same as figure (1), except for Case IIIa with peaks at hours 1 and 13.

DAY	HR	H	T	S	TAU	QUEST	WND	==
1	1	6.3	14.956	34.000	0.50	- 3.5	0.0	0.0
1	2	7.4	14.939	34.000	0.50	-100.8	0.00932	6.822
1	3	8.2	14.935	34.000	0.50	-184.3	0.01800	14.693
1	4	9.9	14.940	34.000	0.50	-248.4	0.02546	22.424
1	5	9.6	14.950	34.000	0.50	-288.7	0.03118	29.404
1	6	10.2	14.961	34.000	0.50	-302.5	0.03477	34.963
1	7	10.9	14.972	34.000	0.50	-288.9	0.03600	38.490
1	8	11.5	14.981	34.000	0.50	-248.7	0.03477	39.380
1	9	12.1	14.985	34.000	0.50	-184.7	0.03118	37.250
1	10	12.7	14.984	34.000	0.50	-101.3	0.02546	31.966
1	11	13.3	14.976	34.000	0.50	- 4.1	0.01800	23.636
1	12	13.7	14.962	34.000	0.50	100.2	0.00932	12.695
1	13	14.0	14.949	34.000	0.50	100.8	0.0	0.0
1	14	14.2	14.936	34.000	0.50	100.8	-.00932	-13.280
1	15	14.2	14.924	34.000	0.50	100.8	-.01800	-25.008
1	16	14.2	14.912	34.000	0.50	100.8	-.02546	-36.303
1	17	14.0	14.899	34.000	0.50	100.8	-.03118	-44.669
1	18	13.9	14.885	34.000	0.50	100.8	-.03477	-49.174
1	19	13.7	14.872	34.000	0.50	100.8	-.03600	-50.291
1	20	13.6	14.859	34.000	0.50	100.8	-.03477	-47.985
1	21	13.4	14.846	34.000	0.50	100.8	-.03118	-42.549
1	22	13.4	14.833	34.000	0.50	100.8	-.02546	-34.564
1	23	13.5	14.819	34.000	0.50	100.8	-.01800	-24.385
1	24	13.7	14.803	34.000	0.50	100.8	-.00932	-13.032
2	1	14.0	14.797	34.000	0.50	- 3.5	0.0	0.0
2	2	14.3	14.797	34.000	0.50	-101.8	0.00932	13.288
2	3	14.7	14.802	34.000	0.50	-184.3	0.01800	25.278
2	4	15.2	14.813	34.000	0.50	-248.4	0.02546	35.240
2	5	15.8	14.824	34.000	0.50	-288.7	0.03118	40.394
2	6	16.4	14.836	34.000	0.50	-302.5	0.03477	55.952
2	7	17.0	14.848	34.000	0.50	-288.9	0.03600	60.189
2	8	17.7	14.858	34.000	0.50	-248.7	0.03477	60.411
2	9	18.3	14.864	34.000	0.50	-184.7	0.03118	56.227
2	10	18.9	14.866	34.000	0.50	-101.3	0.02546	47.504
2	11	19.4	14.862	34.000	0.50	- 4.1	0.01800	34.578
2	12	19.7	14.854	34.000	0.50	+100.2	0.00932	18.302
2	13	19.9	14.846	34.000	0.50	100.8	0.0	0.0
2	14	19.9	14.838	34.000	0.50	100.8	-.00932	-18.611
2	15	19.7	14.831	34.000	0.50	100.8	-.01800	-35.756
2	16	19.4	14.823	34.000	0.50	100.8	-.02546	-49.893
2	17	19.0	14.815	34.000	0.50	100.8	-.03118	-59.922
2	18	18.4	14.806	34.000	0.50	100.8	-.03477	-65.250
2	19	18.0	14.797	34.000	0.50	100.8	-.03600	-65.815
2	20	17.5	14.788	34.000	0.50	100.8	-.03477	-61.984
2	21	17.1	14.779	34.000	0.50	100.8	-.03118	-54.391
2	22	16.9	14.770	34.000	0.50	100.8	-.02546	-43.557
2	23	16.8	14.760	34.000	0.50	100.8	-.01800	-30.470
2	24	16.8	14.750	34.000	0.50	100.8	-.00932	-15.729

(a)

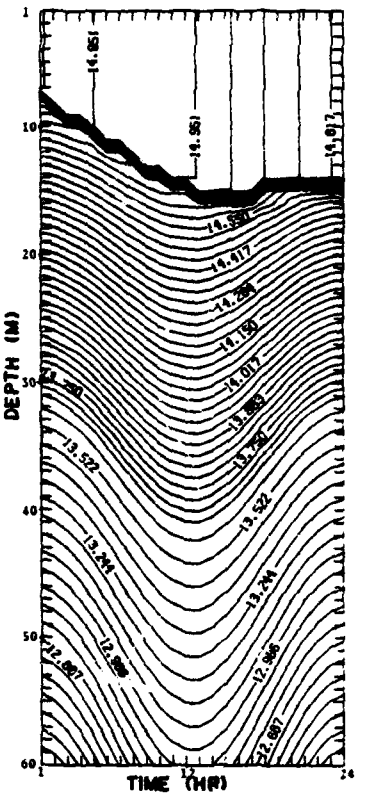

(b)

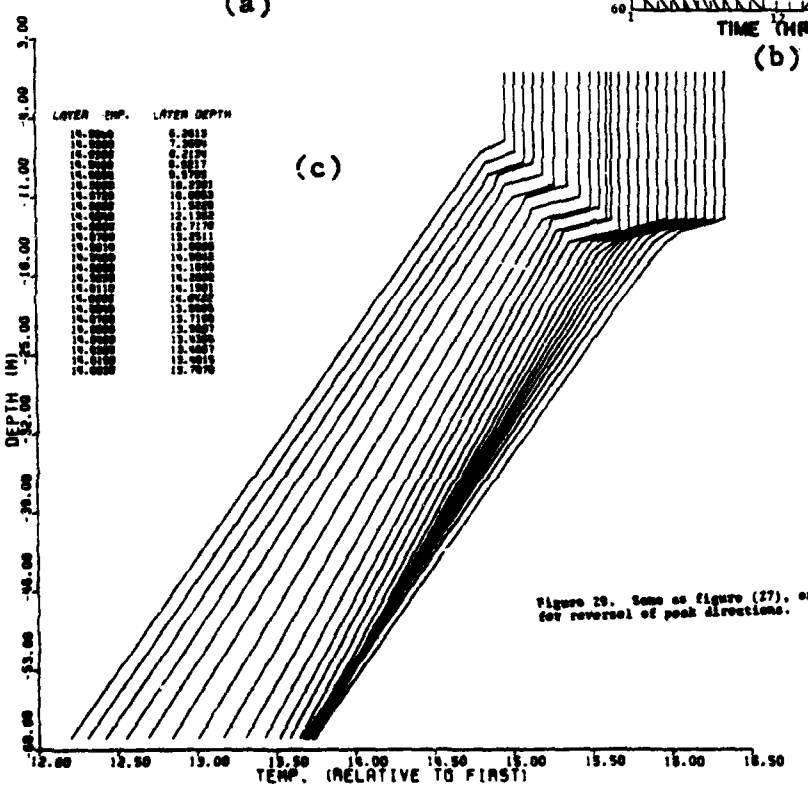

Figure 29. Same as figure (27), except for reversal of peak directions.

DAY	HR	H	T	S	TAU	QNET	WDO	DH
1	1	6.5	14.956	36.000	0.50	- 3.5	0.03600	22.951
1	2	7.7	14.940	36.000	0.50	-101.8	0.03677	26.415
1	3	8.7	14.938	36.000	0.50	-184.3	0.03118	26.586
1	4	9.4	14.944	36.000	0.50	-248.4	0.02546	23.583
1	5	9.9	14.954	36.000	0.50	-288.7	0.01800	17.697
1	6	10.3	14.966	36.000	0.50	-302.5	0.00932	9.555
1	7	10.6	14.977	36.000	0.50	-288.9	0.0	0.0
1	8	10.7	14.985	36.000	0.50	-248.7	-.00932	-10.049
1	9	10.8	14.988	36.000	0.50	-184.7	-.01800	-19.668
1	10	10.8	14.986	36.000	0.50	-101.3	-.02546	-27.938
1	11	10.8	14.975	36.000	0.50	- 4.1	-.03118	-34.248
1	12	10.8	14.956	36.000	0.50	100.2	-.03677	-38.188
1	13	10.8	14.937	36.000	0.50	100.8	-.03600	-39.433
1	14	10.7	14.919	36.000	0.50	100.8	-.03677	-37.988
1	15	10.7	14.908	36.000	0.50	100.8	-.03118	-34.041
1	16	10.8	14.902	36.000	0.50	100.8	-.02546	-27.890
1	17	11.0	14.903	36.000	0.50	100.8	-.01800	-19.982
1	18	11.2	14.904	36.000	0.50	100.8	-.00932	-10.469
1	19	11.5	14.926	36.000	0.50	100.8	0.0	0.0
1	20	12.0	14.910	36.000	0.50	100.8	0.00932	11.115
1	21	12.5	14.794	36.000	0.50	100.8	0.01800	22.316
1	22	13.1	14.779	36.000	0.50	100.8	0.02546	33.028
1	23	13.9	14.765	36.000	0.50	100.8	0.03118	42.562
1	24	14.6	14.751	36.000	0.50	100.8	0.03677	50.051
2	1	15.4	14.746	36.000	0.50	- 3.5	0.03600	54.497
2	2	16.1	14.746	36.000	0.50	-101.8	0.03677	55.139
2	3	16.8	14.752	36.000	0.50	-184.3	0.03118	51.466
2	4	17.3	14.762	36.000	0.50	-248.4	0.02546	43.609
2	5	17.6	14.774	36.000	0.50	-288.7	0.01800	31.624
2	6	17.8	14.786	36.000	0.50	-302.5	0.00932	16.805
2	7	17.8	14.797	36.000	0.50	-288.9	0.0	0.0
2	8	17.7	14.807	36.000	0.50	-248.7	-.00932	-16.565
2	9	17.5	14.813	36.000	0.50	-184.7	-.01800	-31.717
2	10	17.1	14.814	36.000	0.50	-101.3	-.02546	-44.198
2	11	16.8	14.810	36.000	0.50	- 4.1	-.03118	-53.128
2	12	16.4	14.799	36.000	0.50	+100.2	-.03677	-58.058
2	13	16.0	14.789	36.000	0.50	100.8	-.03600	-58.805
2	14	15.7	14.779	36.000	0.50	100.8	-.03677	-55.626
2	15	15.5	14.768	36.000	0.50	100.8	-.03118	-49.008
2	16	15.3	14.757	36.000	0.50	100.8	-.02546	-39.543
2	17	15.3	14.746	36.000	0.50	100.8	-.01800	-27.038
2	18	15.5	14.731	36.000	0.50	100.8	-.00932	-14.472
2	19	15.7	14.720	36.000	0.50	100.8	0.0	0.0
2	20	16.2	14.709	36.000	0.50	100.8	0.00932	15.001
2	21	16.7	14.699	36.000	0.50	100.8	0.01800	29.709
2	22	17.3	14.689	36.000	0.50	100.8	0.02546	43.403
2	23	18.0	14.679	36.000	0.50	100.8	0.03118	55.248
2	24	18.8	14.670	36.000	0.50	100.8	0.03677	64.367

(a)

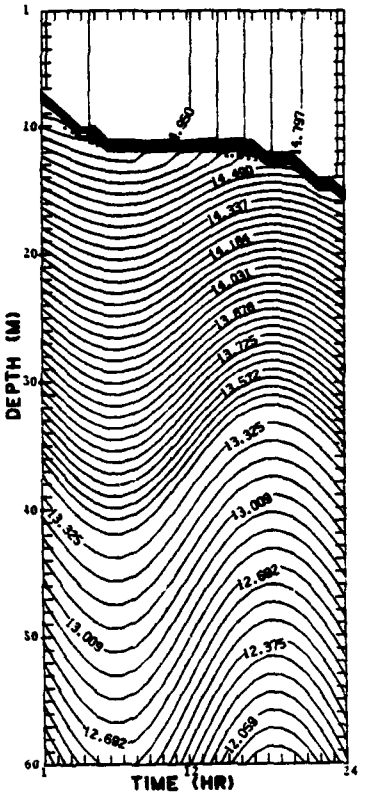

(b)

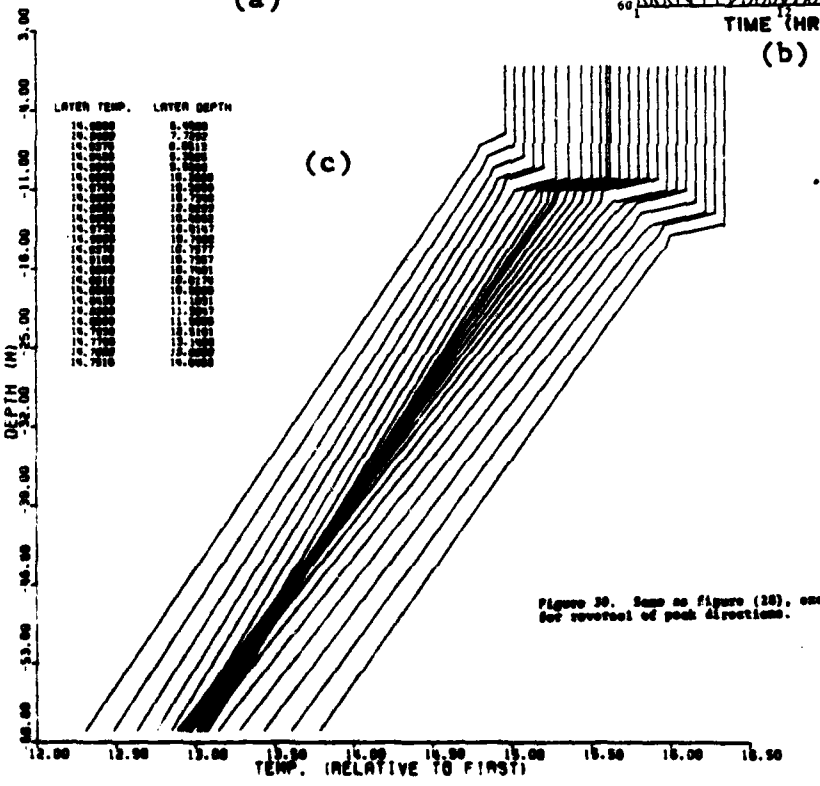

Figure 20. Same as figure (18), except for reversal of peak directions.

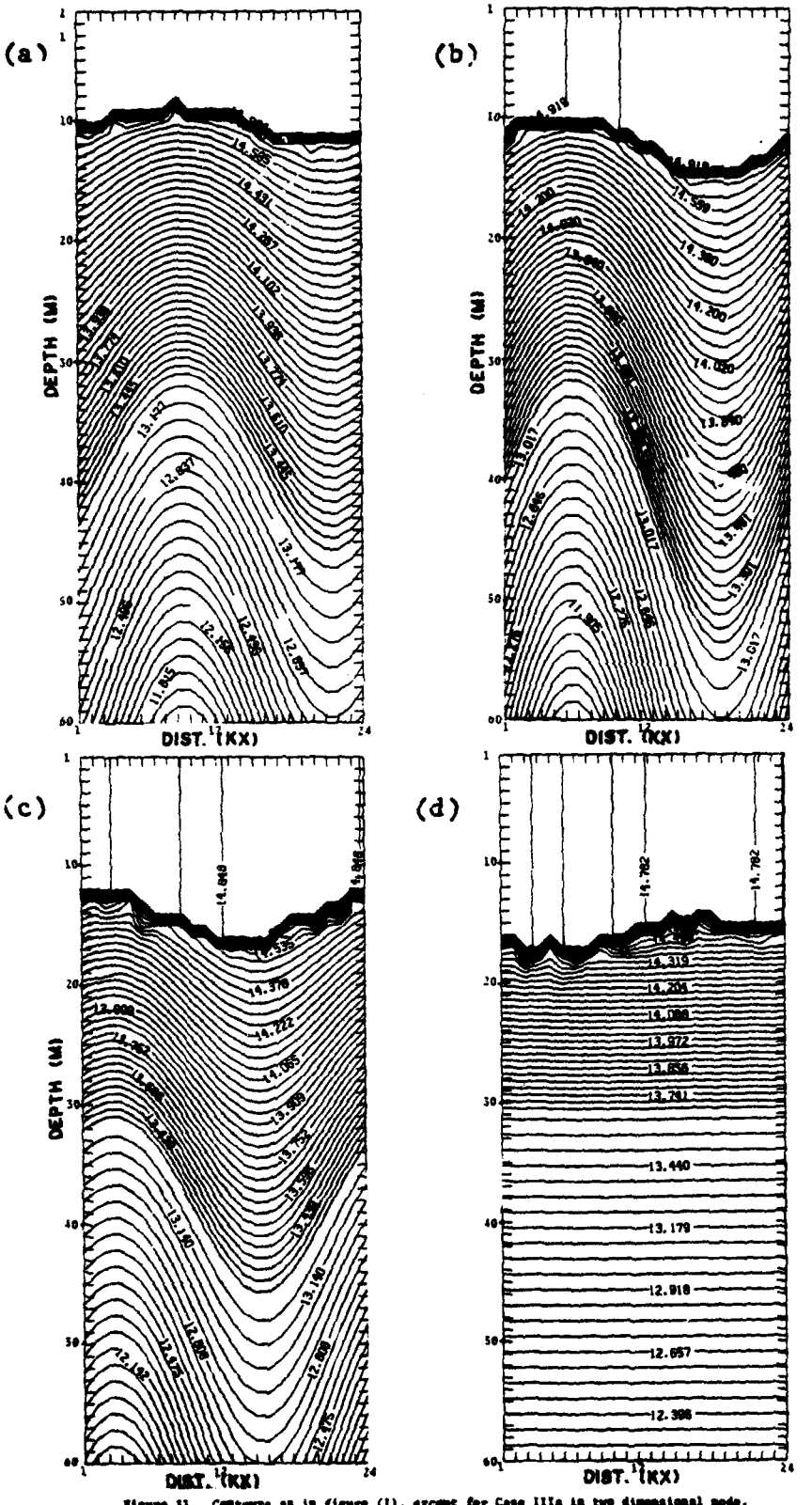

Figure 31. Contours as in figure (1), except for Case IIIa in two dimensional mode. (a), (b), (c), and (d) are hour 6, 12, 18 and 24 respectively.

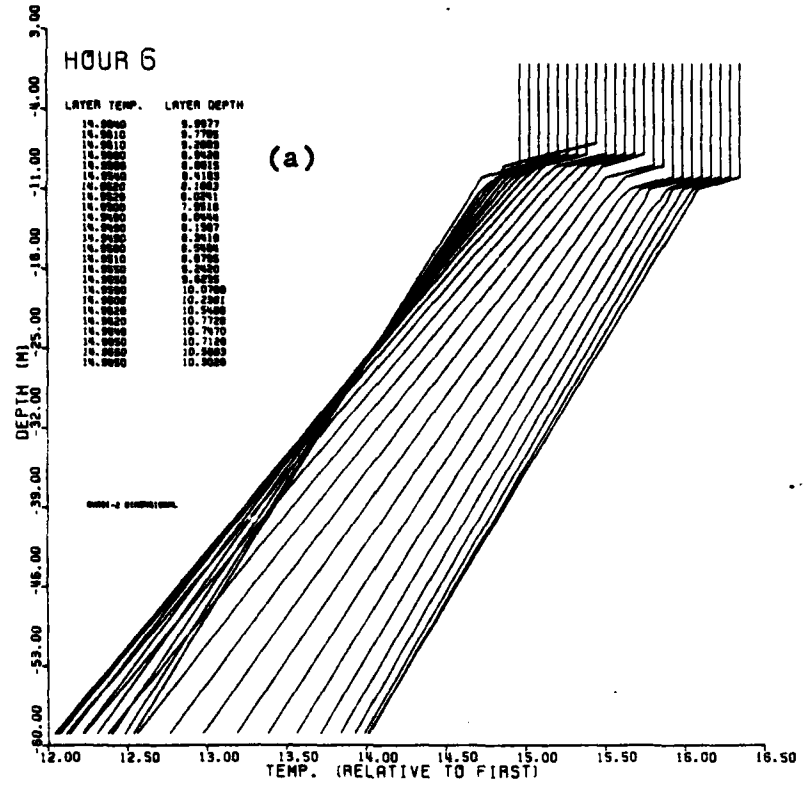

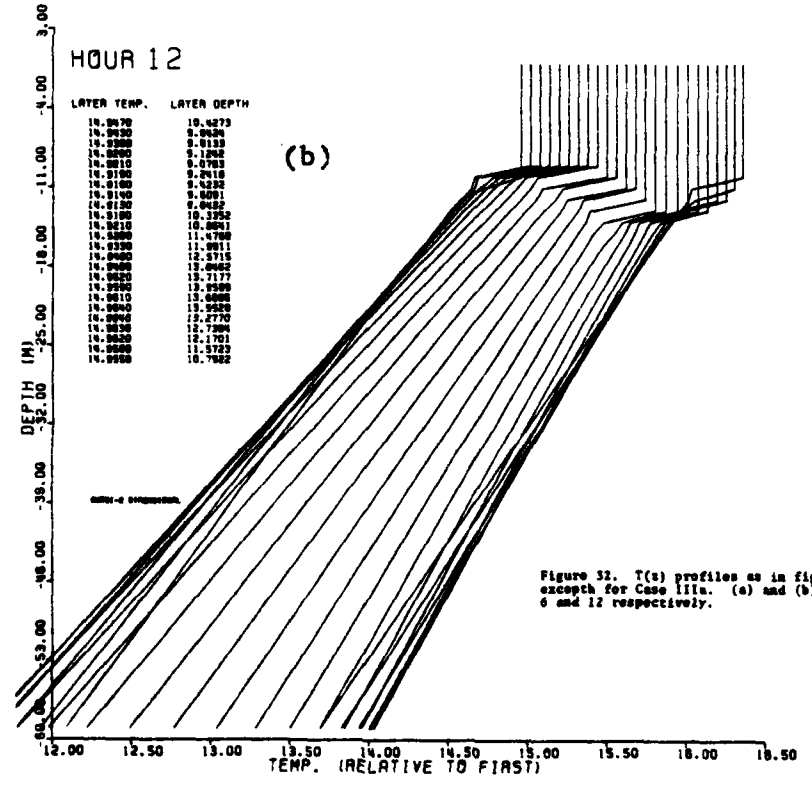

Figure 32. T(z) profiles as in figure (1), excepth for Case IIIa. (a) and (b) are hour 6 and 12 respectively.

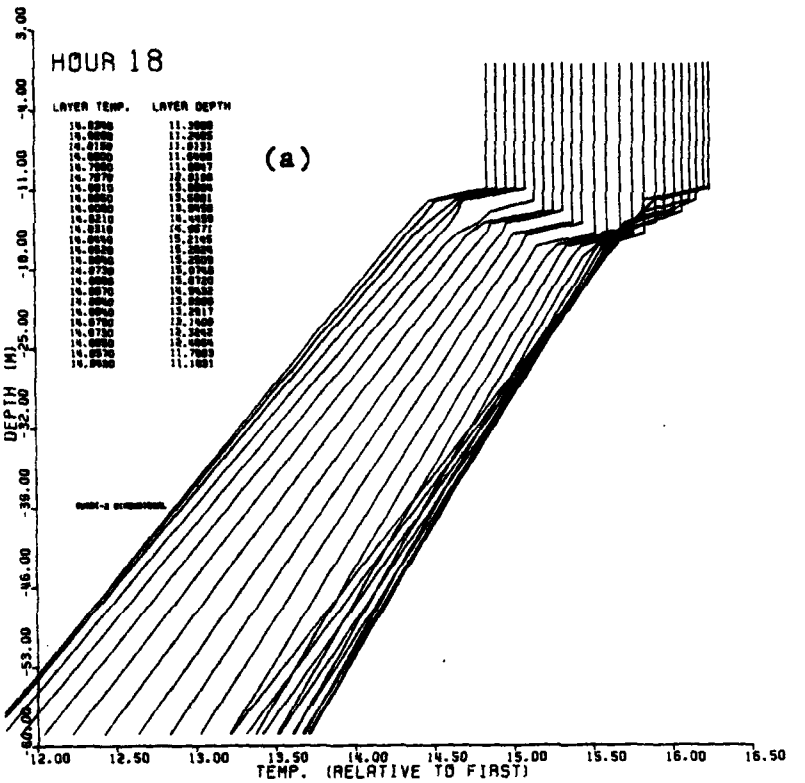

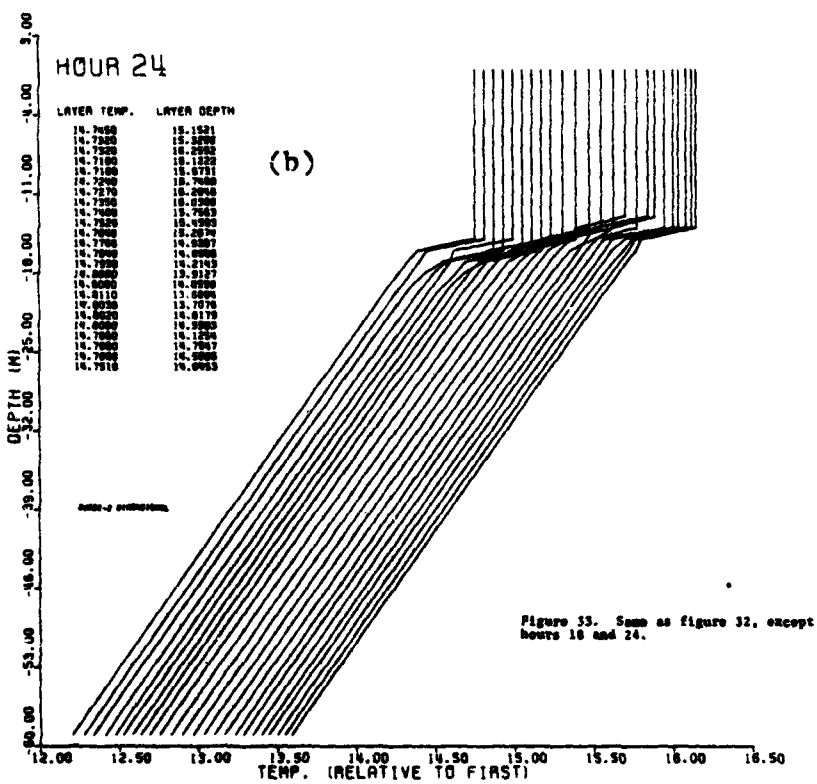

Figure 33. Same as figure 32, except for hours 18 and 24.

DAY	HR	H	T	S	TAU	QNET	WDD	DH
1	1	49.5	15.001	34.000	0.50	- 55.7	0.0	0.0
1	2	17.9	15.009	34.000	0.50	-201.5	-.00932	-16.793
1	3	15.9	15.024	34.000	0.50	-326.8	-.01800	-28.950
1	4	12.7	15.047	34.000	0.50	-423.0	-.02546	-32.856
1	5	11.7	15.075	34.000	0.50	-483.5	-.03118	-37.199
1	6	11.4	15.104	34.000	0.50	-504.2	-.03477	-40.436
1	7	11.3	15.132	34.000	0.50	-483.7	-.03600	-41.530
1	8	11.4	15.154	34.000	0.50	-423.5	-.03477	-40.316
1	9	11.6	15.168	34.000	0.50	-327.5	-.03118	-36.803
1	10	12.0	15.174	34.000	0.50	-202.4	-.02546	-30.875
1	11	12.5	15.169	34.000	0.50	- 56.6	-.01800	-22.641
1	12	13.2	15.155	34.000	0.50	99.9	-.00932	-12.376
1	13	14.1	15.142	34.000	0.50	100.8	0.0	0.0
1	14	15.1	15.130	34.000	0.50	100.8	0.00932	14.028
1	15	16.3	15.119	34.000	0.50	100.8	0.01800	29.136
1	16	17.7	15.110	34.000	0.50	100.8	0.02546	44.423
1	17	19.2	15.101	34.000	0.50	100.8	0.03118	59.808
1	18	20.8	15.093	34.000	0.50	100.8	0.03477	71.045
1	19	22.5	15.086	34.000	0.50	100.8	0.03600	79.525
1	20	24.2	15.080	34.000	0.50	100.8	0.03477	82.842
1	21	26.0	15.074	34.000	0.50	100.8	0.03118	79.704
1	22	27.6	15.069	34.000	0.50	100.8	0.02546	69.157
1	23	29.1	15.064	34.000	0.50	100.8	0.01800	51.856
1	24	30.3	15.060	34.000	0.50	100.8	0.00932	28.137
2	1	30.8	15.060	34.000	0.50	- 55.7	0.0	0.0
2	2	20.9	15.068	34.000	0.50	-201.5	-.00932	-19.593
2	3	15.1	15.083	34.000	0.50	-326.8	-.01800	-27.473
2	4	12.9	15.103	34.000	0.50	-423.0	-.02546	-33.187
2	5	11.7	15.124	34.000	0.50	-483.5	-.03118	-36.969
2	6	11.3	15.144	34.000	0.50	-504.2	-.03477	-39.896
2	7	11.2	15.161	34.000	0.50	-483.5	-.03600	-41.192
2	8	11.3	15.173	34.000	0.50	-423.5	-.03477	-40.094
2	9	11.6	15.178	34.000	0.50	-327.5	-.03118	-36.673
2	10	11.9	15.174	34.000	0.50	-202.4	-.02546	-30.800
2	11	12.4	15.159	34.000	0.50	- 56.6	-.01800	-22.569
2	12	13.2	15.133	34.000	0.50	99.9	-.00932	-12.336
2	13	14.1	15.102	34.000	0.50	100.8	0.0	0.0
2	14	15.1	15.190	34.000	0.50	100.8	0.00932	14.013
2	15	16.3	15.179	34.000	0.50	100.8	0.01800	29.163
2	16	17.7	15.169	34.000	0.50	100.8	0.02546	44.461
2	17	19.2	15.160	34.000	0.50	100.8	0.03118	58.869
2	18	20.8	15.153	34.000	0.50	100.8	0.03477	71.122
2	19	22.5	15.146	34.000	0.50	100.8	0.03600	79.577
2	20	24.2	15.139	34.000	0.50	100.8	0.03477	82.821
2	21	25.9	15.134	34.000	0.50	100.8	0.03118	79.552
2	22	27.4	15.128	34.000	0.50	100.8	0.02546	68.985
2	23	28.8	15.124	34.000	0.50	100.8	0.01800	51.351
2	24	29.8	15.119	34.000	0.50	100.8	0.00932	27.646

(a)

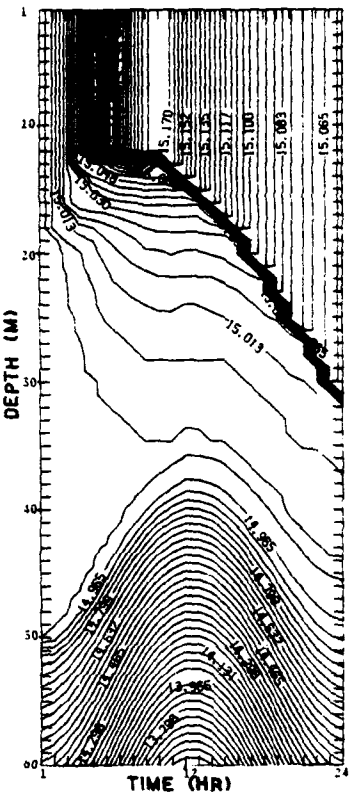

(b)

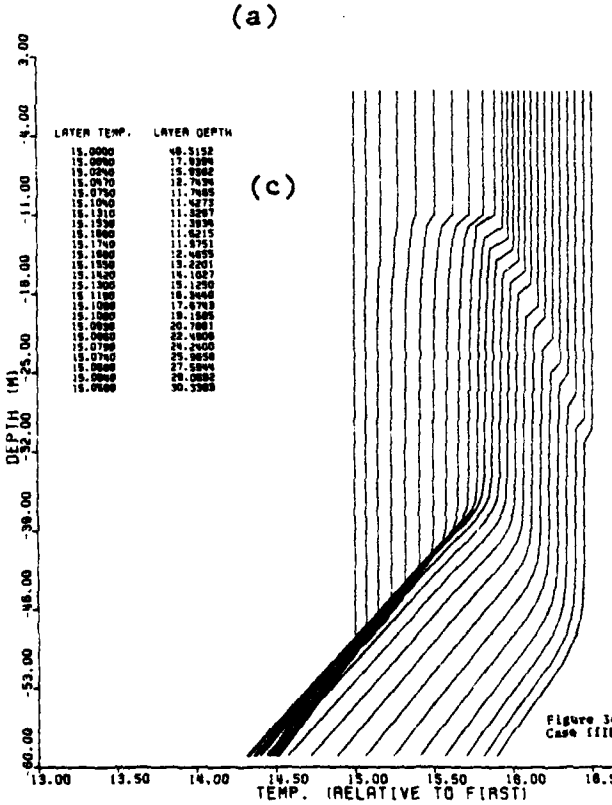

(c)

Figure 34. Same as figure (1), except for Case IIIb with peaks at hours 7 and 19.

DAY	HR	Z	T	S	TAU	QNET	WDO	DZ
1	1	47.8	15.001	34.000	0.50	- 55.7	-.03600	-175.086
1	2	17.7	15.009	34.000	0.50	-201.5	-.03477	- 62.538
1	3	15.8	15.024	34.000	0.50	-326.8	-.03118	- 50.044
1	4	12.8	15.047	34.000	0.50	-423.0	-.02546	- 32.932
1	5	11.9	15.075	34.000	0.50	-483.5	-.01800	- 21.607
1	6	11.7	15.104	34.000	0.50	-504.2	-.00932	- 10.945
1	7	12.0	15.131	34.000	0.50	-483.7	0.0	0.0
1	8	12.4	15.154	34.000	0.50	-423.5	0.00932	11.562
1	9	13.1	15.168	34.000	0.50	-327.5	0.01800	23.468
1	10	14.0	15.175	34.000	0.50	-202.4	0.02546	35.288
1	11	15.2	15.172	34.000	0.50	- 56.6	0.03118	46.708
1	12	16.7	15.161	34.000	0.50	99.9	0.03477	56.954
1	13	18.0	15.152	34.000	0.50	100.8	0.03600	63.705
1	14	19.4	15.143	34.000	0.50	100.8	0.03477	66.297
1	15	20.8	15.135	34.000	0.50	100.8	0.03118	63.716
1	16	22.0	15.128	34.000	0.50	100.8	0.02546	55.248
1	17	23.1	15.122	34.000	0.50	100.8	0.01800	41.146
1	18	24.0	15.116	34.000	0.50	100.8	0.00932	22.239
1	19	24.7	15.110	34.000	0.50	100.8	0.0	0.0
1	20	25.1	15.104	34.000	0.50	100.8	-.00932	- 23.531
1	21	25.4	15.099	34.000	0.50	100.8	-.01800	- 46.145
1	22	25.5	15.093	34.000	0.50	100.8	-.02546	- 65.790
1	23	25.5	15.088	34.000	0.50	100.8	-.03118	- 80.740
1	24	25.4	15.083	34.000	0.50	100.8	-.03477	- 89.980
2	1	25.0	15.083	34.000	0.50	- 55.7	-.03600	- 91.646
2	2	22.1	15.090	34.000	0.50	-201.5	-.03477	- 78.064
2	3	14.7	15.106	34.000	0.50	-326.8	-.03118	- 46.456
2	4	13.0	15.128	34.000	0.50	-423.0	-.02546	- 33.442
2	5	11.8	15.157	34.000	0.50	-483.5	-.01800	- 21.441
2	6	11.7	15.186	34.000	0.50	-504.2	-.00932	- 10.915
2	7	11.9	15.214	34.000	0.50	-483.7	0.0	0.0
2	8	12.4	15.236	34.000	0.50	-423.5	0.00932	11.456
2	9	12.9	15.251	34.000	0.50	-327.5	0.01800	23.239
2	10	13.9	15.257	34.000	0.50	-202.4	0.02546	35.035
2	11	15.0	15.254	34.000	0.50	- 56.6	0.03118	46.189
2	12	16.4	15.243	34.000	0.50	99.9	0.03477	56.054
2	13	17.8	15.233	34.000	0.50	100.8	0.03600	63.043
2	14	19.2	15.225	34.000	0.50	100.8	0.03477	65.623
2	15	20.6	15.217	34.000	0.50	100.8	0.03118	63.110
2	16	21.8	15.210	34.000	0.50	100.8	0.02546	54.870
2	17	22.9	15.203	34.000	0.50	100.8	0.01800	40.923
2	18	23.9	15.197	34.000	0.50	100.8	0.00932	22.134
2	19	24.6	15.191	34.000	0.50	100.8	0.0	0.0
2	20	25.1	15.185	34.000	0.50	100.8	-.00932	- 23.462
2	21	25.3	15.180	34.000	0.50	100.8	-.01800	- 46.025
2	22	25.4	15.175	34.000	0.50	100.8	-.02546	- 65.615
2	23	25.3	15.169	34.000	0.50	100.8	-.03118	- 80.218
2	24	25.1	15.164	34.000	0.50	100.8	-.03477	- 88.884

(a)

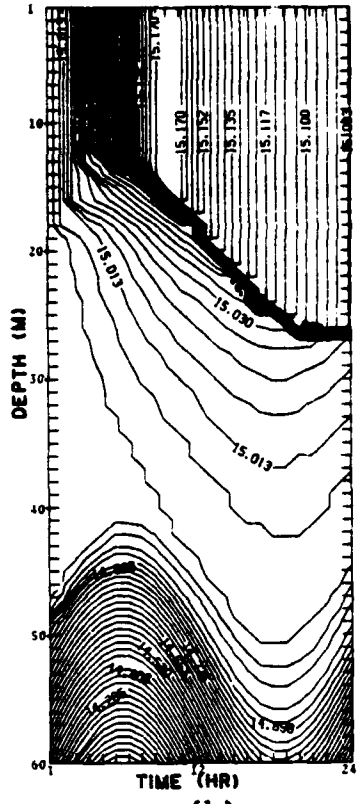

(b)

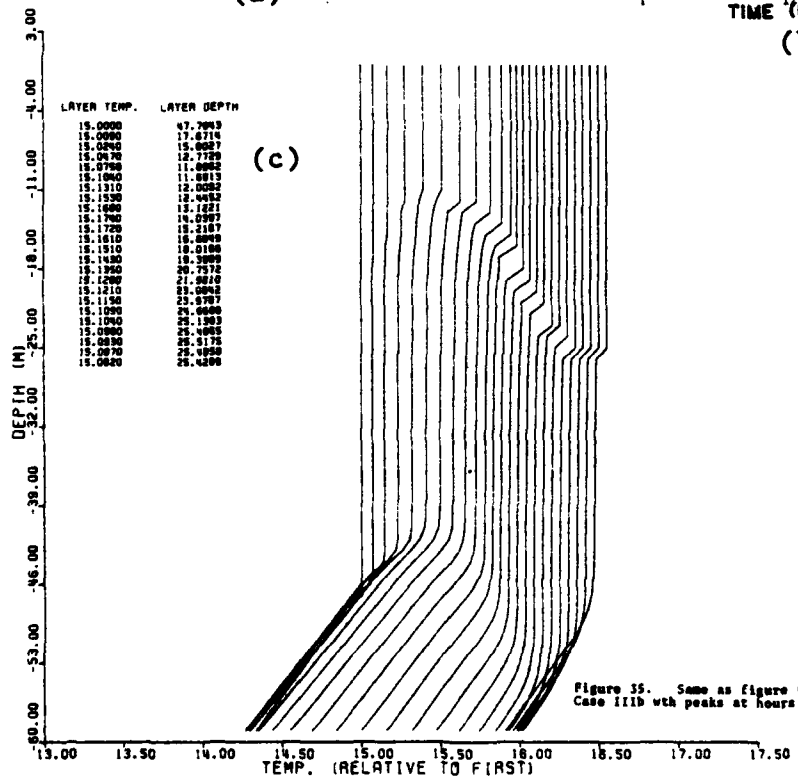

(c)

Figure 35. Same as figure (1), except for Case IIIb wth peaks at hours 1 and 13.

DAY	HR	H	T	S	TAU	QNET	VDO	DH
1	1	49.5	15.001	34.000	0.50	- 55.7	-.00000	- 0.004
1	2	18.3	15.009	34.000	0.50	-201.5	0.00932	16.951
1	3	16.4	15.024	34.000	0.50	-326.8	0.01800	29.388
1	4	13.3	15.047	34.000	0.50	-423.0	0.02546	33.425
1	5	12.4	15.076	34.000	0.50	-483.5	0.03118	38.007
1	6	12.1	15.105	34.000	0.50	-504.2	0.03477	41.405
1	7	12.7	15.133	34.000	0.50	-483.7	0.03600	44.890
1	8	13.5	15.155	34.000	0.50	-423.5	0.03477	46.079
1	9	14.3	15.169	34.000	0.50	-327.5	0.03118	44.043
1	10	15.3	15.176	34.000	0.50	-202.4	0.02546	38.499
1	11	16.4	15.174	34.000	0.50	- 56.6	0.01800	29.185
1	12	17.3	15.164	34.000	0.50	99.9	0.00932	16.060
1	13	18.1	15.155	34.000	0.50	100.8	0.0	0.0
1	14	18.7	15.147	34.000	0.50	100.8	-.00932	-17.521
1	15	19.2	15.139	34.000	0.50	100.8	-.01800	-34.806
1	16	19.5	15.131	34.000	0.50	100.8	-.02546	-50.246
1	17	19.7	15.123	34.000	0.50	100.8	-.03118	-62.429
1	18	19.8	15.116	34.000	0.50	100.8	-.03477	-70.201
1	19	20.0	15.108	34.000	0.50	100.8	-.03600	-73.174
1	20	20.1	15.101	34.000	0.50	100.8	-.03477	-71.243
1	21	20.4	15.094	34.000	0.50	100.8	-.03118	-64.744
1	22	20.9	15.086	34.000	0.50	100.8	-.02546	-53.760
1	23	21.5	15.079	34.000	0.50	100.8	-.01800	-38.968
1	24	22.3	15.073	34.000	0.50	100.8	-.00932	-20.873
2	1	23.0	15.073	34.000	0.50	- 55.7	0.0	0.0
2	2	23.2	15.080	34.000	0.50	-201.5	0.00932	21.500
2	3	15.2	15.096	34.000	0.50	-326.8	0.01800	37.045
2	4	13.5	15.119	34.000	0.50	-423.0	0.02546	34.017
2	5	12.3	15.147	34.000	0.50	-483.5	0.03118	37.696
2	6	12.1	15.177	34.000	0.50	-504.2	0.03477	41.307
2	7	12.6	15.204	34.000	0.50	-483.7	0.03600	44.728
2	8	13.4	15.226	34.000	0.50	-423.5	0.03477	45.938
2	9	14.4	15.241	34.000	0.50	-327.5	0.03118	44.147
2	10	15.4	15.247	34.000	0.50	-202.4	0.02546	38.760
2	11	16.4	15.246	34.000	0.50	- 56.6	0.01800	29.171
2	12	17.3	15.236	34.000	0.50	99.9	0.00932	16.051
2	13	18.1	15.227	34.000	0.50	100.8	0.0	0.0
2	14	18.7	15.218	34.000	0.50	100.8	-.00932	-17.491
2	15	19.1	15.210	34.000	0.50	100.8	-.01800	-34.714
2	16	19.4	15.202	34.000	0.50	100.8	-.02546	-50.044
2	17	19.6	15.195	34.000	0.50	100.8	-.03118	-62.132
2	18	19.7	15.187	34.000	0.50	100.8	-.03477	-69.824
2	19	19.9	15.180	34.000	0.50	100.8	-.03600	-72.794
2	20	20.1	15.172	34.000	0.50	100.8	-.03477	-70.952
2	21	20.4	15.165	34.000	0.50	100.8	-.03118	-64.569
2	22	20.8	15.158	34.000	0.50	100.8	-.02546	-53.691
2	23	21.4	15.151	34.000	0.50	100.8	-.01800	-38.870
2	24	22.1	15.144	34.000	0.50	100.8	-.00932	-20.717

(a)

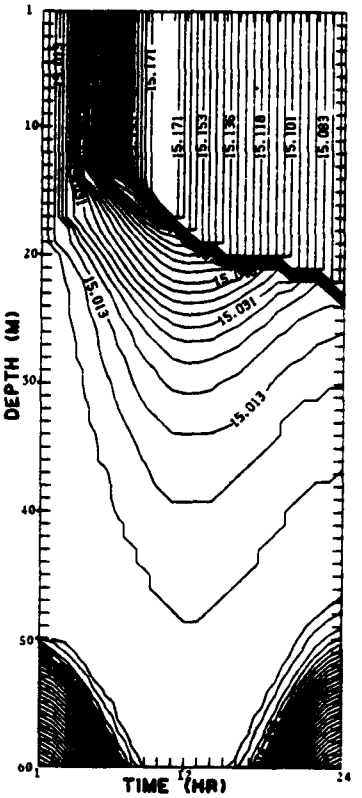

(b)

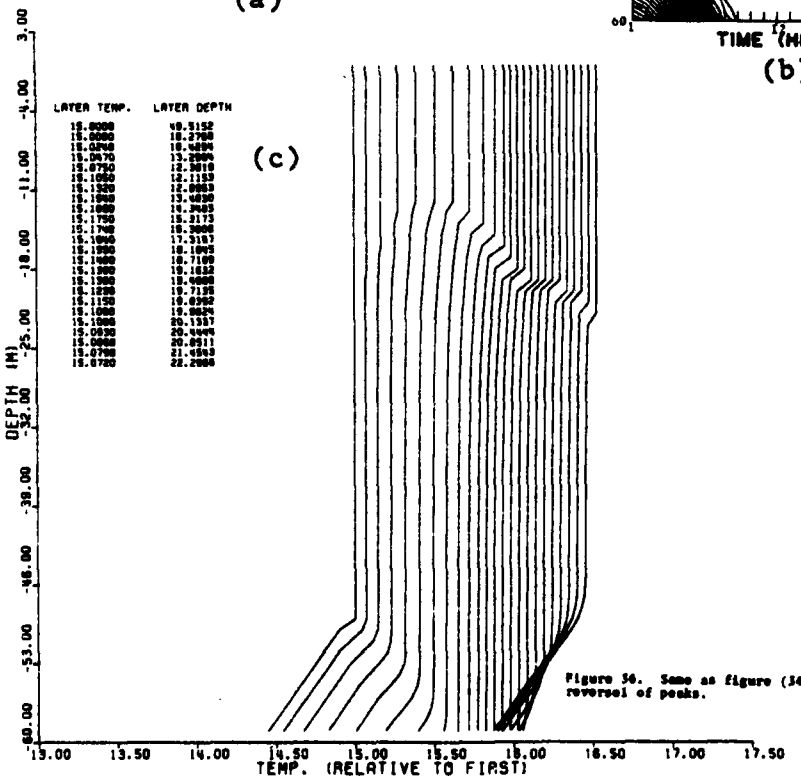

(c)

Figure 36. Same as figure (34), except for reversal of peaks.

DAY	HR	W	T	S	TAU	QNET	WDD	DH
1	1	51.3	15.001	34.000	0.50	- 55.7	0.03600	181.500
1	2	18.6	15.009	34.000	0.50	-201.5	0.03477	63.428
1	3	16.6	15.016	34.000	0.50	-326.8	0.03118	50.859
1	4	13.3	15.048	34.000	0.50	-423.0	0.02546	33.347
1	5	12.2	15.076	34.000	0.50	-483.5	0.01800	21.811
1	6	11.8	15.105	34.000	0.50	-504.2	0.00932	10.985
1	7	12.3	15.132	34.000	0.50	-483.7	0.0	0.0
1	8	12.5	15.154	34.000	0.50	-423.5	-.00932	-11.731
1	9	12.8	15.168	34.000	0.50	-327.5	-.01800	-23.279
1	10	13.1	15.174	34.000	0.50	-202.4	-.02546	-33.653
1	11	13.4	15.171	34.000	0.50	- 56.6	-.03118	-42.378
1	12	13.8	15.158	34.000	0.50	+ 99.9	-.03477	-48.937
1	13	14.2	15.146	34.000	0.50	100.8	-.03600	-52.123
1	14	14.7	15.134	34.000	0.50	100.8	-.03477	-51.925
1	15	15.1	15.123	34.000	0.50	100.8	-.03118	-47.952
1	16	15.7	15.112	34.000	0.50	100.8	-.02546	-40.601
1	17	16.4	15.102	34.000	0.50	100.8	-.01800	-29.866
1	18	17.3	15.092	34.000	0.50	100.8	-.00932	-16.219
1	19	18.4	15.084	34.000	0.50	100.8	-.00000	- 0.001
1	20	19.7	15.075	34.000	0.50	100.8	0.00932	18.261
1	21	21.2	15.068	34.000	0.50	100.8	0.01800	37.866
1	22	23.0	15.061	34.000	0.50	100.8	0.02546	57.770
1	23	25.0	15.055	34.000	0.50	100.8	0.03118	76.611
1	24	27.1	15.050	34.000	0.50	100.8	0.03477	92.697
2	1	28.8	15.050	34.000	0.50	- 55.7	0.03600	101.842
2	2	22.4	15.058	34.000	0.50	-201.5	0.03477	76.651
2	3	15.5	15.074	34.000	0.50	-326.8	0.03118	47.686
2	4	13.5	15.096	34.000	0.50	-423.0	0.02546	33.808
2	5	12.1	15.125	34.000	0.50	-483.5	0.01800	21.659
2	6	11.8	15.154	34.000	0.50	-504.2	0.00932	10.958
2	7	11.8	15.183	34.000	0.50	-483.7	0.0	0.0
2	8	12.2	15.205	34.000	0.50	-423.5	-.00932	-11.408
2	9	12.5	15.219	34.000	0.50	-327.5	-.01800	-22.716
2	10	12.8	15.225	34.000	0.50	-202.4	-.02546	-33.123
2	11	13.2	15.222	34.000	0.50	- 56.6	-.03118	-41.676
2	12	13.6	15.209	34.000	0.50	99.9	-.03477	-48.187
2	13	14.0	15.196	34.000	0.50	100.8	-.03600	-51.414
2	14	14.4	15.184	34.000	0.50	100.8	-.03477	-51.021
2	15	14.9	15.173	34.000	0.50	100.8	-.03118	-47.287
2	16	15.5	15.163	34.000	0.50	100.8	-.02546	-40.053
2	17	16.3	15.153	34.000	0.50	100.8	-.01800	-29.606
2	18	17.2	15.143	34.000	0.50	100.8	-.00932	-16.140
2	19	18.4	15.133	34.000	0.50	100.8	-.00000	- 0.001
2	20	19.7	15.125	34.000	0.50	100.8	0.00932	18.264
2	21	21.2	15.117	34.000	0.50	100.8	0.01800	37.875
2	22	23.0	15.111	34.000	0.50	100.8	0.02546	57.776
2	23	24.9	15.105	34.000	0.50	100.8	0.03118	76.284
2	24	26.8	15.099	34.000	0.50	100.8	0.03477	91.479

(a)

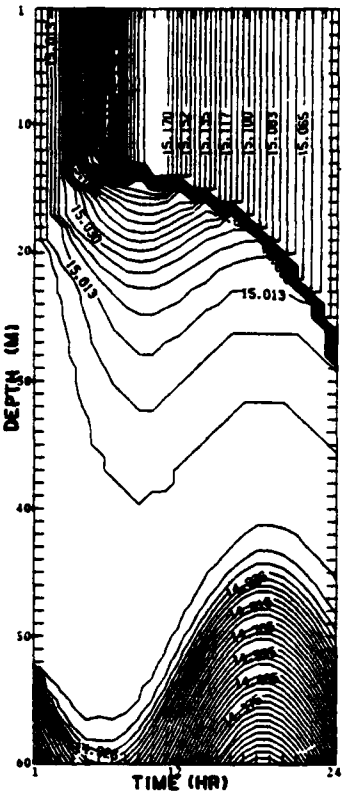

(b)

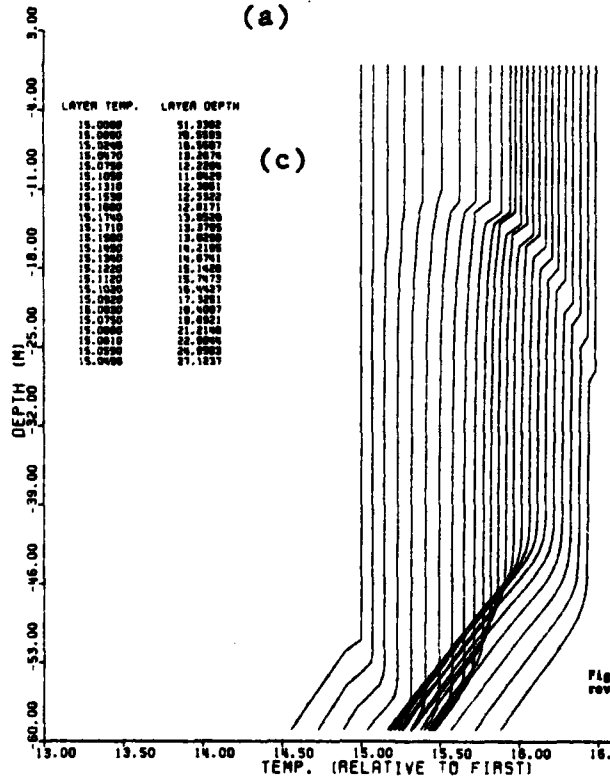

(c)

Figure 37. Same as figure (35), except for reversal of peaks.

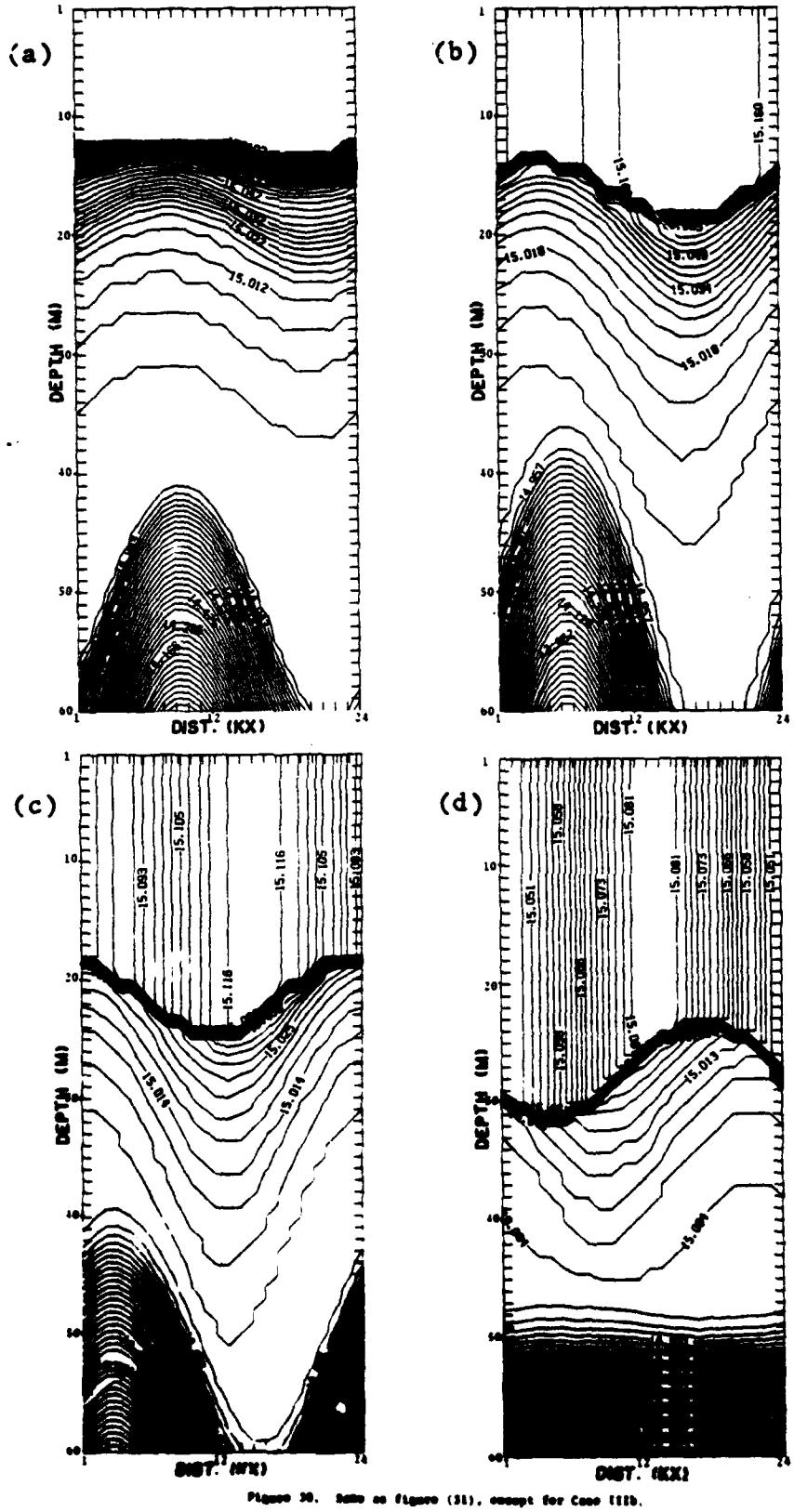

Figure 30. Same as figure (31), except for Case IIIb.

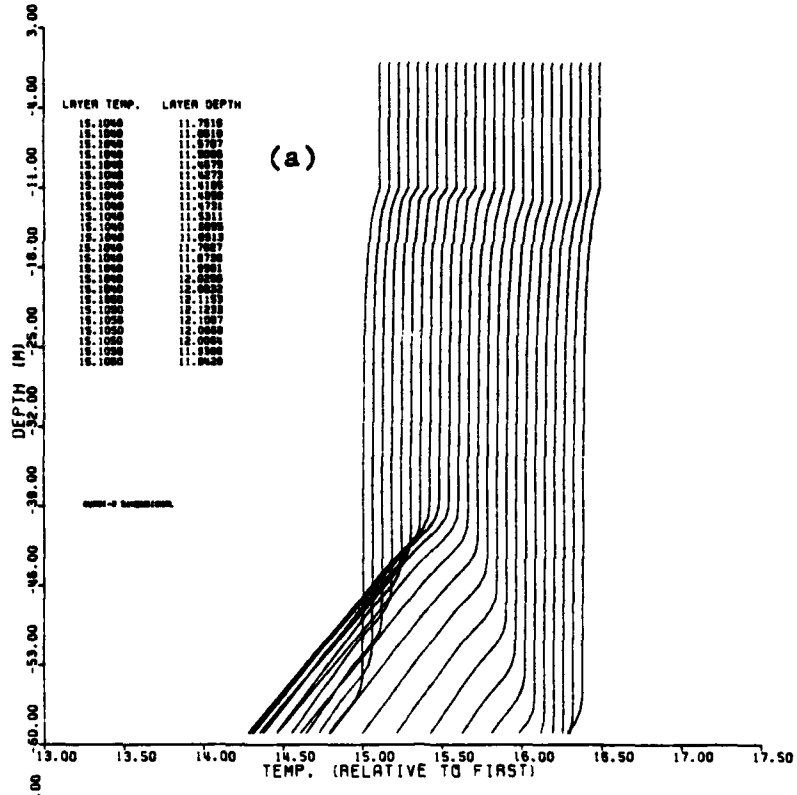

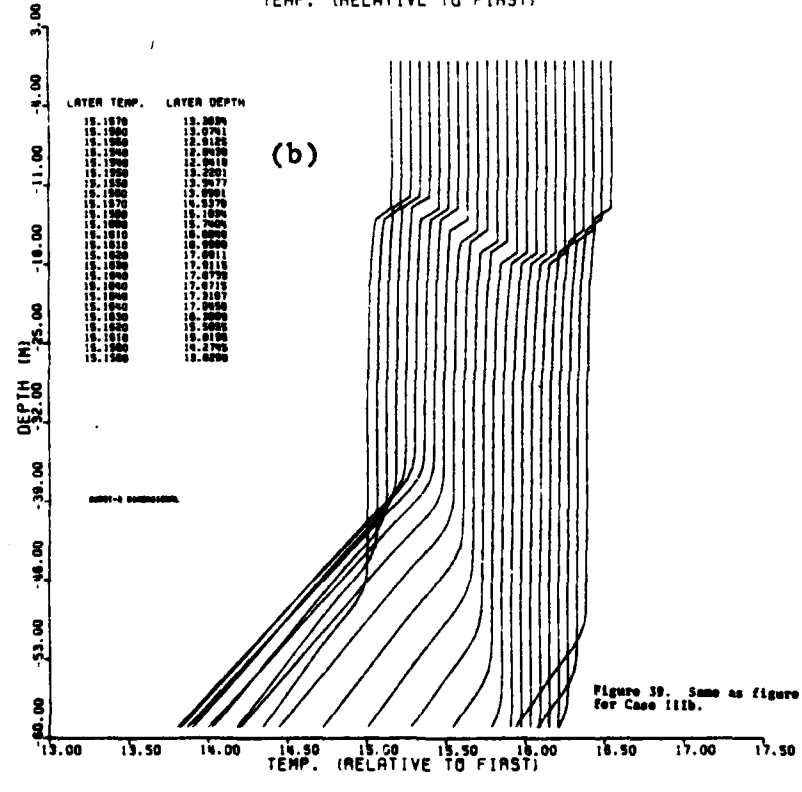

Figure 39. Same as figure (32), except for Case IIIb.

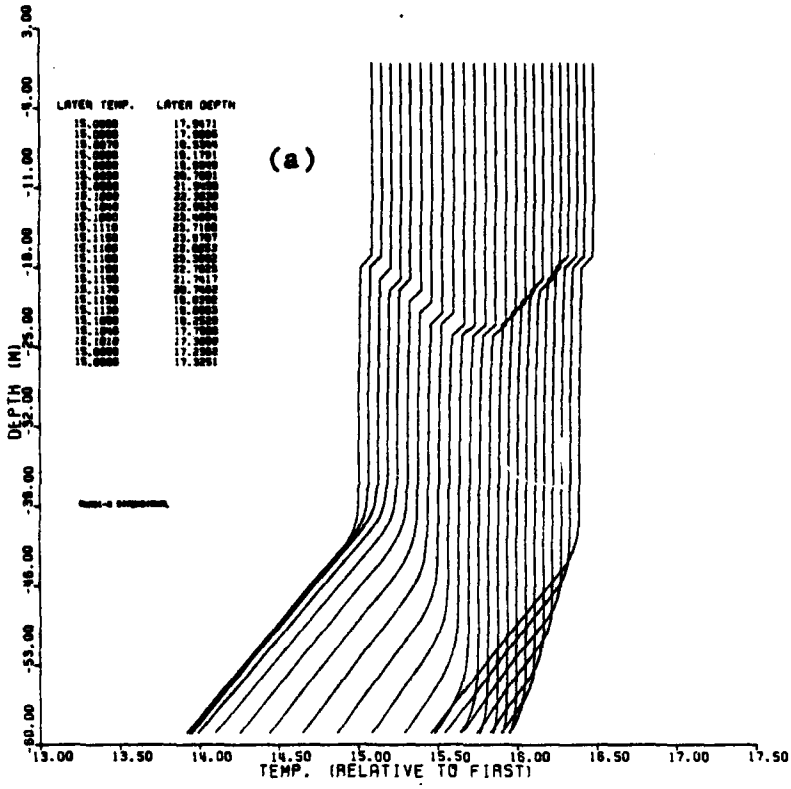

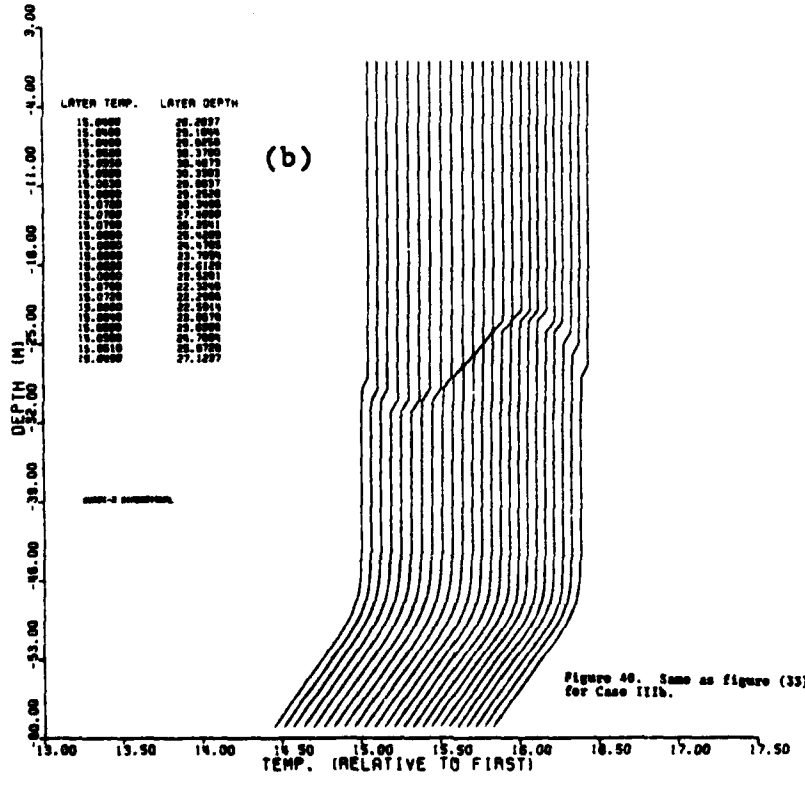

Figure 40. Same as figure (33), except for Case IIIb.

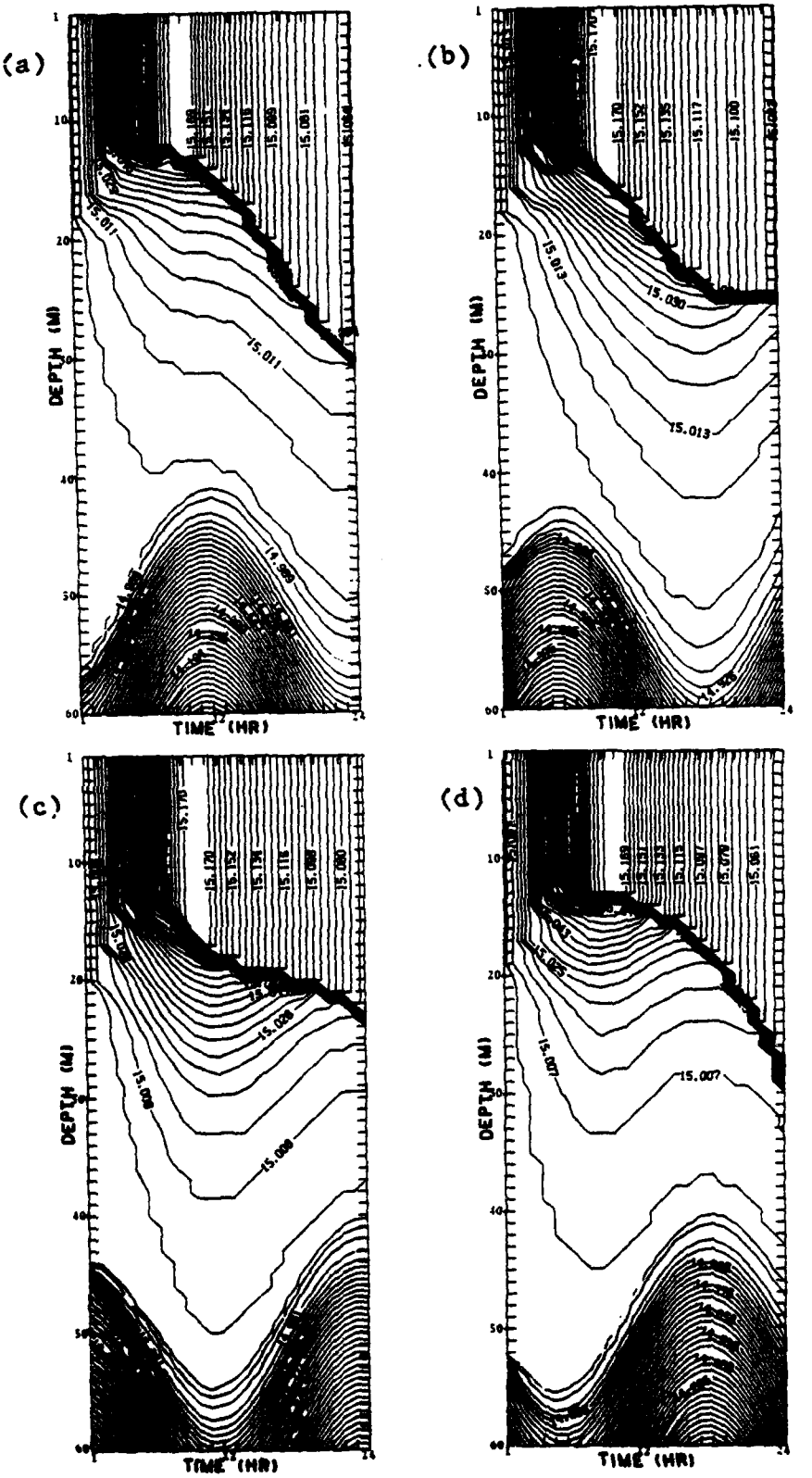

Figure 41. Contours as in figure (1), except for Case IVa. (a), (b), (c), and (d) have the maximum upward motion at hour 6, 24, 18 and 12 respectively.

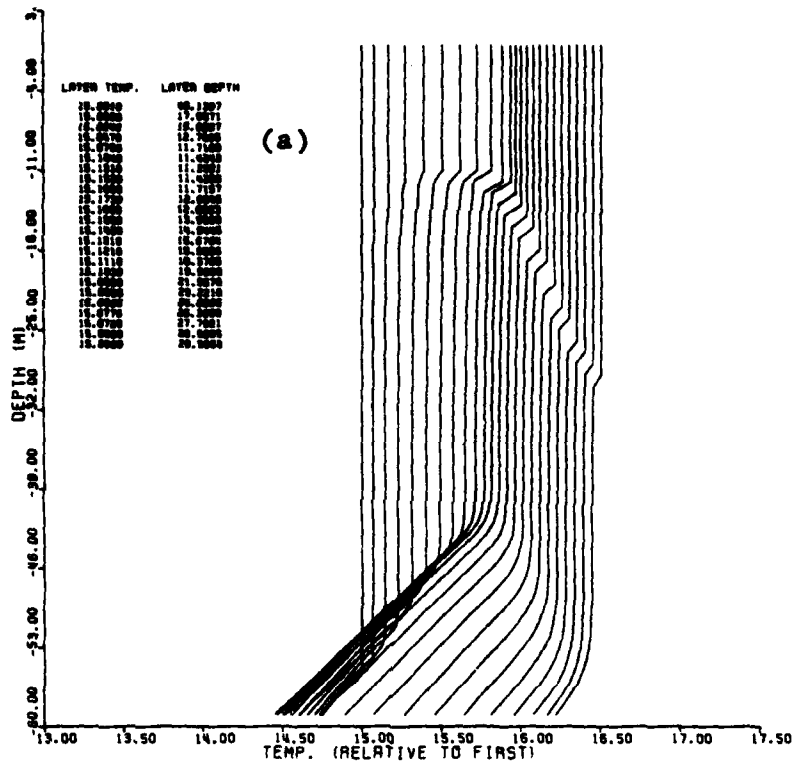

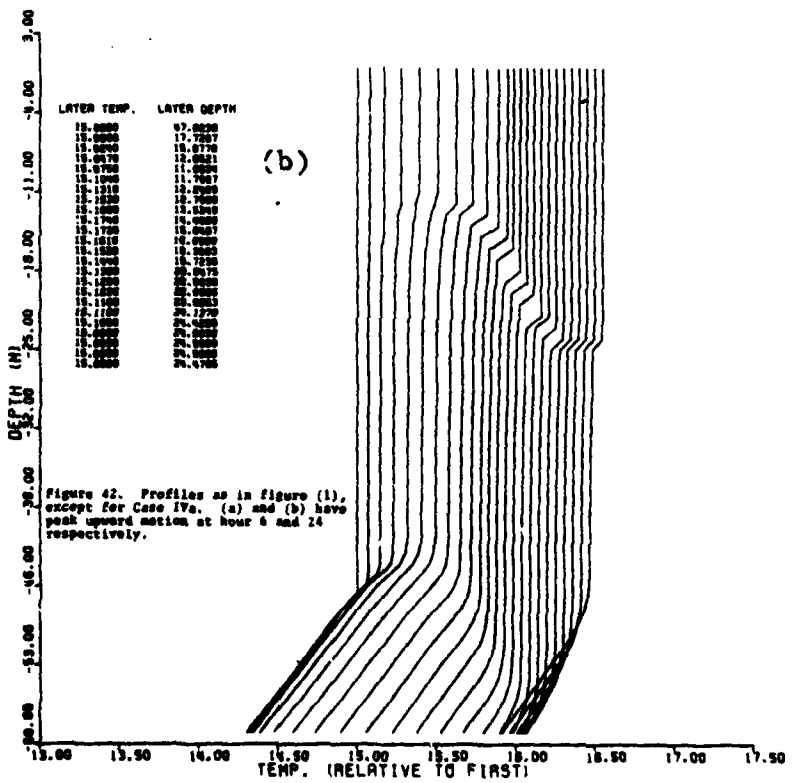

Figure 42. Profiles as in figure (1), except for Case IVa. (a) and (b) have peak upward motion at hour 6 and 24 respectively.

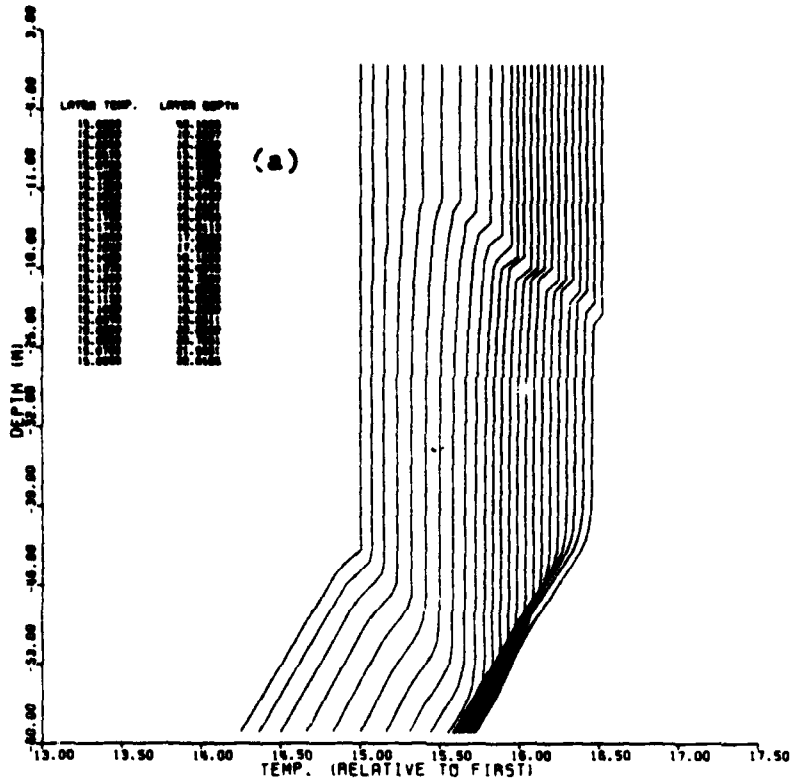

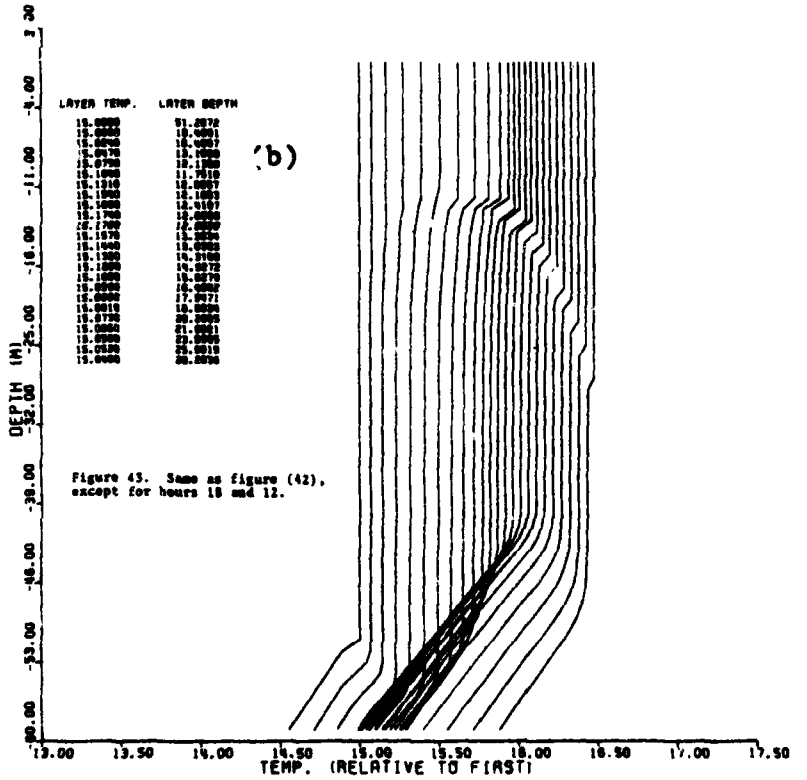

Figure 43. Same as figure (42), except for hours 18 and 12.

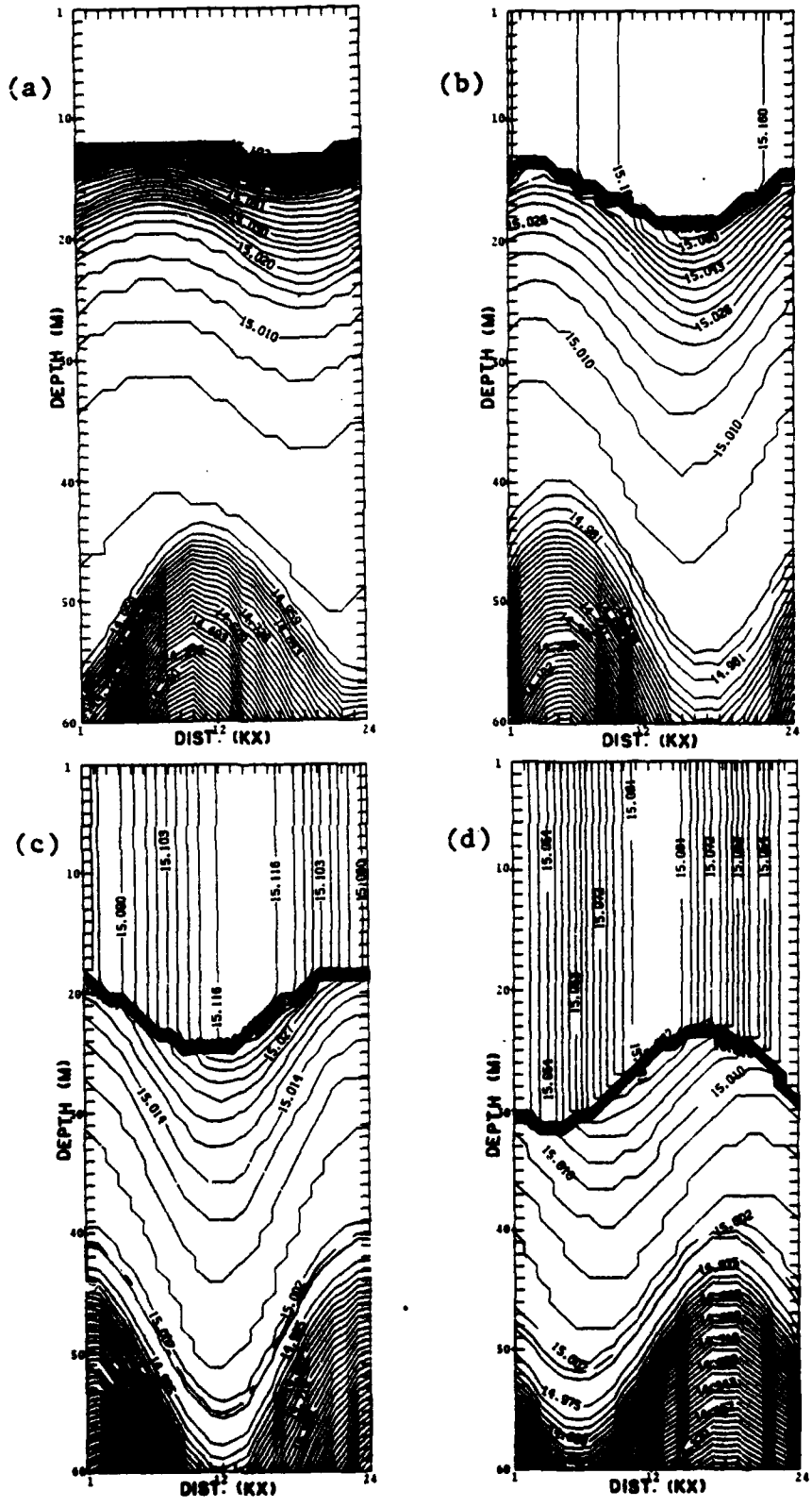

Figure 44. Same as figure (31), except for Case IVa.

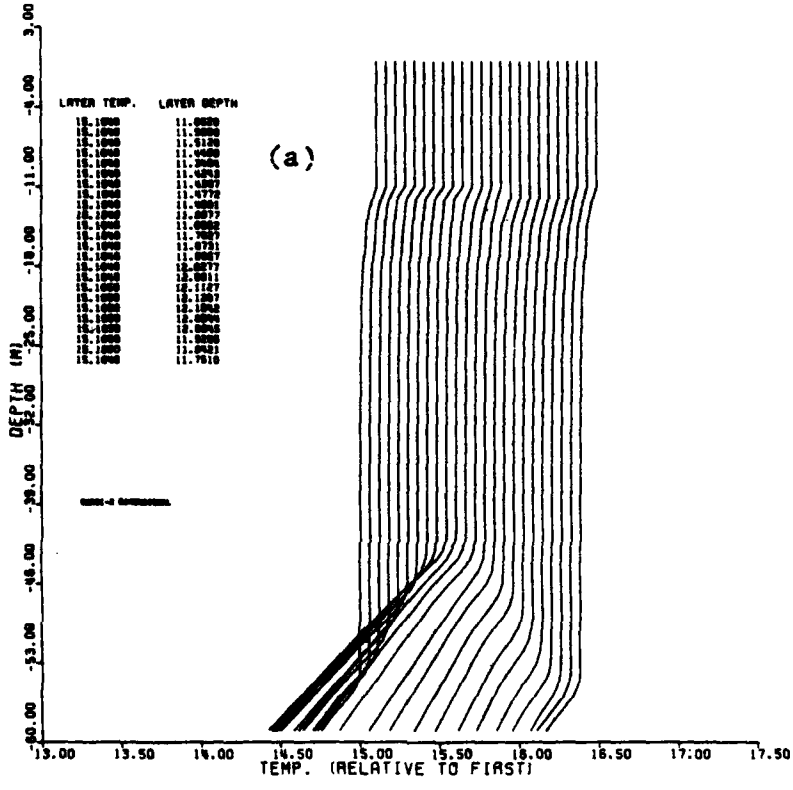

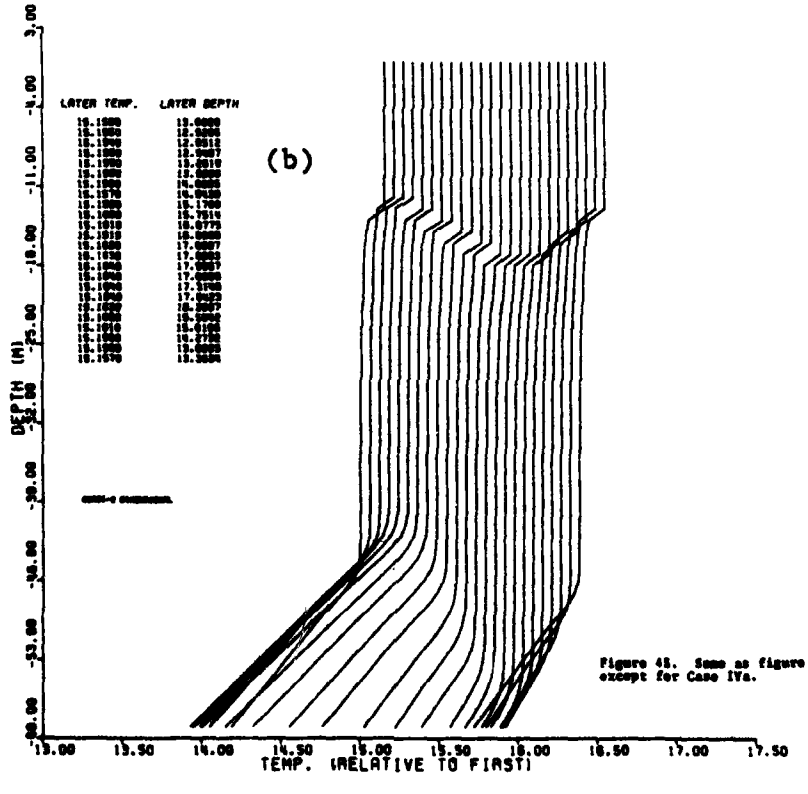

Figure 48. Same as figure (52), except for Case IVa.

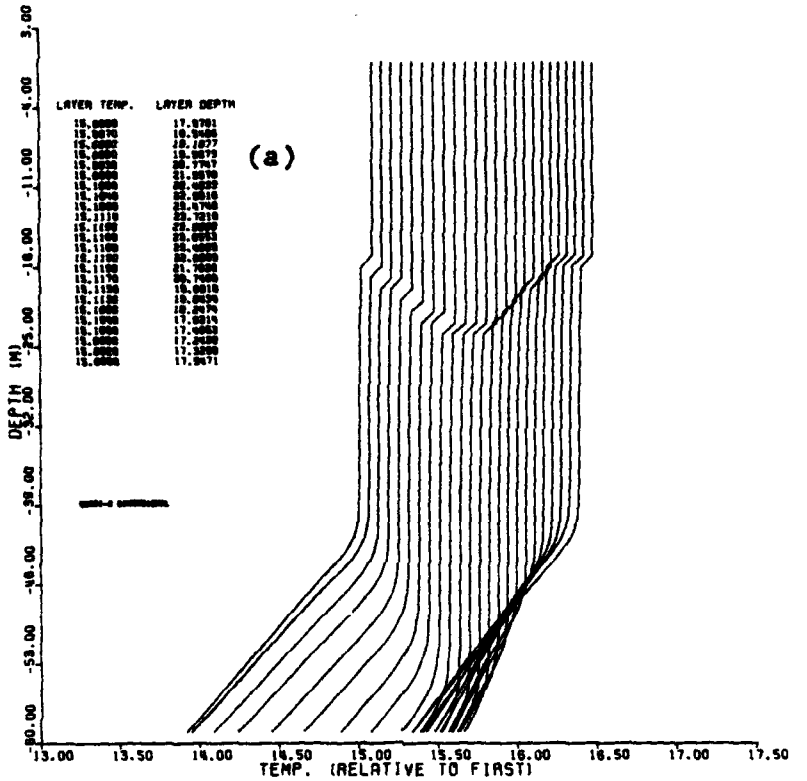

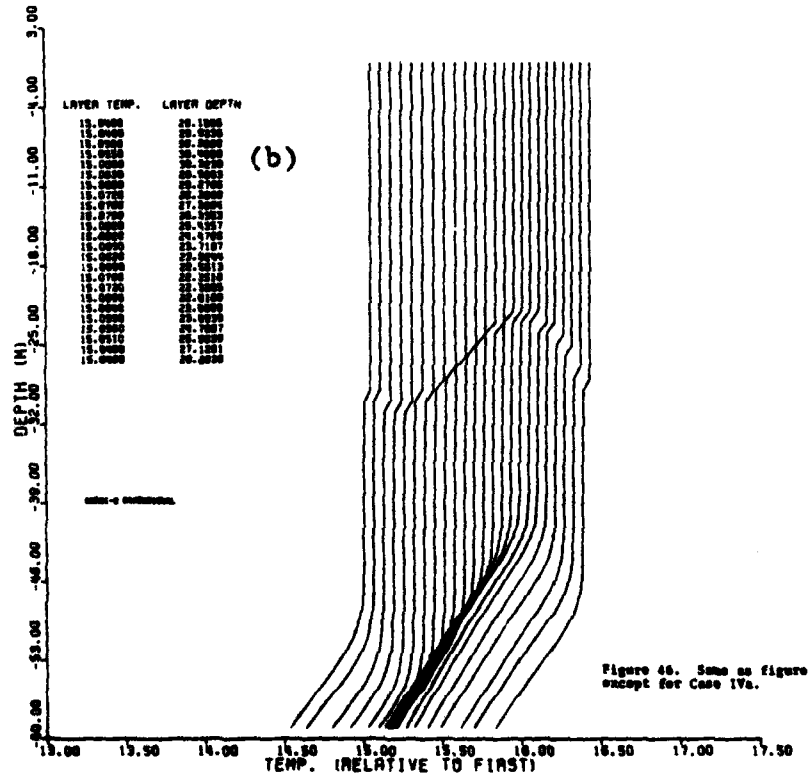

Figure 46. Same as figure (35), except for Case IVa.

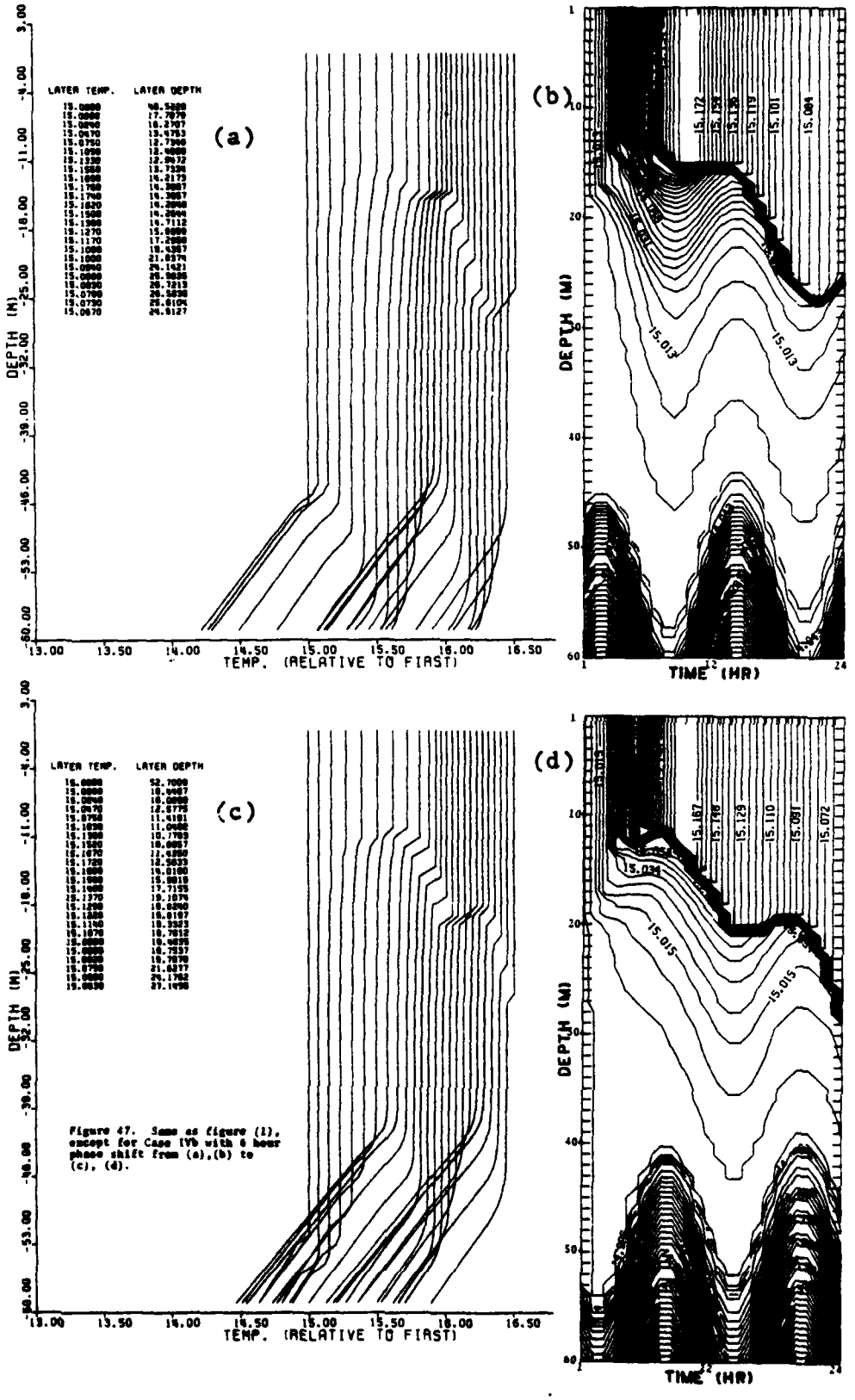

Figure 47. Same as figure (1), except for Case IVb with 6 hour phase shift from (a),(b) to (c), (d).

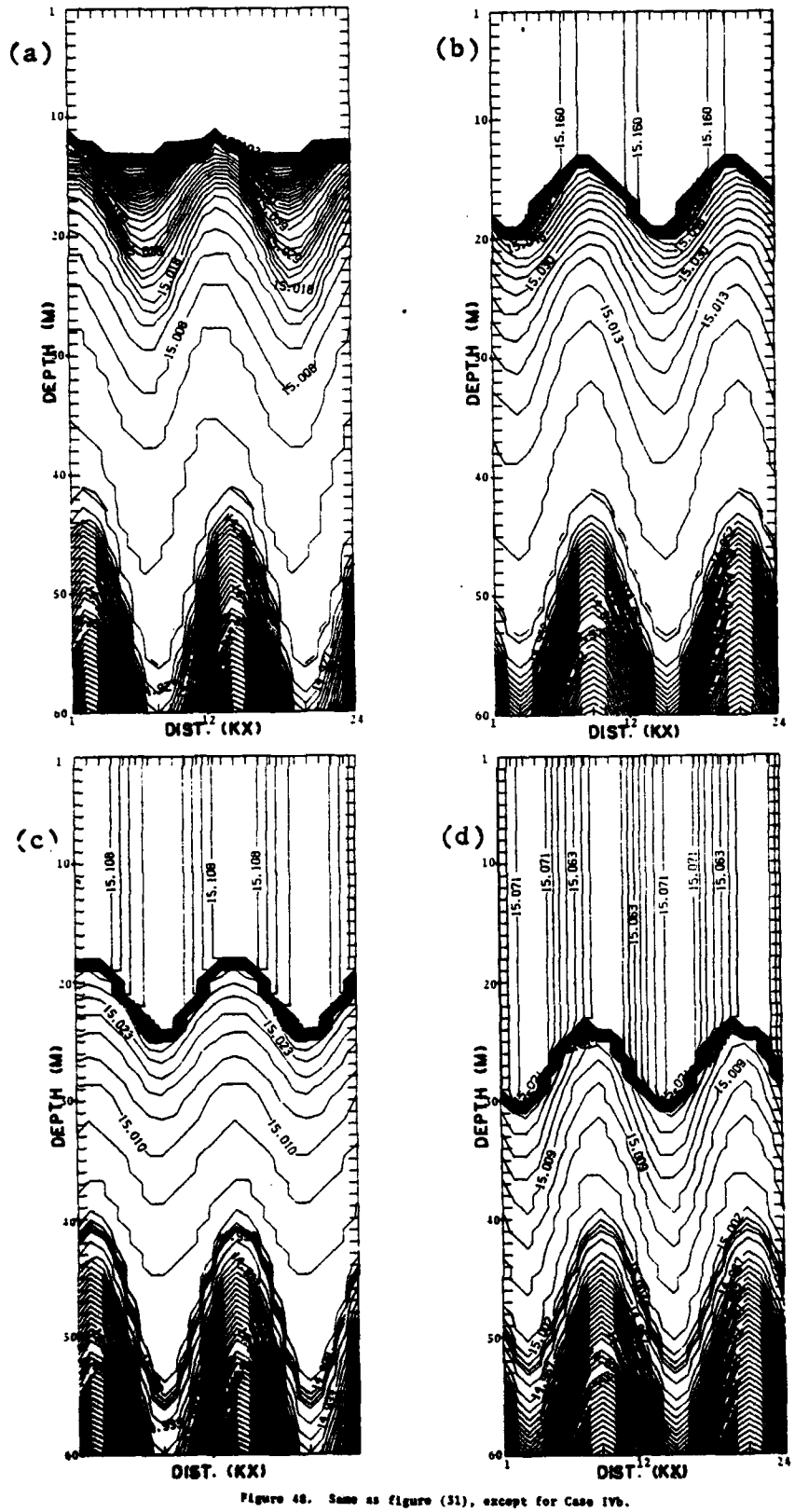

Figure 48. Same as figure (31), except for Case IVb.

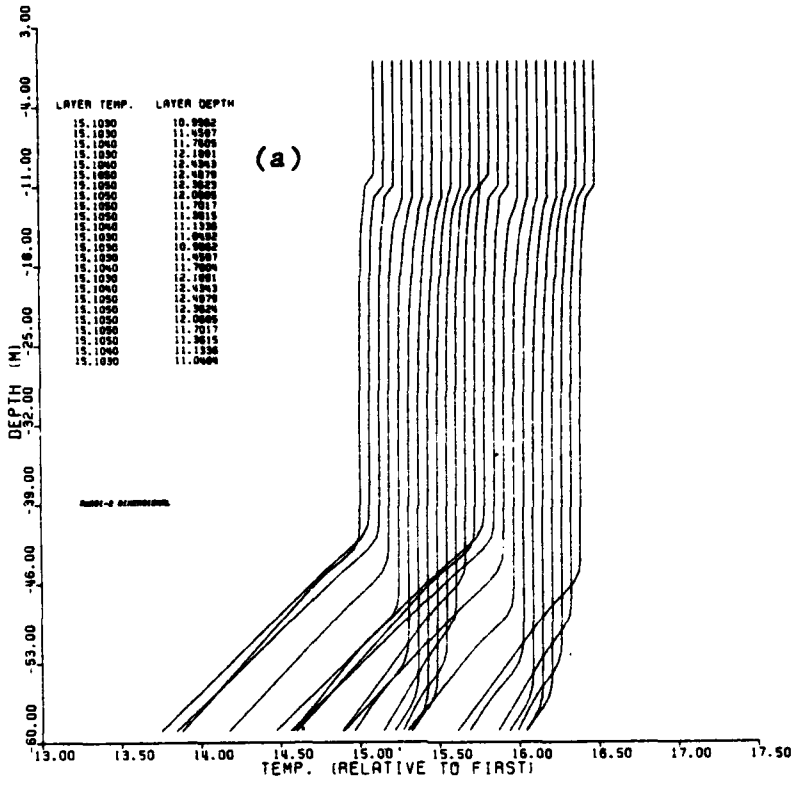

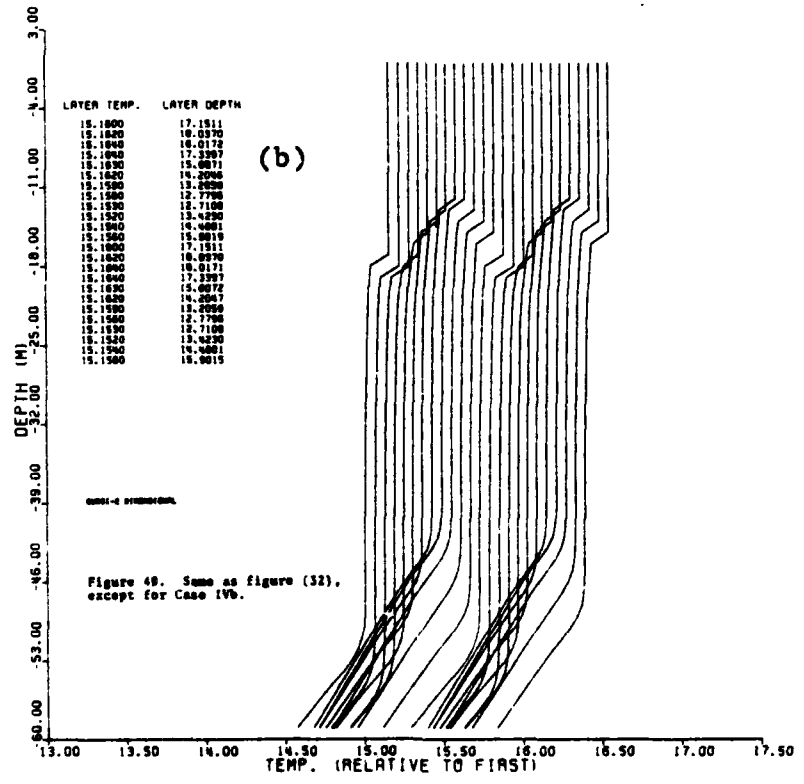

Figure 48. Same as figure (32), except for Case IVb.

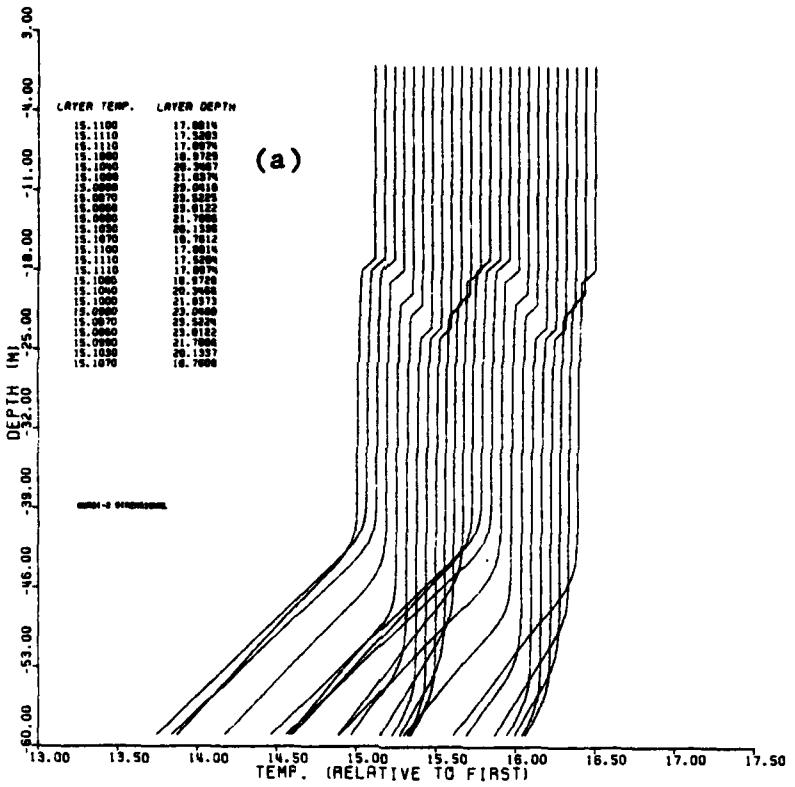

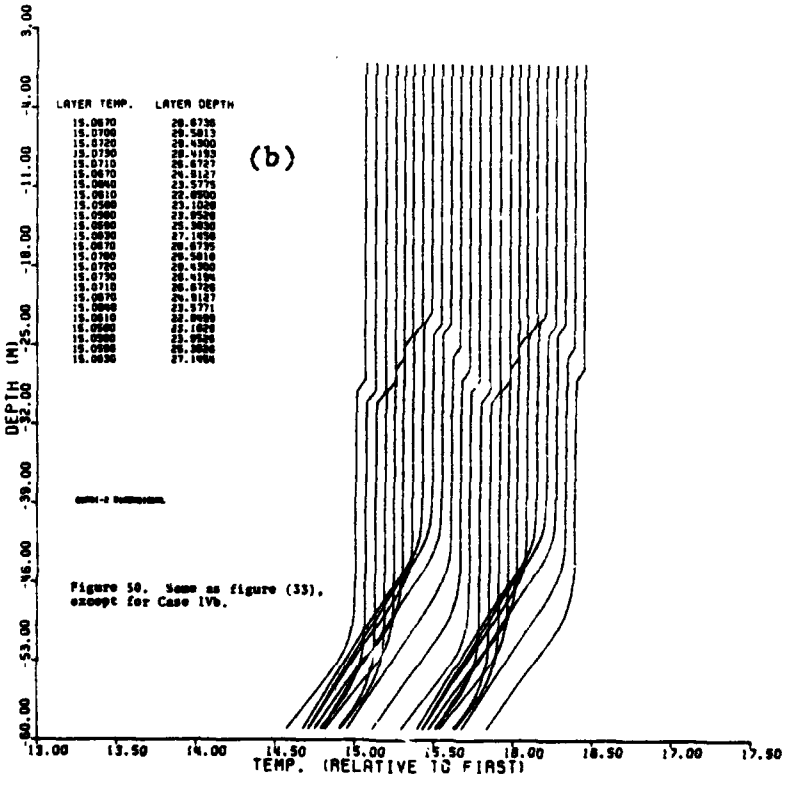

Figure 50. Same as figure (33), except for Case IVb.

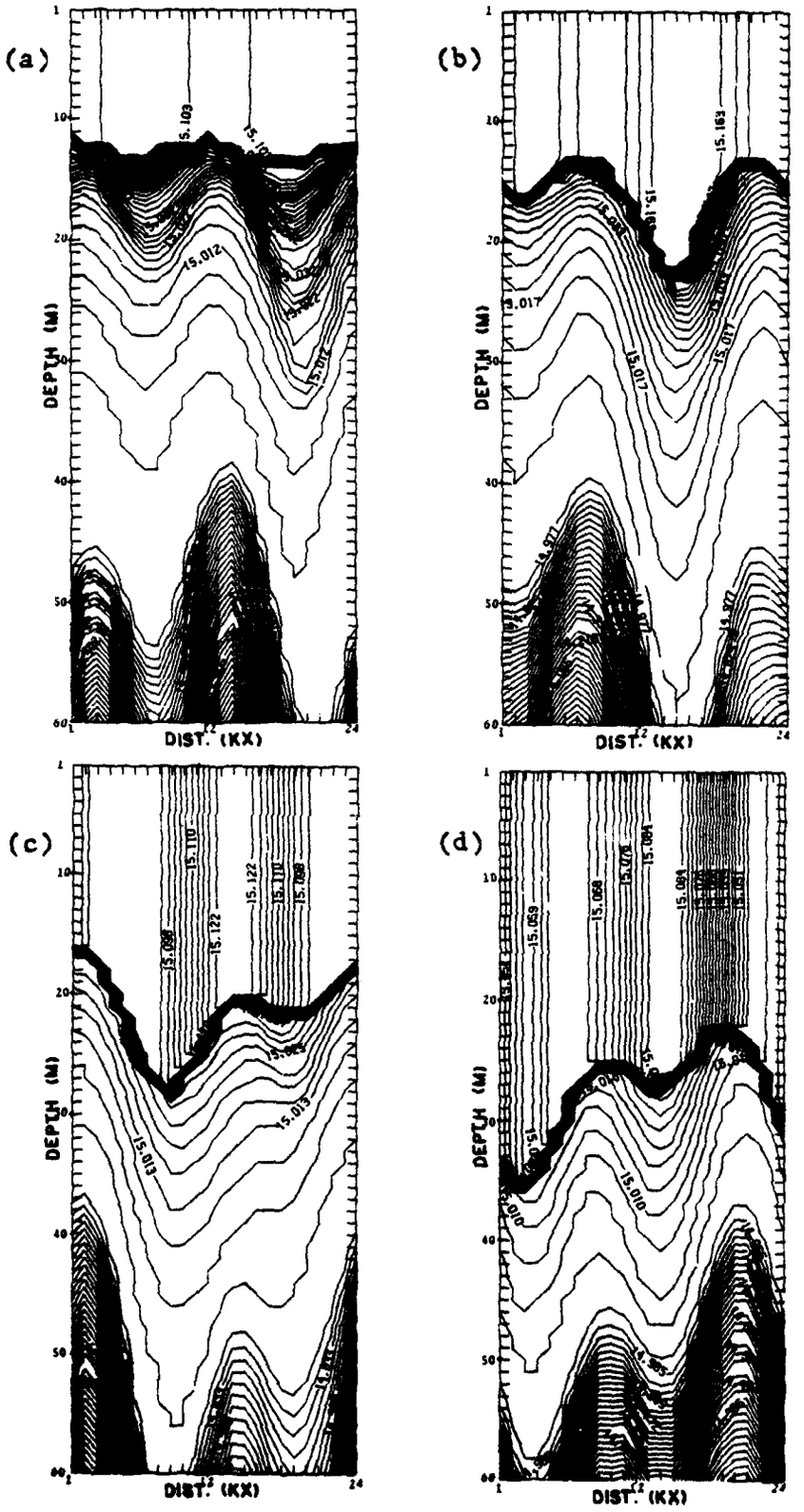

Figure 51. Same as figure (31), except for Case Va.

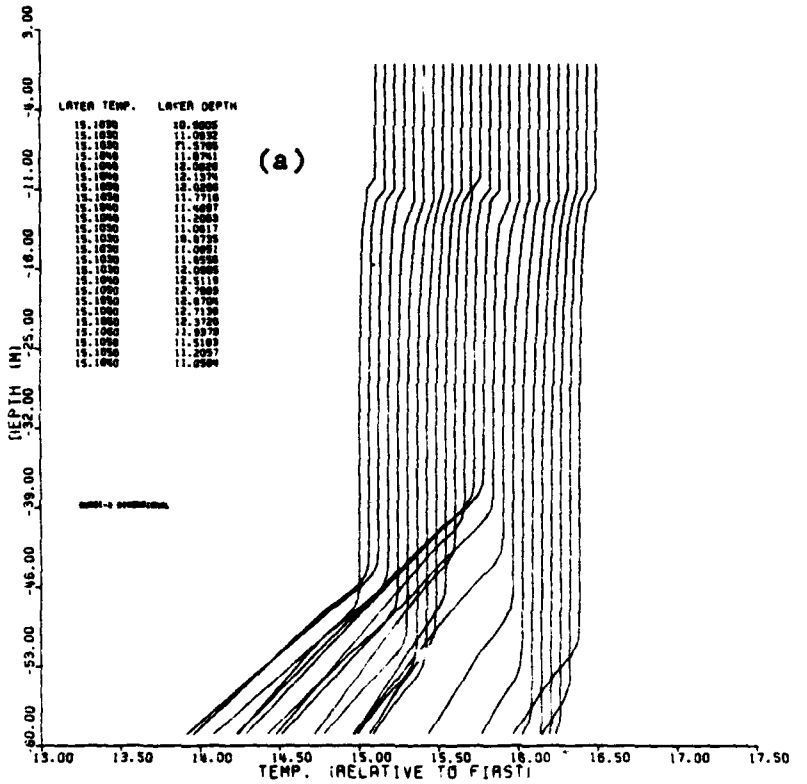

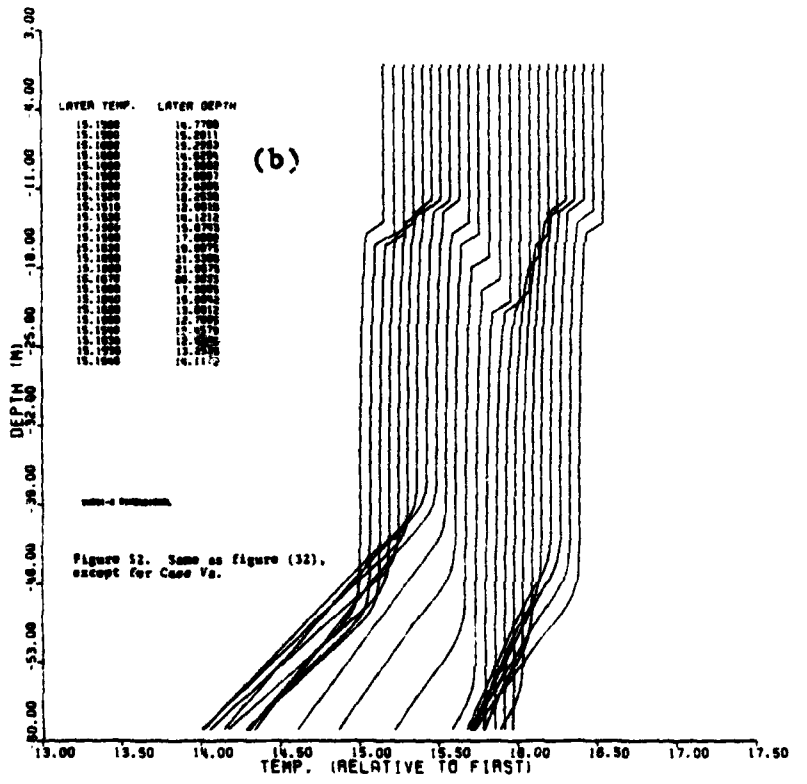

Figure 12. Same as figure (32), except for Case Va.

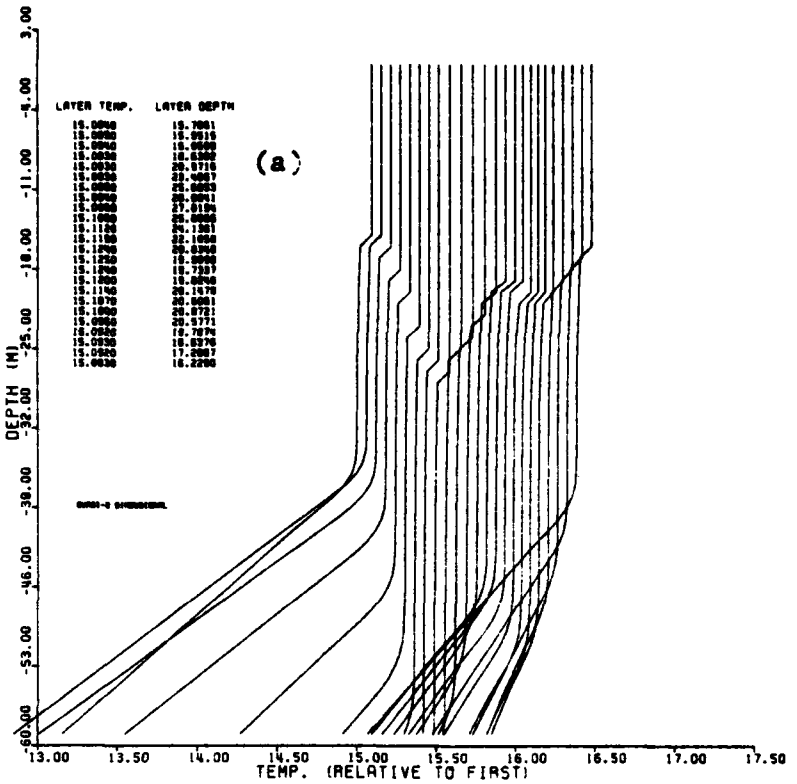

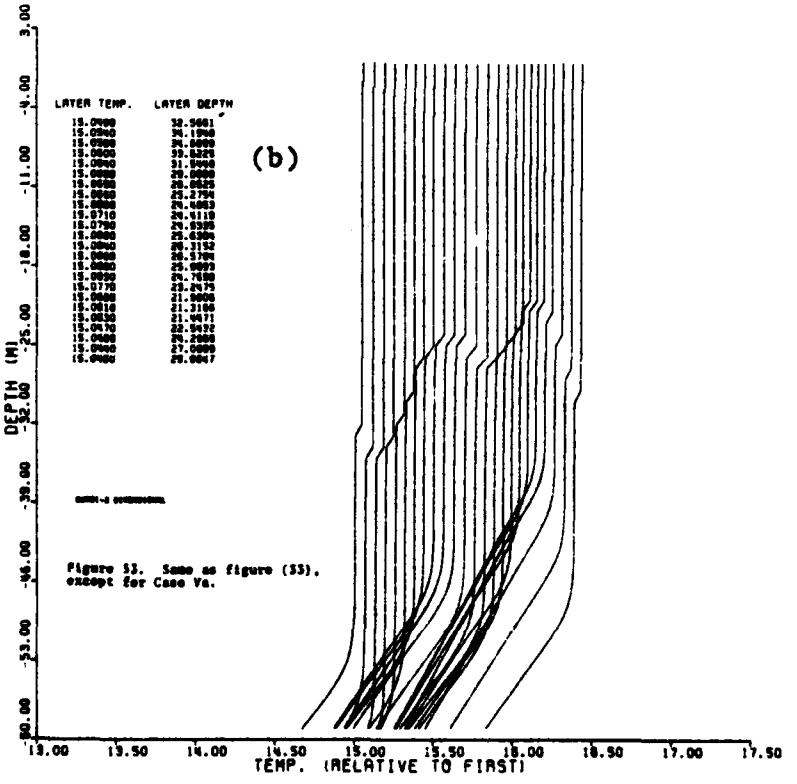

Figure 53. Same as figure (33), except for Case Vb.

BIBLIOGRAPHY

Adamec, D., R. L. Elsberry, R. W. Garwood and R. L. Haney, 1981: An embedded mixed-layer-ocean circulation model. Dynamics of Atmospheres and Oceans, 6, 69-96.

Apel, J. R., 1982: Personal communication.

Bell, T. H., 1978: Radiation damping of inertial oscillations in the upper ocean. Journal of Fluid Mechanics, 88, 289-308.

Butler, W. A., 1981: A study of horizontal sea surface temperature variability. M.S. thesis, Naval Postgraduate School.

Cushman-Roisin, B., 1981: Effects of horizontal advection on upper ocean mixing: A case of frontogenesis. Journal of Physical Oceanography, 11, 1345-1356.

De Szoeke, R. A., 1980: On the effects of horizontal variability of wind stress on the dynamics of the ocean mixed layer. Journal of Physical Oceanography, 10, 1439-1454.

Dillon, T. M. and D. R. Caldwell, 1977: Temperature microstructure profiles at ocean station P: Preliminary results from the MILE experiment. School of Oceanography Oregon State University.

Foo, E., 1981: A two dimensional diabatic isopycnal model-simulating the coastal upwelling front. Journal of Physical Oceanography, 11, 604-626.

Garwood, R. W., 1976: A general model of the ocean mixed layer using a two-component turbulent kinetic energy budget with mean turbulent field closure. Ph. D. thesis, University of Washington, (NOAA Tech. Rep. ERL 384-PMEL 27).

Garwood, R. W., 1977: An oceanic mixed layer model capable of simulating cyclic states. Journal of Physical Oceanography, 7, 455-468.

Garwood, R. W., R. W. Fett, K. M. Rabe and H. W. Brandli, 1981: Ocean frontal formation due to shallow water cooling effects as observed by satellite and simulated by a numerical model. Journal of Geophysical Research, 86, 11000-11012.

Holloway, G., 1980: Oceanic internal waves are not weak waves. Journal of Physical Oceanography, 10, 906-914.

Kantha, L. H., 1977: Note on the role of internal waves in thermocline erosion. Modeling and Prediction of the Upper Layers of the Ocean, Edited by E. B. Kraus, Pergamon Press, 173-177.

Kantha, L. H., O. M. Phillips and R. S. Azad, 1977: On turbulent entrainment at a stable density interface. Journal of Fluid Mechanics, 79, 753-768.

Kraus, E. B. and J. S. Turner, 1967: A one-dimensional model of the seasonal thermocline. Tellus, 19, 90-105.

Linden, P. F., 1975: The deepening of a mixed layer in a stratified fluid. Journal of Fluid Mechanics, 71, 385-405.

Pinkel, R., 1981: Observations of the near-surface internal wavefield. Journal of Physical Oceanography, 11, 1248-1257.

Price, J. F., 1981: Upper ocean response to a hurricane. Journal of Physical Oceanography, 11, 153-175.

Price, J. F., C. N. K. Mooers and J. C. Van Leer, 1978: Observation and simulation of storm-induced mixed-layer deepening. Journal of Physical Oceanography, 8, 582-599.

Roth, M. W., M. G. Briscoe and C. H. Mc Comas III, 1981: Internal waves in the upper ocean. Journal of Physical Oceanography, 11, 1234-1247.

Shook, R. E., 1980: The one-dimensionality of the upper ocean mixing and the role of advection during the POLE experiment. M. S. thesis, Naval Postgraduate School.

Simpson, J. J. and C. A. Paulson, 1979: Observations of upper ocean temperature and salinity structure during the POLE experiment. Journal of Physical Oceanography, 9, 869-883.

Simpson, J. J. and C. A. Paulson, 1980: Small scale sea surface temperature structure. Journal of Physical Oceanography, 10, 399-410.

Spigel, R. H., 1980: Coupling of internal wave motion with entrainment at the density interface of a two-layer lake. Journal of Physical Oceanography, 10, 144-155.

Townsend, A. A., 1968: Excitation of internal waves in a stably-stratified atmosphere with considerable wind-shear. Journal of Fluid Mechanics, 32, 145-171.

INITIAL DISTRIBUTION LIST

		No. Copies
1.	Defense Technical Information Center Cameron Station Alexandria, VA 22314	2
2.	Library, Code 0142 Naval Postgraduate School Monterey, CA 93940	2
3.	Chairman, Code 68Mr Department of Oceanography Naval Postgraduate School Monterey, CA 93940	1
4.	Chairman, Code 63Rd Department of Meteorology Naval Postgraduate School Monterey, CA 93940	1
5.	Professor R. W. Garwood, Code 68Gd Department of Oceanography Naval Postgraduate School Monterey, CA 93940	2
6.	Professor R. T. Williams, Code 63 Wu Department of Meteorology Naval Postgraduate School Monterey, CA 93940	1
7.	Professor K. L. Davidson, Code 63 Ds Department of Meteorology Naval Postgraduate School Monterey, CA 93940	1
8.	Professor R. L. Elsberry, Code 63Es Department of Meteorology Naval Postgraduate School Monterey, CA 93940	1
9.	Professor R. L. Haney, Code 63Hy Department of Meteorology Naval Postgraduate School Monterey, CA 93940	1
10.	Mr. P. C. Gallacher, Code 63Ga Department of Meteorology Naval Postgraduate School Monterey, CA 93940	1

11. Naval Oceanographic Office — 2
NSTL Station
Bay St. Louis, MS 39522
Attn: Lieutenant R. J. Burger

12. Director — 1
Naval Oceanography Command
Naval Observatory
34th and Massachusetts Avenue NW
Washington, D. C. 20390

13. Commander — 1
Naval Oceanography Command
NSTL Station
Bay St. Louis, MS 39522

14. Captain C. H. Bassett Code 00 — 1
Naval Oceanographic Office
NSTL Station
Bay St. Louis, MS 39522

15. Commanding Officer — 1
Naval Oceanographic Office
NSTL Station
Bay St. Louis, MS 39522

16. Commanding Officer — 1
Fleet Numerical Oceanography Center
Monterey, CA 93940

17. Commanding Officer — 1
Naval Ocean Research and Development Activity
NSTL Station
Bay St. Louis, MS 39522

18. Dr. S. Piacsek, Code 320 — 1
Naval Ocean Research and Development Activity
NSTL Station
Bay St. Louis, MS 39522

19. Commanding Officer — 1
Naval Environmental Prediction Research Facility
Monterey, CA 93940

20. Chairman, Oceanography Department — 1
U.S. Naval Academy
Annapolis, MD 21402

21. Chief of Naval Research — 1
800 N. Quincy Street
Arlington, VA 22217

22. Office of Naval Research (Code 420) 1
Naval Ocean Research and Development Activity
NSTL Station
Bay St. Louis, MS 39522

23. Scientific Liaison Office 1
Office of Naval Research
Scripps Institution of Oceanography
La Jolla, CA 93037

24. Library 1
Department of Oceanography
University of Washington
Seattle, WA 98105

25. Library 1
CICESE
P. O. Box 4803
San Ysidro, CA 92073

26. Library 1
School of Oceanography
Oregon State University
Corvallis, OR 97331

27. Commander 1
Oceanography Systems Pacific
Box 1390
Pearl Harbor, HI 96860